EVALUATING THE EFFECTS OF MAJOR ASSUMPTIONS IN LAYERED ELASTIC THEORY ON RAILROAD TRACK RESPONSE PREDICTION THROUGH THE DEVELOPMENT OF AN IMPROVED TRACK ANALYSIS SOFTWARE

by

Sadichchha Sharma

A thesis

submitted in partial fulfillment

of the requirements for the degree of

Master of Science in Civil Engineering

Boise State University

December 2016

BOISE STATE UNIVERSITY GRADUATE COLLEGE

DEFENSE COMMITTEE AND FINAL READING APPROVALS

of the thesis submitted by

Sadichchha Sharma

Thesis Title: Evaluating the Effects of Major Assumptions in Layered Elastic Theory on Railroad Track Response Prediction through the Development of an Improved Track Analysis Software

Date of Final Oral Examination: 30 September 2016

The following individuals read and discussed the thesis submitted by student Sadichchha Sharma, and they evaluated the presentation and response to questions during the final oral examination. They found that the student passed the final oral examination.

Debakanta Mishra, Ph.D.	Chair, Supervisory Committee
Bhaskar Chittoori, Ph.D.	Member, Supervisory Committee
Arvin Farid, Ph.D.	Member, Supervisory Committee

The final reading approval of the thesis was granted by Debakanta Mishra, Ph.D., Chair of the Supervisory Committee. The thesis was approved by the Graduate College.

Dedicated to my late grandparents: Shanti - Ved Ballav Sharma and Bhawa - Shyam Krishna Pandey

ACKNOWLEDGMENTS

ABSTRACT

Railway transportation has been recently gaining popularity due to its efficiency and environmental-friendly technology which has led to its increased usage for both passenger and freight transport. For railway transport to be a sustainable component of the transportation infrastructure in the United States, adequate structural and functional design of track components is essential. This is primarily dependent on thorough understanding of track mechanics and track structural response under loading, and can be accomplished through mechanistic analysis of railway track structure response under loading. Considering the need for a mechanistic track analysis program that can serve as a link between the state of art in research and state of practice in railroad engineering, one of the objectives of this research effort was to develop an advanced, easy-to-use track analysis program for use by both researchers and practitioners working in the field of railroad engineering. This was accomplished through development of a modified version of GEOTRACK (a track analysis program originally developed in the 1980's at the University of Massachusetts, Amherst), called GEOTRACK-2016 on the MATLAB$^{\circledR}$ platform. GEOTRACK utilizes the principles of layered elastic analysis to predict the responses of track super- and sub-structure under vertical quasi-static loading. The first task towards the achievement of this objective involved interpretation of different elements of Layered Elastic Theory as implemented in the original version of GEOTRACK. Results produced by the new version of the software were compared with those from the original version to ensure the accuracy of all modifications. Field instrumentation data obtained from a recently completed research effort was used to constitute a 'control section' for these analyses. A parametric analysis was subsequently carried out to quantify the

effects of different track design parameters on overall track modulus. All results were observed to comply with the trends reported in published literature. The other objective of this Master's thesis was to evaluate the limitations introduced to analysis results when layered elastic theory is used for the analysis of in-service railroad track structures. For this purpose, a commercially available Finite Element package (ABAQUS) was used to model the control section and the track responses under loading were compared under similar loading configurations to those analyzed using GEOTRACK-2016. These comparisons revealed a close match between the results and thus established GEOTRACK-2016 as an accurate, easy-to-use track analysis tool. An intuitive Graphical user Interface (GUI) was also developed for GEOTRACK-2016 to facilitate easy adoption by practicing engineers. Detailed discussions on different tasks undertaken during this research effort have been presented in this Master's thesis.

TABLE OF CONTENTS

LIST OF TABLES

LIST OF FIGURES

CHAPTER 1

INTRODUCTION

1.1   Introduction

The railway system is a vital component of the transportation infrastructure in the United States. Construction of the Baltimore and Ohio Railroad in 1828 marked the beginning of a new era in the country's transportation infrastructure. Following this event, modern railroads promptly entered the U.S., and the golden age for railroads began, which lasted approximately from 1880 till 1920 [1]. In the later years, the railroad industry started facing adversities as other modes of transportation such as airplanes and automobiles started attracting larger portions of the traveling population due to better operational speeds and cost-effectiveness. Upon enactment of the Interstate Highway System Act in 1956, better highways and roads started being built throughout the country, and railroads were slowly abandoned with preference given to personal automobiles [2]. However, after long years of being depicted as a dying industry, the railroad industry has recently made a strong comeback. According to the Association of American Railroads (AAR) [3], *"In 2010, U.S. Class-I freight railroads delivered 955,000 carloads of finished automobiles; in 2015, they delivered 1.45 million carloads, a 52% increase."* Drastic increase in domestic and international freight volumes in the US was observed between 1998 and 2010, and the volume in 2020 is expected to increase by 49% compared to that in 2010 [4]. Furthermore, the volume of freight traffic increased by 72% from 1990 to 2010. As of 2011, there were more than 10 billion unlinked passenger train trips in the US [5].

This growth of the railroad industry can be attributed to increased speed and fuel-efficiency; this has resulted in constantly increasing demand for improved railway infrastructure. Greenhouse gas emissions associated with gasoline-powered automobiles necessitate the use of "greener"transportation modes. According to an AAR report [6], as of 2015, in spite of accounting for 42% of the total amount of freight transported by volume in the US, freight railroads contributed only 0.6% to the total greenhouse gas emissions. Figure 1.1 shows the percentage of greenhouse emissions due to railroads. The AAR report [6] also claims that on average, railroads are four times more fuel efficient than trucks, yet only account for 10% of greenhouse emissions compared to trucks.
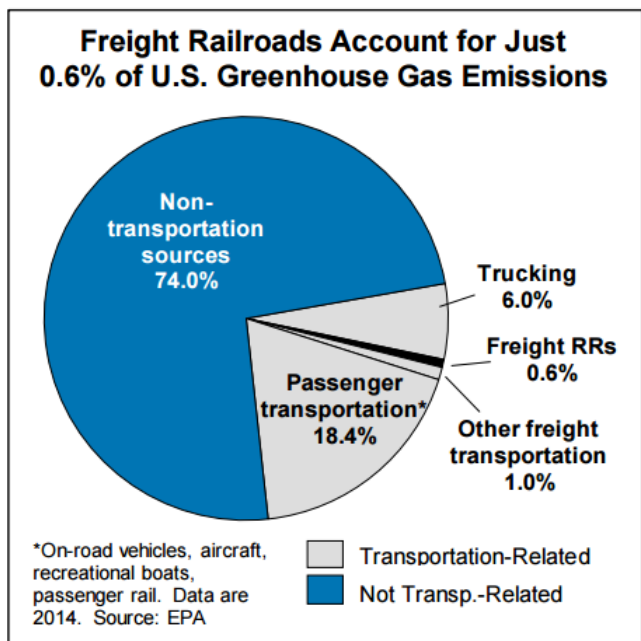
Figure 1.1: Comparing the Relative Contributions of Different Sources towards Total Greenhouse Gas Emissions [4]

A report published by the American Public Transportation Association (APTA) in 2009 indicated that every $1 billion investment in rail transport system creates 24,000 jobs, and every dollar a community invests in railways results in approximately $4 of economic returns [5]. This combined with ever-increasing gasoline prices and

environmental concerns emphasizes the need for a more reliable rail network for both freight as well as passenger transport.

Recent government initiatives since 2008 have kick-started a move towards improved passenger rail networks connecting different parts of the US. Initiatives such as the 'All Aboard Florida' [7], 'Chicago CREATE Plan' [8] and the 'California High Speed Rail', [7] have paved the way for a developed passenger rail network in different parts of the country. Rather than constructing a completely new track network for passenger train traffic, the concept of "shared-use corridors" involving the operation of high-speed passenger trains and slower freight trains along the same set of tracks is being explored for implementation in the US. This presents a particular challenge in front of railroad engineers as the track behavior and performance standards are completely different for these two types of track operations. Factors contributing to these differences include but are not limited to: (i) different operating speeds, (ii) different axle loads, and (iii) varying profile smoothness requirements, etc. A thorough understanding of the mechanics of track behavior is critical to facilitate the development and for the maintenance of reliable passenger and freight railroad networks. Significant research and developmental efforts are required for better understanding of track behavior, and also to develop optimized network operational strategies. Consequently, there is always the need for better understanding of track structure response under loading. Railway track analysis helps in developing better understanding of these responses such as stresses, strains and deflections (both elastic as well as plastic) under train loading.

1.2   Background and Problem Statement

Talbot's method, developed by A.N. Talbot in the 1920's, is one of the oldest approaches to railroad track substructure analysis under loading [9]. This method uses several simplifying assumptions such as the beam-on-elastic-foundation approach and the one-layer substratum supposition. Considering the major shortcomings of such

traditional approaches, significant efforts have been directed towards the development of computer programs for substructure analysis for both railroads and pavements under loading. Some notable compter programs developed for the analysis of multi-layer pavement systems are the 'CHEVRON N-LAYER' computer program [10], the BItumen Stress Analysis in Roads (BISAR) computer program [11] and the LEAF program [12]. Meanwhile, computer programs such as KENTRACK [9], ILLITRACK [13] and GEOTRACK [14] have been developed over the years for the analysis of railway track structures as multi-layer systems.

Recently, there has been significant development in the field of railroad track analysis using advanced computational methods such as the Finite Element method. Although such advanced methods have the potential to analyze more complex geometries and layer configurations, they require high computational effort and special sets of user skills. Moreover, simple methods such as the one developed by Talbot represent the track support through a single set of properties only, and cannot account for variations in material properties across different substructure layers. An intermediate solution that is more realistic than the simplified Talbot's method (which cannot analyze multi-layer systems) but is more convenient to use by practitioning engineers as Finite Element method, is desirable. An example of such a railroad track analysis program is GEOTRACK.

GEOTRACK is a computer program for track structure analysis under vertical quasi-static loading and was developed at the University of Massachusetts, Amherst, USA by Chang, Adegoke and Selig in 1980 [14]. It was developed as an improvement to the Multi-Layer Track Analysis (MULTA) program [15]. GEOTRACK can be used to calculate different track response values in the superstructure as well as substructure; the outputs being: (a) Superstructure: Rail Deflection, Rail Seat Force, Tie Deflection, Tie Bending Moment, Rail Bending Moment; (b) Substructure: Vertical Deflection within the Ballast, Subballast, and Subgrade layers, Complete

Stress State within the Substructure, Bulk Stress, and Stress States at Different Points; (c) <u>Overall Track Structure</u>: Track Modulus [16]. The original version of GEOTRACK, written in the VAX FORTRAN language, was only compatible with VAX machines that used punch cards for inputs. This version was later modified in 1987 for use on microcomputers [17]. It was last modified for execution on the WINDOWS operating system in 1992. Since then, no subsequent developmental efforts have focused on further development of this software. The source code for the executable version of the program is not available because of software transfer right issues. The currently available code corresponds to the original version written in VAX FORTRAN, and cannot be executed on modern operating systems. Advent of modern operating systems has rendered the current executable version of GEO-TRACK incompatible with most computers. This has proved to be a significant obstacle against wide-spread use of this program by researchers and practitioners in the railroad industry. Absence of detailed supporting documentation for the current version of the source code makes the interpretation of the underlying algorithm an extremely challenging task. Considering the wide recognition of GEOTRACK as a validated track analysis program, this research effort focused on developing an improved version of this software. Once the underlying algorithm of the code is interpreted, it would facilitate further upgrade of the software by future researchers. The lack of knowledge transfer caused by this uncompilable version of GEOTRACK was the primary motivation behind selecting this program for upgrade and improvement into a newer version of 'GEOTRACK-2016' under the scope of this Master's thesis work.

1.3 Research Objective and Tasks

Considering the need of an easy-to-use mechanistic track analysis program that can serve as a link between high-level research and practice in the field, one of the objectives of this research effort was to develop an advanced, easy-to-use track analysis

program for use by both researchers and practitioners working in the field of railroad engineering. GEOTRACK-2016, based on the MATLAB$^{\circledR}$ platform was developed as a product of this research undertaking. The theory employed by this newly developed railroad track analysis program is Layered Elastic (LE) Analysis. The LE theory has been used for analysis by several computer programs since 1940s, and the "same code" for analysis has been passed on for generations. Therefore, another objective of this research effort was to analyze the accuracy of the LE algorithm used by such computer programs. This was achieved by assessing the assumptions of LE theory, comparing the analysis results with those generated from analysis using the Finite Element method.

Different tasks carried out to accomplish the overall research objectives are briefly outlined below:

1. Extensive review of published literature to gather information on different railroad track analysis models and computer programs, for interpretation of the algorithms inherent in the Layered Elastic analysis and its formulation.

2. Development of 'GEOTRACK-2016' on MATLAB$^{\circledR}$platform. Further sub-tasks included:

   2.1. Elimination of the compilation errors in the available source code to facilitate compilation on modern Operating Systems.

   2.2. Elimination of runtime errors during execution to generate desired output file(s).

   2.3. Modification of the inherent algorithm in the available source code to match the output from GEOTRACK for WINDOWS.

   2.4. Rewriting the code for GEOTRACK to develop a newer version of the GEOTRACK software on the MATLAB$^{\circledR}$platform.

3. Conducting a parametric study with GEOTRACK-2016 to evaluate the effects of different track parameters on track modulus and comparing against the trends observed in the past.

4. Analysis of the assumptions inherent to Layered Elastic analysis through side-by-side comparisons with results from Finite Element modeling and analysis.

5. Incorporation of advanced features and enhancement of analysis capabilities in GEOTRACK-2016. New capabilities and features include:

   5.1. An intuitive Graphical User Interface (GUI) with enhanced pre- and post-processing capabilities and expedited generation of input files.

   5.2. A batch-mode in the program facilitating simultaneous parametric analysis of different design alternatives.

   5.3. Enhanced plotting and data visualization capabilities.

   5.4. Calculation of bending stresses in the rails.

   5.5. Incorporation of Talbot's dynamic factor to account for dynamic effects of loading.

   5.6. Ability to query track response at desired points of interest.

1.4   Outline of the Thesis

Chapter 2 of this Master's thesis presents findings from an extensive review of published literature on different track analysis theories. A brief background on two railroad track analysis computer programs: KENTRACK and ILLITRACK has also been presented. Chapter 3 presents a detailed discussion of the layered elastic theory and relevant equations. Subsequently, a theoretical formulation of the analysis scheme in GEOTRACK is presented.

Detailed descriptions of different tasks undertaken during the development of GEOTRACK-2016 are presented in Chapter 4. The process of compiling the software

through elimination of different errors and development of the MATLAB$^{\circledR}$-based software are discussed. Verification of the modified code through comparison of the analysis results with those generated by GEOTRACK for WINDOWS is also discussed. Chapter 5 presents results from a parametric study performed using GEOTRACK-2016 to evaluate the effects of different track design and construction parameters on the overall track modulus value. The use of Finite Element analysis to analyze the assumptions of Layered Elastic analysis is also discussed in this chapter.

Chapter 6 introduces the enhanced analysis capabilities implemented in GEOTRA-CK-2016. The ability to calculate rail bending stresses, the ability to calculate dynamic load factors, and the ability to query track response at desired points of interest along with plotting and data-visualization modules are discussed. Chapter 7 presents a summary of the research tasks and provides recommendations for future research and developmental efforts.

CHAPTER 2

REVIEW OF PUBLISHED LITERATURE

As already discussed, the objective of this research effort was to develop an easy-to-use software program for railroad track analysis. To accomplish this objective, a proper understanding of different track components and their contributions to track structural performance is essential. In-depth understanding of different track analysis methods and advantages and limitations of each would also aid the accomplishment of individual tasks in this research. Hence, an extensive literature review of the track components and different available track analysis methods was undertaken, and the findings have been presented in this chapter. These track analysis methods include the concept of Beam on Elastic Foundation, the Pasternak Foundation, Filonenko-Borodich Foundation and Kerr Foundation models. Subsequently, two of the currently available computer programs for railroad track analysis have also been introduced. Towards the end of the chapter, models incorporating moving loads and finite element modeling of high speed rails have also been briefly introduced.

2.1 Conventional Track Structure Components

Railroad tracks can be ballasted or ballast-less (slab track). Ballasted railroad tracks are also known as conventional railroad tracks. The focus of this research is on conventional track structures, and therefore, all discussions presented in this chapter pertain to conventional track structure.

Railway track systems are constructed to provide a smooth and safe running surface for trains. A railway track system comprises two main components: super-

structure and substructure. A typical railway track superstructure consists of rails, railpads and fastening systems and cross-ties (also called ties or sleepers). The substructure consists of the ballast, subballast and subgrade layers. The superstructure is separated from the substructure by the tie-ballast interface. Figure 2.1 shows the components of a typical ballasted track structure [16].
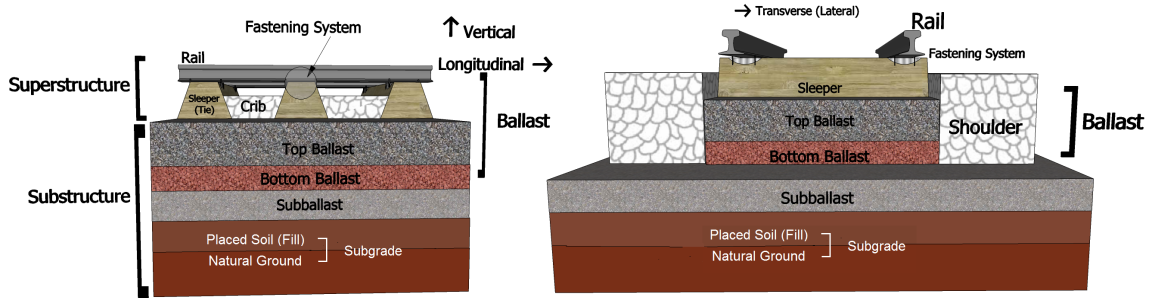
Figure 2.1: Railway Track Structure Components (a) Longitudinal View (b) Transverse View (modified from [16])

2.1.1 Superstructure

The railway track superstructure consists of rails, railpads and fastening systems and cross-ties; and comprises the primary load carrying elements of the track that transfer train-induced loads to the track substructure. The superstructure is designed and constructed to resist vertical and lateral loads imposed by the train traffic while undergoing only small elastic and permanent deformations [18].

Rails: Rails are longitudinal steel members that provide smooth and continuous running surfaces for train wheels. Rails should securely support wheel loads in the vertical, lateral, and longitudinal directions and present sufficient stiffness to function as beams that distribute train-induced wheel loads onto the ties. They also act as electrical conductors for the signaling system. The standard gage between two rails is 1435 mm (56.5 inches) in North America. Typical rail sizes, and corresponding properties used in North America are shown in Table 2.1 [16].

* 1 lb = 4.45 N;   1 yd = 914.4 mm;   1 in = 25.4 mm

Table 2.1: Rail Properties Used in North America

Rail Size	Mass (lb/yd)	Cross-Sectional Area (in^2)	Moment of Inertia (in^4)
100 RE	101.5	9.9	49.0
115 RE	114.7	11.2	65.6
132 RE	132.1	12.9	88.2
136 RE	136.2	13.3	94.9
140 RE	140.6	13.8	96.8

Railpads and Fastening Systems: Railpads are provided between rails and cross-ties to provide resiliency to the rail-tie system, insulation for track signals, and also to reduce rail-tie contact deterioration. The purpose of fastening systems is to restrain the rails against cross-ties and resist the relative movements. The stiffness value for the fastening system component is significantly lower compared to that of railpads; therefore the effect of fastening is normally neglected and railpad stiffness is given more importance during track analysis.

Cross-Ties: Cross-ties are laid transversely to support rails. They receive loads from the rails and transmit them on to the ballast with reduced contact pressures. Cross-ties also hold the rails and fastening systems to maintain track gauge, level, and alignment. They restrict lateral, vertical, and longitudinal movements of the rails.

The most commonly used materials for manufacturing of cross-ties are wood (timber) and reinforced concrete. Researchers in the past have argued that concrete ties are heavier and more durable than wood ties [16]. They also provide better fastening than wood ties. However, wood ties are easier to handle than concrete ties and also do not require pads to provide resiliency. According to the Railway Tie Association (RTA), as of 2006, *"Wood maintains a 93%+ share of the market for ties installed in North America; whereas concrete maintains about 6.5% market share"* [19]. Typical tie dimensions and center to center spacing used in the North America are shown in Table 2.2 [16].

Table 2.2: Typical Mainline Railroad Tie Dimensions and Center to Center Spacing Used in North America

Material	Width (*in.*)	Length (*in.*)	Spacing (*in.*)
Wood	9.01	102	19.5
Concrete	11.26	103.5	24.01

2.1.2 Substructure

Track substructure consists of foundation layers that support the track superstructure. A typical ballasted railway track substructure consists of the ballast, subballast and subgrade layers.

Ballast: Ballast is the crushed granular layer of relatively uniform size placed as the topmost layer of the substructure where ties are embedded. A typical ballast layer comprises gravel-size (nominal 20 to 50 mm diameter, with most particle between 6 and 64 mm diameter) crushed rock [16]. The ballast layer transmits forces from ties to a larger area underneath and provides vertical, lateral, and longitudinal resistance helping maintain the track alignment. It provides resiliency and elasticity to the track and also provides electrical resistance. The ballast layer also helps provide improved drainage to the track. Drainage is very important in the track because excessive water in the substructure causes problems of increased plastic strain accumulation, decreased stiffness, decreased strength, and loss of subgrade strength. Other disadvantages of poor drainage include subgrade intrusion into ballast, ballast degradation and cross-tie attrition, and frost heave and thaw softening [16].

Sub-ballast: The sub-ballast layer is usually placed between the ballast and subgrade layers and typically consists of well-graded granular particles. The sub-ballast layer helps reduce the intensity of train-induced stresses transmitted from the ballast to the subgrade. It further acts as a separation layer between the ballast layer and the subgrade and prevents upward migration of fine materials coming from the subgrade.The most common materials used as subballast are crushed natural aggregates and sand-gravel mixtures.

Subgrade: The subgrade layer is the platform upon which the track structure is constructed and has an important effect on overall track performance. It functions as a stable platform for all track components above it, and should ideally resist excessive plastic deformation, massive shear failure, and excessive volume change [16]. Stresses imposed by train loads extend beyond the ballast and subballast layers and are ultimately dissipated into the underlying subgrade layer [16].

Assessing the effects of individual track components on overall track performance for an in-service railroad track can prove to be a tedious undertaking. Therefore, parameters such as indicators like track modulus and track stiffness are used for analyzing the effects of track components on overall track quality and performance. The next section introduces these indicators of overall track quality.

2.2 Structural Indicators of Track Quality

2.2.1 Definition of Track Modulus and Track Stiffness

Track modulus is an important indicator of track quality and performance. It is defined as the supporting force per unit length of track per unit vertical deflection, and presents a measure of the vertical stiffness of the rail foundation [20]. On the other hand, track stiffness is a measure of the vertical stiffness of the entire track structure [21]. If a concentrated vertical force, P, from the train wheel produces a maximum vertical rail deflection, δ_{max}, under the wheel, q being the vertical foundation supporting force per unit length, track modulus, u, and track stiffness, k, can be defined by Equations 2.1 and 2.2 respectively [21].

$$u = \frac{q}{\delta_{max}} \tag{2.1}$$

$$k = \frac{P}{\delta_{max}} \tag{2.2}$$

Note that although several research literatures use 'track modulus' and 'track

stiffness' interchangeably, 'track modulus' is not the same as 'track stiffness'. The relationship between track modulus and track stiffness can be described by Equation 2.3.

$$u = \frac{k^{4/3}}{(64EI)^{1/3}} \qquad (2.3)$$

2.2.2 Methods of Track Modulus Determination

Since the track modulus cannot be calculated directly from properties of individual track components, it must be determined from field measurements of track deflection under loading [16, 20]. Different methods for estimating the track modulus for a given track structure are presented in the following subsections.

Single Point Load Test: The single point load test is considered to be the easiest method for determining the track modulus for an in-service track. In this method, a known vertical load is applied on the top of the rail at a single point and the deflection thus caused, is measured. The track modulus can be estimated using Equation 2.4 [15].

$$u = \frac{(P/y_m)^{4/3}}{(64EI)^{1/3}} \qquad (2.4)$$

where P is the maximum rail-seat load, y_m is the maximum deflection of the rail, and EI is the rail flexural rigidity.

Deflection Basin Test: This method of estimating the track modulus is based on the vertical equilibrium of an infinitely long beam [21]. The track modulus is calculated using Equation 2.5, as the ratio of the applied forces to the total area of track deflection measured as the area between the original rail position and the deflected rail position.

$$u = \frac{\sum_{j=1}^{n} P_j}{A_\delta} = \frac{\sum_{j=1}^{n} P_j}{S \sum_{i=1}^{m} \delta_i} \qquad (2.5)$$

where A_δ is the area of the deflection basin, n is the number of loads, m is the number of ties that deflect under the vertical loads, and S is the center to center tie spacing [21].

To eliminate the effects of slacks in the track, a light and a heavy vertical force may be used instead of a single force. The area is then the difference in the two deflection basin areas, and the load is the difference between the heavy and the light forces [22]. However, this method is not recommended because it requires measurements of displacement at many points and also does not account for flexural rigidity (EI term) of the rail [16].

Multiple Axle Load Test This method is an extension of the single point load test to multiple axle loads. The load is applied using two or three axle bogies on rail vehicles, which is the most convenient method for applying the load [22]. A wheel load superposition analysis is then performed to estimate the value of track modulus. This approach for determining the track modulus is used in the GEOTRACK analysis program.

Pyramid Load Distribution Method This method of calculating track modulus assumes the pressure beneath the rail seat is distributed uniformly across the area of a pyramid spreading downward in the substructure. An equivalent spring stiffness (k_e) for the entire system is used, which accounts for stiffness of the rail pad, tie, ballast, and subgrade separately. The equivalent spring stiffness (k_e) is calculated using Equation 2.6.

$$\frac{1}{k_e} = \frac{1}{k_p} + \frac{1}{k_t} + \frac{1}{a\,k_{bs}} \tag{2.6}$$

where k_p is the stiffness of the railpad, k_t is the vertical stiffness of tie, a is an experimental factor used to account for the continuity of the deflection of trackbed between adjacent ties, and k_{bs} is the combined stiffness of ballast and subgrade.

The distributed track modulus is then calculated using Equation 2.7 [22].

$$u = \frac{k_e}{S} \tag{2.7}$$

where S is the center to center tie spacing. This method presents a quick estimation

approach for determining the track modulus where no direct measurement for deflection under loading is available. Similar to the deflection basin method, the main disadvantage of this method is it does not account for flexural rigidity of the rail [20].

Track modulus is an overall indicator of the entire track quality and performance. It can also serve as a good indicator during parametric analysis to observe how different track parameters affect the overall track structural health. However, for prediction of deflections, stresses and strains, an in-depth analysis of railroad track structure is required. The following section presents overviews and formulations of commonly used railroad track structural analysis approaches.

2.3   Railroad Track Structural Analysis

Railroad track structural analysis helps to better represent the complex interactions among track components and to quantify the response of different track structure components under loading. It also provides a basis for track performance prediction. Since the physical states of ballast, subballast and subgrade are not constant and change with state of stress and time, the analyses are complicated [23]. Nevertheless, various analytical and numerical models have been developed by researchers over the years for track structural analysis. A brief introduction to some of the most commonly used analysis methods has been presented in the following sections.

2.3.1   Determination of Vertical Stresses in the Substructure based on Boussinesq Solution

In its simplest form, a loaded track structure can be viewed as a multi-layer system subjected to vertical loading. Therefore, all analysis methods developed to calculate the track response under loading adopt different algorithms to predict the stresses and strains in a layered system. However, before considering a multilayer system, the first simplification can be to merge the different layers to constitute one substructure layer. This is similar to the homogeneous semi-infinite elastic half-space assumption

proposed by Boussinesq [24]. This half space is assumed to be elastic, and the length of the loaded area is infinitely long. The half space is also assumed to be weightless, and Hooke's law holds true. Extending this theory to the analysis of railroad track structure has the primary limitation that there is no distinction between different substructure layers.
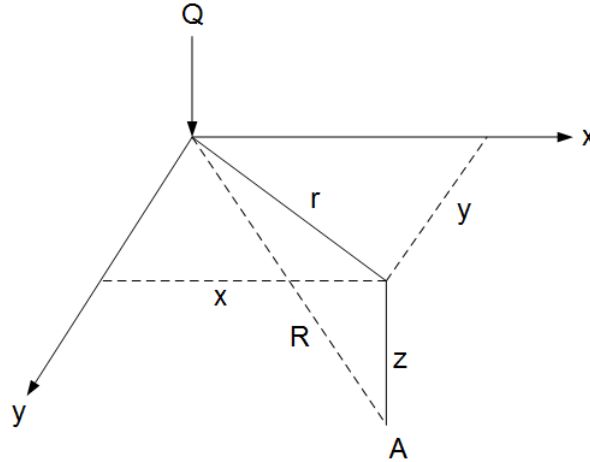
Figure 2.2: Boussinesq Solution for Vertical Stress Determination under Point Load Q

The Boussinesq solution for stresses produced at any point A due to point load Q as shown in Figure 2.2 is given by the following equation.

$$\sigma_z = \frac{Q}{z^2} \frac{3}{2\pi} \times \left[\frac{1}{1 + \left(\frac{r}{z}\right)^2} \right]^{5/2} \tag{2.8}$$

This problem can further be extended to uniformly distributed loads [24] as shown in Figure 2.3.

The vertical pressure (P) at any point in the substructure can be calculated using Equation 2.9.

$$P = \frac{P_0}{\pi} (\alpha + \sin \alpha + \cos 2\beta) \tag{2.9}$$

where P_0 is the pressure on top of the loaded layer, and α and β are the angles as shown in Figure 2.3 [24].
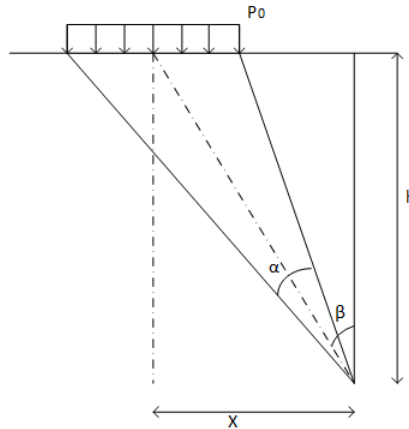
Figure 2.3: Substructure under Load P_o(modified from [24])

The assumption of homogeneity made for Boussinesq's analysis, which does not differentiate between individual substructure layers, is not valid for accurately predicting stresses in a railroad track substructure. In addition, the vertical pressure calculated is independent of the depth (h) in Equation 2.9, which is not realistic. A correction factor was thus introduced by Salem in 1996 [24]. The modified equation is given as follows.

$$P = \frac{P_0}{\pi}\left(\frac{48-h}{22}\right)(\alpha + \sin\alpha + \cos 2\beta) \tag{2.10}$$

where h is the depth of the point where pressure is being calculated.

Note that in the above formulations of Boussinesq's theory, the loading is directly applied on top of the half-space. One method of incorporating the effect of the superstructure in a track system is provided by the theory of Beam on Elastic Foundation.

2.3.2   Beam on Elastic Foundation (BOEF)

Considering that the load transmission to a railroad track is achieved through the movement of a wheel over a long beam, one simple analysis approach involves the application of the Beam on Elastic Foundation theory. The BOEF theory can be applied to calculate rail and tie deflections, bending moments and shear forces in the rail, and rail seat force, ballast pressure and vertical stress between the tie and the

ballast. In the BOEF theory, the rail is simplified as an infinitely long Euler-Bernoulli beam supported by evenly distributed linear springs representing a continuous elastic foundation (the dense liquid or Winkler foundation).

Euler-Bernoulli Beam: Euler-Bernoulli beam theory, developed by Leonard Euler and Jacob Bernoulli in 1750s [25] is a simplification of the linear theory of elasticity which provides a means of calculating the load-carrying and deflection characteristics of beams. The beam under consideration extends from $x = 0$ to $x = L$, and has a flexural rigidity EI as shown in Figure 2.4.
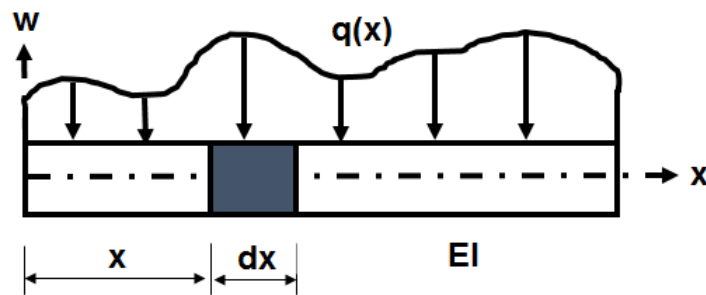
Figure 2.4: Schematic Representation of an Euler-Bernoulli Beam Subjected to a Distributed Loading

Beam deflection (w) at a distance x as shown in Figure 2.4 is described by the differential equation in Equation 2.11.

$$EI\frac{d^4w(x)}{dx^4} = -q(x) \tag{2.11}$$

where $q(x)$ is the distributed load on the beam.

Winkler Base Model: Conventional track systems consist of two parallel continuous beams (the rails), which are fixed at regular intervals on ties supported by the ballast bed from underneath and from the sides. The ballast bed rests on a subballast layer, which rests on the subgrade with the ultimate layer for the load transmission chain being a non-deformable formation. According to Winkler's hypothesis (1867), at each

point of support, the compressive stress is proportional to the compression at that particular point [26],
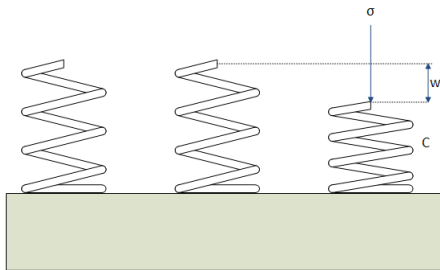
Figure 2.5: Winkler Base Model

$$\sigma(x) = uw(x) \tag{2.12}$$

where $\sigma(x)$ is the compressive stress on the support, u is the foundation modulus, and w is the deflection of support, a shown in Figure 2.5.

For single point load P, the differential equation of the Beam on Elastic Foundation model is given by the following equation.

$$EI\frac{d^4w(x)}{dx^4} + uw(x) = 0 \tag{2.13}$$

where EI is the flexural rigidity of the beam (rail or tie), $w(x)$ is the vertical deflection at point x and u is the Winkler's constant or track modulus.

The solution of the differential equation is given by Equation 2.14.

$$w(x) = \frac{P\beta}{2u}e^{-\beta x}(\cos \beta x + \sin \beta x) \tag{2.14}$$

where $\beta = (\frac{u}{4EI})^{1/4}$. The supporting line force along the beam is calculated as,

$$F(x) = -uw(x) \tag{2.15}$$

The successive differentiation of the solution of the BOEF differential equation gives equations for slope (θ), bending moment (M), and shear force (V) at distance

x from the point load.

$$\theta(x) = -\frac{P\beta}{u}e^{-\beta x}(\sin \beta x) \tag{2.16}$$

$$M(x) = \frac{P}{4\beta}e^{-\beta x}(\cos \beta x - \sin \beta x) \tag{2.17}$$

$$V(x) = -\frac{P}{2}e^{-\beta x}(\cos \beta x) \tag{2.18}$$

Multiple axles can be incorporated in this model using the principle of superposition.

The rail seat load is calculated by the following equation.

$$Q_n = F_n S \tag{2.19}$$

where Q_n is the rail seat load for tie number n, F_n is the supporting line force along the beam for tie number n, and S is the tie spacing.

$$Q_n = F_n S = u w_n S \tag{2.20}$$

where w_n is the deflection of tie number n.

A.N. Talbot used the theory of BOEF for track design and analysis in the 1920s [9]. This is known as "Talbot's Method".

Limitations of the BOEF Approach

The BOEF theory is extensively used, and is one of the simplest and easiest approaches for railroad track analysis under loadings. However, this analysis approach has the following limitations:

1. The track substructure is estimated in terms of one generic track modulus value in the BOEF formulation, but the substructure behavior is complex because there are multiple layers with varying properties. Hence, representation using

a single stiffness value eliminates the possibility for distinguishing between the responses of individual track substructure layers.

2. As per the BOEF theory, the rail is assumed to be supported continuously. However, in a conventional track, the rails are discretely supported by cross-ties.

3. According to the BOEF formulation, in the parts of the track that experience upward deflection, tensile forces will develop in the foundation. But in reality, the unbound nature of ballast layers means that no tensile forces can be mobilized to support any uplifting tendency of the superstructure.

4. The track response is assumed to be linear according to the Winkler formulation; however, geomaterials and most pads do not behave linearly [27].

5. The BOEF model does not take the weight of the rails and ties into account. This can, however, be justified somehow because the weight of rails and ties are negligible compared to the forces exerted by considerably large wheel loads.

6. Shear deformations in the rails are not included since the rail is modeled as Euler-Bernoulli beam.

7. In this model, the Winkler springs are independent of each other, and this model does not consider the interaction among the springs, which is unrealistic.

8. The deflection calculated from the BOEF formulation corresponds to static loading only; the dynamic loads are estimated by increasing the value of static load. Therefore, the effect of dynamic loading is only an approximation, and inertia effects are not taken into consideration during analysis.

Considering that the Beam on Elastic Foundation model does not take into account the interaction among the Winkler springs, several models were developed by researchers in the past to overcome this limitation. Some of these models are discussed in the following sections.

2.3.3 Filonenko-Borodich Foundation

In the Filonenko-Borodich model developed in 1940 [28], the springs are not independent of each other and the movement of one spring influences the movement of other springs (unlike the BOEF model). This is achieved by attaching the top ends of the springs to a thin elastic membrane stretched under a constant tension T as shown in Figure 2.6. No shear stiffness is considered for this membrane.
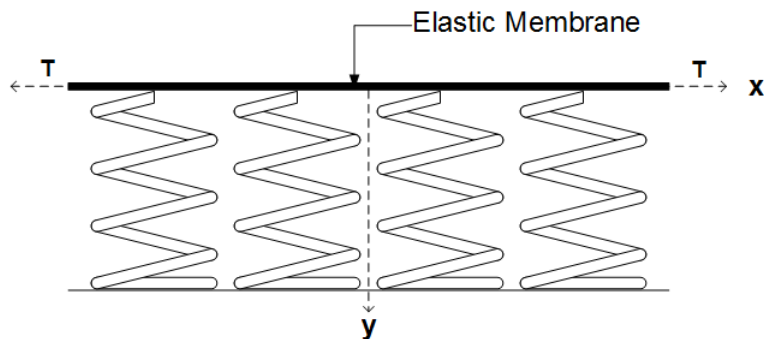
Figure 2.6: Schematic Representation of Basic Filonenko-Borodich Foundation

The equilibrium in the vertical direction of the beam element gives the following equation [29].

$$ky - T\frac{d^2y}{dx^2} = 0 \qquad (2.21)$$

where P is the pressure, y is the vertical deflection, T is the constant tensional force and k is the spring constant.

As mentioned, the Filonenko-Borodich Foundation model considers a tension membrane effect but does not consider the shear interaction among individual spring elements. The following models consider shear interaction among the springs.

2.3.4 Pasternak Foundation

The Pasternak Foundation model, developed by P.L. Pasternak in 1954 [30], assumes shear interactions between Winkler springs that both the BOEF and Filonenko-Borodich Foundation models fail to consider. This is obtained by connecting the

ends of the springs to a beam that comprises incompressible vertical elements. These vertical elements deform by transverse shear as shown in Figure 2.7. Equation 2.22 presents the formulation of the Pasternak Foundation.
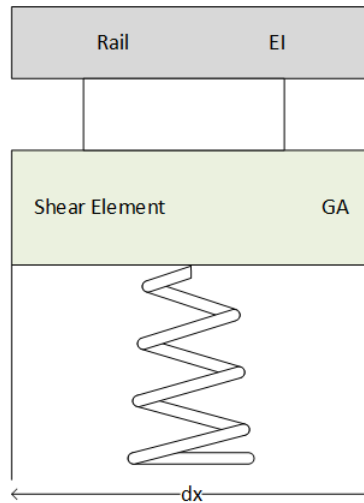
Figure 2.7: Schematic Representation of Pasternak Foundation

$$ky - G\frac{d^2y}{dx^2} = 0 \tag{2.22}$$

where G is the shear modulus of the shear element, y is the deflection and k is the track modulus of the foundation [31]. The physical equivalency of the Pasternak Foundation with the Filonenko-Borodich Foundation is implied by the equation, where "T" of Filonenko-Borodich model is replaced by "G" in the Pasternak model [31].

2.3.5   Kerr Foundation

In the Kerr Foundation model, a shear element is introduced in between the Winkler's foundation and the rail such that different spring constants above and below the shear element can be modeled [31]. Figure 2.8 shows a schematic representation of the model.

The governing differential equation for the pressure-deflection relationship can be expressed as follows [31].
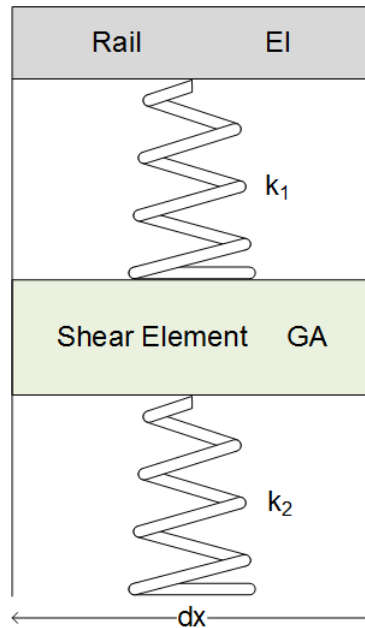
Figure 2.8: Schematic Representation of Kerr Foundation

$$(1 + \frac{k_1}{k_2})p = \frac{G}{k_1}\frac{d^2p}{dx^2} + k_2y - G\frac{d^2y}{dx^2} \qquad (2.23)$$

where p is the pressure, and k_1 and k_2 are the spring constants for the Winkler's foundation above and below the shear element respectively, and y is the deflection of the first layer [31].

Filonenko-Borodich Foundation, Pasternak Foundation, and Kerr models are models that attempt to overcome some limitations in the BOEF theory. They, however, have several limitations, e.g. they do not account for different number of layers in substructure. The next subsection will introduce the Layered Elastic Theory, which can be used to model a railroad track substructure as a multilayered system.

2.3.6 Layered Elastic Theory

The Layered Elastic Theory (LET) was introduced by Burmister [32], who developed analytical solutions for a two-layered system under loading and later extended it to a three-layered system. This theory can further be extended for different number of layers. The LET can be used to model a railroad track substructure as a multilayered

system and assumes all layers to be linear, elastic, infinite in the horizontal direction and having uniform thicknesses. The applied load is distributed over a circular area, and there are no initial stresses or strains in the system.

To perform a Layered Elastic Analysis, the modulus of elasticity and Poisson's ratio of each layer, layer thicknesses, and loading magnitude and geometry are the input parameters. The solution involves the following steps [33]:

1. Present stresses, strains, and deflections in terms of Burmister's Biharmonic functions.

2. Assemble boundary conditions.

3. Solve a system of linear equations to determine the coefficients of Burmister's functions.

4. Determine stresses, strains, and deflections using Burmister's coefficients.

Since the GEOTRACK software program is based on the principles of Layered Elastic analysis, a detailed description of different steps and governing equations of LET are presented in Chapter 3 of this Master's thesis.

2.3.7 Currently Available Track Analysis Computer Programs

Although several researchers have focused extensively on analyzing railroad track behavior under loading, the number of dedicated software programs developed for this purpose have been limited. Background and salient features of some of these computer programs are discussed in this section.

ILLITRACK

ILLITRACK (developed at the University of Illinois by Robnett et al. in 1976 [13]) is a model based on the application of the finite-element method for the analysis of track structures. It consists of two two-dimensional models, transverse and longitudinal (See Figure 2.9). The output from the longitudinal model is employed as the input for the transverse model. This results in forming a three-dimensional effect using two

two-dimensional models. In the longitudinal analysis, two types of elements applied are [34]:

1. Beam-spring elements to represent the rail tie structure as a continuous beam supported on a series of linear springs

2. Rectangular planar elements to represent the ballast-subballast-subgrade structure.

In the transverse analysis, the tie is located on top of the ballast-subballast-subgrade system. Maximum vertical displacements and forces obtained from the longitudinal analysis are applied to the rail. The tie is considered as a two dimensional body or a beam and the rectangular planar elements from longitudinal analysis are used in the system. This model gives moments and deflections of rail, tie reaction and distribution of stresses as output.
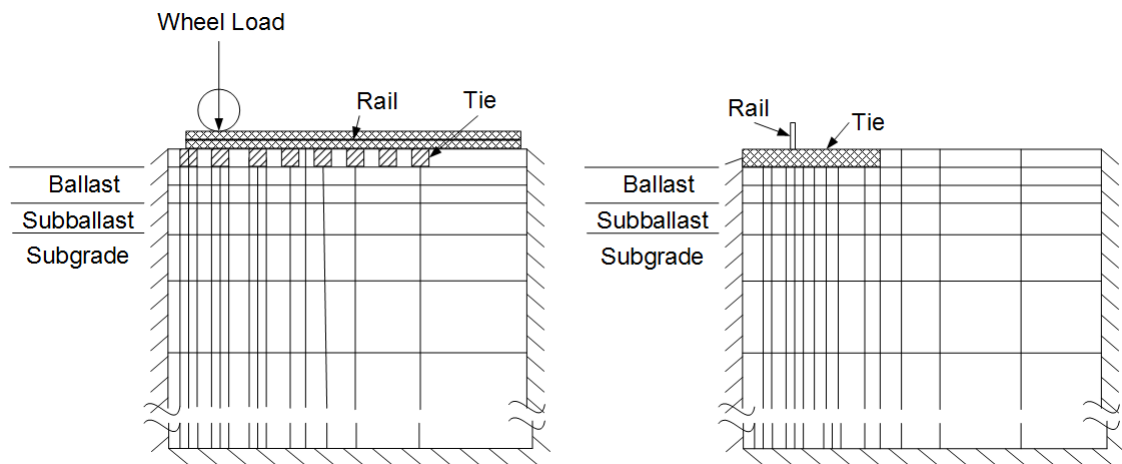
Figure 2.9: Two-Dimensional Finite Element Meshes as Employed in ILLITRACK (a) Longitudinal and (b) Transverse (modified from [16])

KENTRACK

KENTRACK is a multi-layer elastic finite-element computer program, which was developed at the University of Kentucky to analyze railroad track beds in the 1980s [9]. It was developed specifically for track structures incorporating hot-mix asphalt

underlayment between the ballast and subgrade [16]. However, this model can be extended for the design and analysis of conventional tracks and concrete-slab tracks. Railroad track analysis using the KENTRACK program is particularly applicable during the structural design of track beds subjected to heavy-axle loads and high-speed train traffic. the following two types of failure criteria that have been included in the program:

1. Maximum vertical compressive stress/strain in ballast or subgrade to control permanent deformation

2. Maximum horizontal tensile strain in the bottom of the asphalt layer to control fatigue cracking

The analysis procedure in KENTRACK utilizes both the finite-element method and layered elastic theory. The finite-element method is used to calculate the stresses and strains in the rails and ties. Rails and ties are modeled as beam elements, and the fasteners between the rails and ties are modeled as spring elements. The stresses obtained below the ties are applied as circular loads on the top layer. Multilayered Elastic Theory is used to calculate the stresses and strains in different layers. The track responses are linked to damage accumulation using empirical 'damage functions'. These empirical equations specify the total number of allowable load repetitions until a particular track component fails under loading. Using KENTRACK, the service life of the layers can be predicted using the following equation [35].

$$L = \frac{1}{\sum_{i=1}^{n} \frac{N_p}{N_a}} \tag{2.24}$$

where L is the design life in years, N_p is the predicted number of repetitions during each period, N_a is the allowed number of repetitions during each period, and n is the number of periods (for KENTRACK, this is four seasons [34]).

Comparison between Different Track Analysis Computer Programs

Table 2.3 presents a comparison of different features in the currently available computer programs for railroad track analysis. Note that only commonly available computer programs have been included here, and specialized codes developed by different researchers and not widely available to users, have been eliminated from this list.

Table 2.3: Comparison between Different Track Analysis Computer Programs

	ILLITRACK	KENTRACK	*GEOTRACK
Underlying Theory	Finite Element (FE) Analysis	FE Analysis & Layered Elastic Theory	Layered Elastic Theory
Trackbed Type	All Granular	Asphalt Underlayment, All Granular & Combination	All Granular
Dimension	Simulated Pseudo-3D	3D	3D
Source Code Language	Information Not Available	FORTRAN	VAX FORTRAN
Output	Rail Moment & Deflection, Tie Reactions, Stresses & Deformation in Trackbed	Asphalt Tensile Strain, Subgrade Compressive Stress, Predicted Asphalt & Subgrade Life	Rail & Tie Deflection, Rail Seat Force, Tie & Rail Bending Moment, Vertical Deflection & Stress States within Substructure & Track Modulus
Presence of GUI	Information Not Available	Yes	No
Parametric Analysis	Information Not Available	No	No
Graphing & Plotting Abilities	Information Not Available	No	No

*GEOTRACK refers to GEOTRACK VAX Version

2.3.8 Advanced Models

The railroad track analysis models discussed thus far do not take into account the dynamic aspects of train loading. Nonetheless, when a track is subjected to moving loads, the deflections and stresses are largely magnified in comparison to those imposed by a static load of the same magnitude. To overcome the drawbacks of the previous models, improved models have been developed by researchers, analysing dynamic effects of loading. Researchers have also used advanced analysis methods such as the finite-element method to model the railroad tracks.

In 1996, Thambiratnam and Zhuge [36] developed a procedure based on the finite-element method for dynamic analysis of a beam on elastic foundation subjected to a moving point load. In the model, the elastic foundation is represented by springs, and the moving load is modeled as a sprung mass and is assumed to travel along the rail at a constant speed. As cited by Arlaud et al. [37], researchers like Hall [38], Araujo [39], Kouroussis et al. [40], Ju and Li [41], Banimahd and Woodward [42], etc. have also used three-dimensional finite-element models to represent railroad tracks. However, using a 3D finite-element based models for track analysis would require large computational time and storage capacities. To overcome these drawbacks, researchers like Paixao et al. [43] have used two-dimensional finite-element models (as cited by Arlaud et al. [37]).

While the 2-D models provide some understanding of the problem, 3-D models are required to achieve accuracy in the results. A special symmetry is considered by some researchers, viz. Gardien and Stuit [44], Yang and Hung [45], and Yang et al. [46], considering the railroad track as invariant in the rail direction; and hence these models can be considered to be intermediate between 2-D and 3-D analysis, hence known as '2.5-D'. The approximations implied on the track geometry are because of the discontinuity of the cross-ties.

Along with the movement of the train loads, when the high speed of trains is taken

into account, proper modeling of the railway track system and the loading is required to obtain realistic results. In 2007, Correia et al. [47] used three finite-element codes, DIANA, PLAXIS, and ANSYS to generate two-dimensional models for the dynamic performance of a high-speed train tracks, with operational speeds of 195 miles/hour. An agreement between the rail track performance and induced vibrations predicted by all three FEM codes was observed. There are significant ongoing research and developments in the field of railroads, with considerable effort directed towards the analysis of railroad track structures. However, detailed discussion of these advanced models is beyond the scope of this Master's thesis.

All the discussions presented thus far are the research in the field of railroad engineering. The current practice in the field is different as it involves traditional methods of design; which are discussed in the following section.

2.4   Current Practice in Railroad Track Analysis

As mentioned earlier, the current practice in railroad industry still involves empirical and traditional methods of design, rather than the advanced ongoing research in the field. This section discusses the determination of the ballast depth required to protect the subgrade from excessive stresses using the current method of practice used by The calculation of average ballast pressure at the base of tie used by the American Railway Engineering and Maintenance-of-Way Association (AREMA). The calculation of average ballast pressure at the base of the tie is given by Equation 2.25 [48].

$$P_a = \frac{\left[2\,P(1 + \frac{IF}{100})(\frac{DF}{100})\right]}{A} \tag{2.25}$$

where P_a is the average ballast pressure at base of tie, P is the wheel loading in lb, IF is the impact factor in percentage calculated using Equation 2.26, and DF is the distribution factor in percentage. 47% of axle load is assumed to be applied to each tie on either side of the applied load.

$$IF = \frac{33S}{100D} \tag{2.26}$$

where S is the train speed in mph and D is the diameter of the train wheel in $inch$. The ballast depth required to protect the subgrade from excessive stresses can then be calculated using Equation 2.27.

$$h = \left(16.8\frac{p_a}{p_c}\right)^{\frac{4}{5}} \tag{2.27}$$

where h is the ballast depth, p_c is the allowable subgrade pressure in psi.

Calculation of ballast pressure using empirical equation as shown in Equation 2.25 does not incorporate the rails, and the substructure into the equation. This implies that change in rail properties and substructure stiffness would not have any effect in the ballast pressure, which is not a realistic representation of actual railroad track behavior. Such empirical relationships generally do not have a firm scientific basis and hence there is the need to incorporate mechanistic components into design. For practitioners to use a mechanistic design, a usable analysis software is required.

2.5   Summary

This chapter briefly introduced different components of a typical ballasted railroad track structure. This was followed by discussions on the concept of track modulus, and different methods for estimating the modulus of a track system. Discussions on different track analysis methods were also presented, highlighting the salient features and limitations of each. A brief overview on commonly used railroad track analysis computer programs, KENTRACK and ILLITRACK was also presented, comparing the features of these available computer programs. An overview of the attempts made to more realistically incorporate moving loads and high speed trains, using finite element methods, was also presented. The trend in current practice has been briefly discussed and the necessity of a mechanistic design component has also been

established in this chapter. The next chapter will present the theoretical formulations included in Layered Elastic Analysis (an easy to implement analysis method that incorporates mechanics into track analysis) of railroad tracks, which constitutes the underlying algorithm for the GEOTRACK program.

CHAPTER 3

LAYERED ELASTIC THEORY AND ITS IMPLEMENTATION IN GEOTRACK

GEOTRACK is a computer program for determining the response of railroad track structures under quasi-static loading. Originally developed by Chang, Adegoke and Selig in 1980, the GEOTRACK program is based on Burmister's principles of Multi-layered Elastic Theory [14]. This chapter discusses different aspects of Layered Elastic Theory and its implementation in the underlying algorithm for GEOTRACK.

The GEOTRACK program considers a section of the track spanning eleven ties (five on each side of the central tie) assuming that ties outside that zone are not influenced by the applied loads [49]. This assumption has been justified by researchers in the past for a real railroad track structure [16]. Figure 3.1 [14] presents a schematic of different track components considered by GEOTRACK.

The rails are represented as Euler-Bernoulli beams supported by a number of concentrated reactions, one at each tie location. The rails span eleven ties and are free to rotate at the ends as well as at each tie location [49]. The ties are also represented as Euler-Bernoulli beams and are divided into ten equal rectangular segments with the reaction forces due to the underlying ballast layer represented as concentrated forces at the center of each segment. The force is applied on the ballast surface layers in the form of a uniform pressure over a circular area, calculated from individual tie segment dimensions. Note that conversion of the rectangular tie segments into circular areas for load application on top of the ballast layer is necessary as layered elastic analysis considers only circular loading geometry [32].
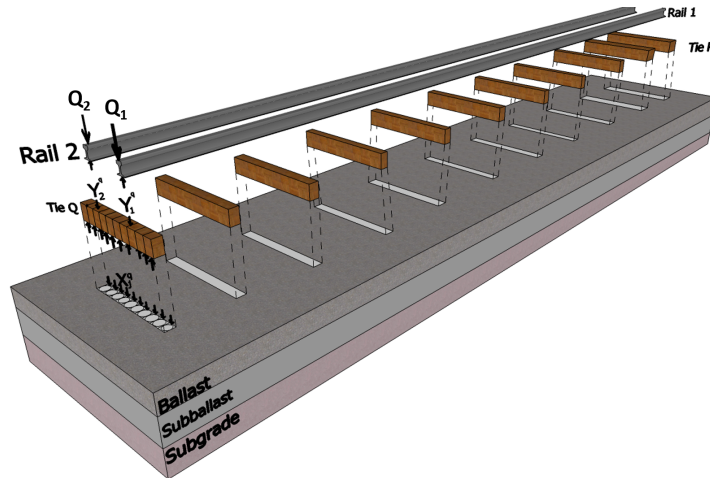
Figure 3.1: Forces and Elements in GEOTRACK

The connections between rails and ties are represented as bi-directional linear springs (capable of resisting tensile as well as compressive forces). The ballast, subballast and subgrade layers are represented as a series of linear elastic layers, each corresponding to unique modulus of elasticity (E) and Poisson's ratio (ν) values. All layers are assumed to be of infinite extent in the horizontal direction and are placed on a semi-infinite elastic half space. Considering the inherent assumptions associated with multilayer elastic theory, it is important to note that GEOTRACK cannot model spatial variations within a particular substructure layer or geometric variations such as those introduced by track shoulders or track substructure drainage features.

3.1 Foundation Flexibility Matrix

*The following discussions are largely based on a paper by Chang et al. [14]. As in the theory of multi-layered elastic analysis, analysis of a track structures using GEOTRACK involves formulation and subsequent solving of a series of simultaneous equations. First, the foundation flexibility matrix of the system comprising the ballast, subballast and subgrade layers is obtained using the Burmister's analytical solutions [50], which is represented by the following equation.

$$\delta_i^p = S_{ij}^{pq} X_j^q \tag{3.1}$$

where δ_i^p is the deflection at the intersection of rail i, and tie p, X_j^q is the tie-ballast force acting on the jth segment of tie q representing the uniform pressure distributed over the circular area, S_{ij}^{pq} is the vertical deflection of the ith segment of tie p obtained due to the unit load distribution as a uniform pressure over the equivalent circular area of the jth segment of tie q. The foundation flexibility matrix S_{ij}^{pq} can be visualized as the inverse of the stiffness matrix commonly used in Finite Element type formulations.
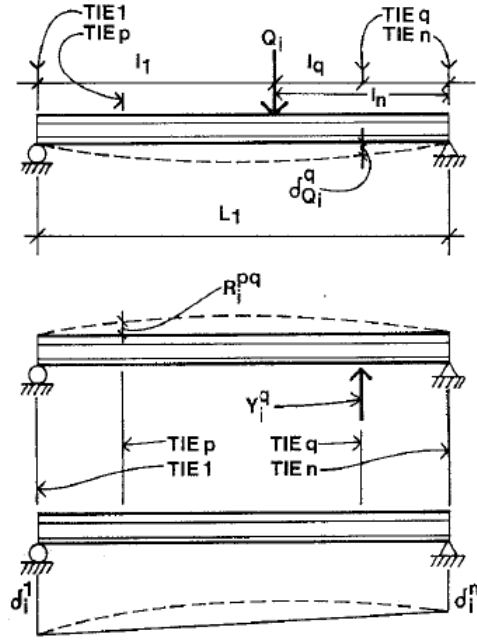
Figure 3.2: Schematics Illustrating Different Load and Deflection Components Considered during Formulation of the Foundation Flexibility Matrix in GEOTRACK [5]

3.2 Combined Flexibility Matrix

The flexibility matrix of the foundation is combined with the flexibility matrix of the rail-tie structure, and compatibility of displacements and equilibrium of forces between bottom of rail-tie structure and top of foundation are imposed for overall
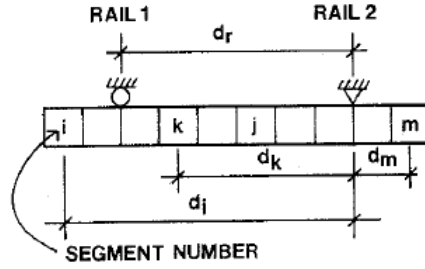
Figure 3.3: A Tie Used in GEOTRACK Showing Ten Segments [5]

solution. The solution of the set of equations gives the tie-ballast pressure, displacements and stresses at required points in the layers [14].

$$Vertical\,Force\,Equilibrium: \sum_{j=1}^{m} X_j^q = \sum_{i=1}^{2} Y_i^q \qquad (3.2)$$

$$Moment\,Equilibrium: \sum_{j=1}^{m} X_{ij}^q d_j = Y_i^q d_r \qquad (3.3)$$

$$Rail\,Moment\,Equilibrium: \sum_{q=1}^{n} Y_i^q l_q = 0 \qquad (3.4)$$

$$Rail\,Force\,Equilibrium: \sum_{q=1}^{n} Y_i^q = Q_i \qquad (3.5)$$

where Y_i^q is the rail seat force acting between rail i and Tie q; (i = 1, 2), d_j is the distance from the center of segment j in a particular tie to rail 2 (moment is taken about rail 2), d_r is the distance from rail center of rail 1 to center of rail 2, l_q is the distance measured from wheel load position to tie q and Q_i is the wheel load. These terms have been schematically illustrated in Figure 3.2 [14] and Figure 3.3 [14].

The multilayer theory developed by Burmister uses the equilibrium and compatibility equations from the theory of elasticity. Figure 3.4 presents the schematic of a 3-layer track substructure illustrating the important layer properties used in the formulation of layered elastic theory. The equations comprising Layered Elastic Theory for the infinitesimal block as shown in Figure 3.5 are presented below [51, 52, 50].
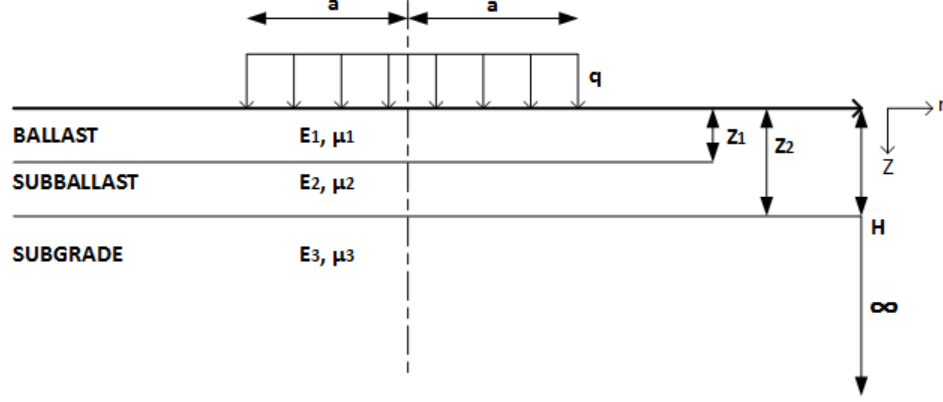
Figure 3.4: Schematic of the Cross-Section of Track for Layered Elastic Model

3.3 Equilibrium Equations

In cylindrical coordinates, the equilibrium in the radial and transverse direction can be expressed as,

$$\frac{\delta\sigma_r}{\delta r} + \frac{\delta\tau_{rz}}{\delta z} + \frac{\sigma_r - \sigma_\theta}{r} = 0 \tag{3.6}$$

$$\frac{\delta\tau_{rz}}{\delta r} + \frac{\delta\sigma_z}{\delta z} + \frac{\tau_{rz}}{r} = 0 \tag{3.7}$$

3.4 Compatibility Equations

Since literature suggests that deriving the equations of compatibility in Cylindrical coordinates is a cumbersome process, the derivation of compatibility equations is first done for Cartesian coordinates. In Cartesian coordinates, the normal strains (ϵ_x, ϵ_y and ϵ_z) and shearing strains (γ_{xy}, γ_{yz} and γ_{zx}) can be written as Equation 3.8 through Equation 3.10.

$$\frac{\delta^2\epsilon_x}{\delta y^2} + \frac{\delta^2\epsilon_y}{\delta x^2} = \frac{\delta^2\gamma_{xy}}{\delta x\,\delta y} \tag{3.8}$$

$$\frac{\delta^2\epsilon_y}{\delta z^2} + \frac{\delta^2\epsilon_z}{\delta y^2} = \frac{\delta^2\gamma_{yz}}{\delta y\,\delta z} \tag{3.9}$$

$$\frac{\delta^2\epsilon_z}{\delta x^2} + \frac{\delta^2\epsilon_x}{\delta z^2} = \frac{\delta^2\gamma_{zx}}{\delta z\,\delta x} \tag{3.10}$$

These are the compatibility equations expressed in terms of strains. Similarly,
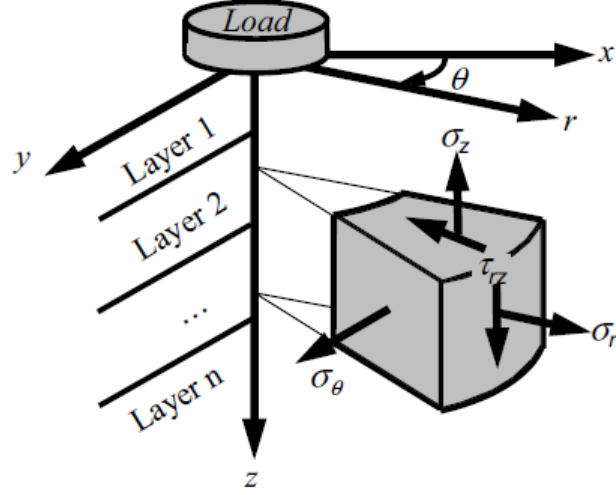
Figure 3.5: Stresses Acting on an Element [34]

the normal stresses (σ_x, σ_y and σ_z) and shearing stresses (τ_{xy}, τ_{yz} and τ_{zx}) can be represented by Equation 3.11 through Equation 3.13.

$$\frac{\delta \tau_{xy}}{\delta x} + \frac{\delta \tau_{yz}}{\delta z} = -\frac{\delta \sigma_y}{\delta y} \tag{3.11}$$

$$\frac{\delta \tau_{yz}}{\delta y} + \frac{\delta \tau_{zx}}{\delta x} = -\frac{\delta \sigma_z}{\delta z} \tag{3.12}$$

$$\frac{\delta \tau_{xy}}{\delta y} + \frac{\delta \tau_{xz}}{\delta z} = -\frac{\delta \sigma_x}{\delta x} \tag{3.13}$$

The above equations can be mathematically manipulated to be expressed in the form of Equation 3.14. All the in-between steps of the derivation have been provided in Appendix A.

$$\nabla^2 \phi - \nabla^2 \sigma_z - \frac{\delta^2 \phi}{\delta z^2} - \nu \nabla^2 \sigma_z = 0 \tag{3.14}$$

where, ∇^2 is the Laplace Operator represented as $\nabla^2 = (\frac{\delta^2}{\delta x^2} + \frac{\delta^2}{\delta y^2} + \frac{\delta^2}{\delta z^2})$ and ϕ is the bulk stress represented as $\phi = \sigma_x + \sigma_y + \sigma_z$.

Equation 3.14 can be reduced to $(1 - \nu)\nabla^2 \phi = 0$. Since ν (Poisson's ratio) can never be equal to 1,

$$\nabla^2\phi = 0 \tag{3.15}$$

3.5 Beltrami-Mitchell Equations

The Beltrami-Mitchell equations are used to convert the compatibility equations from Cartesian coordinates to Cylindrical coordinates. For the body considered in Figure 3.5, the Beltrami-Mitchell equation [53] are,

$$\frac{\delta^2\phi}{\delta x\,\delta y} + (1+\nu)\nabla^2\tau_{xy} = 0 \tag{3.16}$$

$$\frac{\delta^2\phi}{\delta y\,\delta z} + (1+\nu)\nabla^2\tau_{yz} = 0 \tag{3.17}$$

$$\frac{\delta^2\phi}{\delta z\,\delta x} + (1+\nu)\nabla^2\tau_{xz} = 0 \tag{3.18}$$

The concept of stress functions are used to further simplify and reduce the equations.

3.6 Compatibility Equations in Cylindrical Coordinates

The compatibility equations in Cylindrical co-ordinates can be written as Equation 3.19 through Equation 3.22.

$$\nabla^2\sigma_r - \frac{2}{r^2}(\sigma_r - \sigma_\theta) + \frac{1}{1+\nu}\frac{\delta^2\phi}{\delta r^2} = 0 \tag{3.19}$$

$$\nabla^2\sigma_\theta + \frac{2}{r^2}(\sigma_r - \sigma_\theta) + \frac{1}{1+\nu}\frac{1}{r}\frac{\delta\phi}{\delta r} = 0 \tag{3.20}$$

$$\nabla^2\sigma_z + \frac{1}{1+\nu}\frac{\delta^2\phi}{\delta z^2} = 0 \tag{3.21}$$

$$\nabla^2\tau_{rz} - \frac{1}{r^2}\tau_{rz} + \frac{1}{1+\nu}\frac{\delta^2\phi}{\delta r\,\delta z} = 0 \tag{3.22}$$

where σ_r, σ_θ and σ_z are radial, circumferential and vertical

3.7 General Differential Equations Derivation

To derive the differential equations, which can be used to determine stresses, the equilibrium equations are to be solved and the state of stress are to be expressed in terms of surface forces [54]. However, the equations 3.1 and 3.2 are not sufficient to find the stresses. The equilibrium equations and compatibility equations should be used together to develop equations, which can subsequently be used to determine the stresses. Similar to plane strain theory (since the z-coordinate is very large in comparison to the other two directions) when S is an arbitrary function,

$$\tau_{rz} = -\frac{\delta^2 S}{\delta r\,\delta z} \tag{3.23}$$

When replaced in Equation 3.2, Equation 3.23 transforms to Equation 3.24.

$$-\frac{\delta^3 S}{\delta r^2\,\delta z} + \frac{\delta\sigma_z}{\delta z} - \frac{1}{r}\frac{\delta^2 S}{\delta r\,\delta z} \tag{3.24}$$

Equation 3.24 can be written as $(1 - \nu)\nabla^4 X_0 = 0$.

Since $\nu \neq 1$,

$$\nabla^4 X_0 = 0 \tag{3.25}$$

Equation 3.25 represents the Biharmonic Equation. Making use of the above equations and applying Hooke's law, the displacement in z-direction (w) and in the r-direction (u) can be written as Equation 3.26 and Equation 3.27.

$$w = \frac{1}{E}(1 + \nu)[(1 - 2\nu)\nabla^2 X_0 + \frac{\delta^2 X_0}{\delta r^2} + \frac{1}{r}\frac{\delta X_0}{\delta r}] \tag{3.26}$$

$$u = -\frac{(1 + \nu)}{E}\frac{\delta^2 X_0}{\delta r\delta z} \tag{3.27}$$

where E is the modulus of elasticity of the material in the substructure layer. Let $X = kX_0$, where k is a constant. In addition, let $k = \frac{1}{2(\lambda+\mu)}$, where λ and μ are

Lame's constants, such that

$$\nabla^4 X = 0 \tag{3.28}$$

The normal and shear stresses can be expressed in terms of the Lame's constant using Equations 3.29 and 3.30.

$$\sigma_z = \frac{\delta}{\delta z}[(3\lambda + 4\mu)\nabla^2 X - 2(\lambda + \mu)\frac{\delta^2 X}{\delta z^2}] \tag{3.29}$$

$$\tau_{rz} = \frac{\delta}{\delta r}[(\lambda + 2\mu)\nabla^2 X - 2(\lambda + \mu)\frac{\delta^2 X}{\delta z^2}] \tag{3.30}$$

3.8 Application of boundary and interface conditions

For layered elastic analysis, there is the assumption of continuous surface of contact in the layer interface. The following boundary conditions should satisfy equation 3.28. At upper surface when $z = 0$, the shear stress at the topmost layer is assumed to be zero.

$$\tau_{rz} = 0 \tag{3.31}$$

Also, for radius (r) < radius of load (a),

$$\sigma_z = p[1 - \left(\frac{r}{a}\right)^2] \tag{3.32}$$

For $r > a$,

$$\sigma_z = 0 \tag{3.33}$$

At the interface, there is continuity of vertical stress (σ_z), vertical displacement (w) and shear stress (τ_{rz}), which gives,

$$(\sigma_z)_j = (\sigma_z)_{j+1} \tag{3.34}$$

$$(w_z)_j = (w_z)_{j+1} \tag{3.35}$$

$$(\tau_{rz})_j = (\tau_{rz})_{j+1} \tag{3.36}$$

As z approaches infinity, the stresses and displacements (represented by function X) approach zero. At $z \to \infty$,

$$X \to 0 \tag{3.37}$$

3.9 Using Hankel Transform to Find the Solution of the Biharmonic Function

To determine stresses and displacements, Equation 3.28 is to be solved satisfying the boundary condition. The Biharmonic equation can be transformed to a differential equation using Hankel transform. The Hankel transform of $F_n(H)$ is defined as,

$$F_n(H) = \int_0^\infty f(r) J_n(Hr) r \delta r$$

and using the Hankel inverse when f(r) satisfies the requisite conditions,

$$f(r) = \int_0^\infty F_n(H) J_n(Hr) H \delta H$$

where H is the variable of integration introduced by Hankel transformation and J_n is the Bessel function of the first kind with order n.

The biharmonic function can be represented as,

$$\nabla^4 X = (\frac{\delta^2}{\delta r^2} + \frac{1}{r}\frac{\delta}{\delta r} + \frac{\delta^2}{\delta z^2})(\frac{\delta^2}{\delta r^2} + \frac{1}{r}\frac{\delta}{\delta r} + \frac{\delta^2}{\delta z^2})X = 0 \tag{3.38}$$

Multiplying Equation 3.38 by $J_o(Hr)r$ and integrating with respect to r,

$$\int_0^\infty (\frac{\delta^2 \eta}{\delta r^2} + \frac{1}{r}\frac{\delta \eta}{\delta r} + \frac{\delta^2 \eta}{\delta z^2}) r J_o(H_r) \delta r = 0 \tag{3.39}$$

where,

$$\eta = \frac{\delta^2 X}{\delta r^2} + \frac{1}{r}\frac{\delta X}{\delta r} + \frac{\delta^2 X}{\delta z^2}$$

$$\frac{\delta^2}{\delta z^2}\bar{\eta} + [r\frac{\delta\eta}{\delta r}J_o(H_r)]_0^\infty - \int_0^\infty r\frac{\delta\eta}{\delta r}\frac{\delta}{\delta r}[J_o(H_r)]\delta r = 0 \tag{3.40}$$

where,

$$\bar{\eta} = \int_0^\infty \eta J_o(Hr)r\delta r$$

Since $\frac{\delta\eta}{\delta r}$ is assumed to be finite for all values of r, So,

$$[r\frac{\delta}{\delta r}\eta J_o(Hr)]_0^\infty = 0$$

Since the first derivative of zero order Bessel function is first order Bessel function,

$$\frac{\delta}{\delta r}[J_o(Hr)] = -H[J_1(Hr)]$$

$$\frac{\delta}{\delta r}[rJ_1(Hr)] = (Hr)J_o(Hr)$$

So, the equation becomes,

$$\frac{\delta^2\bar{\eta}}{\delta z^2} - 0 - \int_0^\infty r\frac{\delta}{\delta r}\eta[-HJ_1(Hr)]\delta r = 0$$

$$(\frac{\delta^2}{\delta z^2} - H^2)^2 \int_0^\infty (\frac{\delta^2 X}{\delta r^2} + \frac{1}{r}\frac{\delta X}{\delta r} + \frac{\delta^2 X}{\delta z^2})J_o(Hr)r\delta r = 0$$

When the operations are performed again,

$$\int_0^\infty r\nabla^4 X J_0(Hr)\delta r = (\frac{\delta^2}{\delta z^2} - H^2)^2 \int_0^\infty rX J_o(Hr)\delta r = 0$$

Using G for the zero order Hankel transform which is a function of H & z, $G(H, z)$ can be expressed as Equation 3.41.

$$G(H, z) = \int_0^\infty rX J_o(H_r)\delta r \tag{3.41}$$

$$(\frac{\delta^2}{\delta z^2} - H^2)^2 G(H, z) = 0$$

The solution of which is,

$$G(H, z) = (A + B_z)e^{-Hz} + (C + D_z)e^{Hz} \tag{3.42}$$

where A, B, C and D are the integration constants.

The <u>Normal Stress</u> (σ_z) can be expressed as Equation 3.43.

$$\sigma_z = \frac{\delta}{\delta z}[(3\lambda + 4\mu)\nabla^2 X - 2(\lambda + \mu)\frac{\delta^2 X}{\delta z^2}] \tag{3.43}$$

When Equation 3.43 is multiplied by $rJ_0(Hr)$ and integrated with respect to r,

$$\sigma_z = \int_0^\infty H[(\lambda + 2\mu)\frac{\delta^3 G}{\delta z^3} - (3\lambda + 4\mu)H^2\frac{\delta^3 G}{\delta z^3}]J_o(Hr)\delta H \tag{3.44}$$

Similarly for <u>Shear Stress</u> (τ_{rz}),

$$\tau_{rz} = \frac{\delta}{\delta r}[(\lambda + 2\mu)\nabla^2 X - 2(\lambda + \mu)\frac{\delta^2 X}{\delta z^2}]$$

$$\tau_{rz} = \int_0^\infty H^2[\lambda\frac{\delta^2 G}{\delta z^2} + (\lambda + 2\mu)H^2 G]J_1(Hr)\delta H \tag{3.45}$$

For <u>Vertical Displacement</u> (w),

$$w = \frac{\lambda + 2\mu}{\mu}\nabla^2 X - \frac{\lambda + \mu}{\mu}\frac{\delta^2 X}{\delta z^2}$$

$$w = \int_0^\infty H[\frac{\delta^2 G}{\delta z^2} - \frac{\lambda + 2\mu}{\mu}H^2 G]J_o(Hr)\delta H \tag{3.46}$$

For <u>Radial Displacement</u> (u),

$$u = -\frac{\lambda + \mu}{\mu}\frac{\delta^2 X}{\delta z\delta r}$$

$$u = \frac{\lambda + \mu}{\mu} \int_0^\infty H^2 \frac{\delta G}{\delta z} J_1(Hr) \delta H \tag{3.47}$$

Hankel transform of X (for multi-layered media) for j^{th} layer is,

$$G_j = (A_j + B_{jz})e^{-Hz} + (C_j + D_{jz})e^{Hz} \tag{3.48}$$

3.10 Calculation of the Constants of Integration

Equation 3.48 can be written as Equation 3.49, which when differentiated with respect to z gives Equation 3.50.

$$G_j = (A_j + B_j z)e^{-Hz} + (C_j + D_j z)e^{Hz} \tag{3.49}$$

$$\frac{\delta G_j}{\delta z} = (A_j + B_j z)(-He^{-Hz}) + e^{-Hz}(0 + B_j) + (C_j + D_j z)(He^{Hz}) + e^{Hz}(0 + D_j) \tag{3.50}$$

For $z = 0$ & $j = 1$,

$$\frac{\delta G_j}{\delta z} = -HA_1 + B_1 + HC_1 + D_1 \tag{3.51}$$

$$\frac{\delta^2 G_j}{\delta z^2} = (A_1 H - 2B_1 + C_1 H + 2D_1)H \tag{3.52}$$

$$\frac{\delta^3 G_j}{\delta z^3} = (-A_1 H + 3B_1 + C_1 H + 3D_1)H^2 \tag{3.53}$$

Replacing these equations in Equation 3.48 gives Equation 3.54.

$$(A_1 + C_1)(H\lambda_1 + H\mu_1) = \lambda_1(B_1 - D_1) \tag{3.54}$$

Using the boundary conditions gives rise to Equation 3.55 (detailed description provided in Appendix A).

$$F(H) = 2H^3(A_1 - C_1)(\lambda_1 + \mu_1) + 2H^2\mu_1(B_1 + D_1) \tag{3.55}$$

Using the boundary conditions for any interface gives Equation 3.56.

$$\frac{\delta^2 G_j}{\delta z^2} - \frac{\lambda_j + 2\mu_j}{\mu_j} H^2 G_j = \frac{\delta^2 G_{j+1}}{\delta z^2} - \frac{\lambda_{j+1} + 2\mu_{j+1}}{\mu_{j+1}} H^2 G_{j+1} \tag{3.56}$$

For the nth layer (when n is the number of layers, hence n^{th} layer is the bottom-most layer),

$$G_n = (A_n + B_n z)e^{-Hz} + (C_n D_n z)e^{HZ}$$

When $z \to \infty$,

$$(A_n + B_n z)e^{-Hz} + (C_n D_n z)e^{HZ} = 0$$

which gives,

$$C_n = 0 \tag{3.57}$$

$$D_n = 0 \tag{3.58}$$

There are four constants of integration to be calculated for each layer, which means for n layers, there are $4n$ constants to be calculated. Since C_n and D_n are zeros, there are $(4n - 2)$ constants.

The top layer gives two equations and for n layers with $(n - 1)$ interfaces, there are $4(n - 1)$ equations. The total is $2 + 4(n - 1) = (4n - 2)$ equations for $(4n - 2)$ constants, and all constants of integration can be calculated. Solving these equations results in the calculation of stresses and displacements.

This chapter presented equations inherent to the Layered Elastic theory as incorporated in GEOTRACK. A description of all the tasks undertaken in this research effort along with important functions of GEOTRACK-2016 will be presented in the following chapter.

CHAPTER 4

DEVELOPMENT OF GEOTRACK-2016 ON THE MATLAB$^{\circledR}$ PLATFORM

As previously mentioned, the GEOTRACK analysis software is based on the theory of layered elastic analysis. Therefore, Chapter 3 of this thesis presented the theoretical formulations associated with the analysis of multi-layer systems using the layered elastic analysis approach. Once the underlying theory in LET was reviewed, the next task involved in-depth understanding of the available source code to link different components of the code to different steps in LE analysis. However, prior to that, the original version of the code needed to be modified to facilitate compilation and execution on modern operating systems. This chapter presents different errors in the original version of the source code that made the version uncompilable, and the process adopted to address these errors. The output generated by the modified code was then compared with that for GEOTRACK for WINDOWS to ensure that the modificaions related to debugging did not adversely affect the analysis results. A typical track structure was selected as the control section and was analyzed using GEOTRACK for WINDOWS and the debugged version of the code. A detailed comparison of the analysis results is presented in this chapter. Important functions of GEOTRACK-2016 developed on the MATLAB$^{\circledR}$ platform are discussed. An important point to note is that since the railroad industry in the US widely uses English units, GEOTRACK-2016 has been developed with English units. All the inputs provided by the user and the outputs generated by the software uses the same units.

4.1 Compilation Errors in GEOTRACK (VAX Version)

The original source code for GEOTRACK was written for a system that used punched cards as an input source. Later, the punched cards were translated into a high level programming language that is an extension of FORTRAN called VAX (Virtual Address Extension) FORTRAN used to program machines with the VAX Instruction Set Architecture (ISA) [55]. This code required a VAX Fortran compiler to be compiled and executed. Accordingly, trying to execute the code on modern operating systems resulted in several compilation errors.

For compiling the available code, the GCC (GNU Compiler Collection) FORTRAN (gfortran) compiler was used [56]. Since this compiler does not support the VAX extensions, there were numerous syntactical errors that needed to be addressed before the GCC compiler could successfully compile the code. For ease of development and debugging of GEOTRACK, an Integrated Development Environment (IDE) developed by The Eclipse Foundation called Photran [56] was used. Since the GCC is only available on Linux operating systems, installation of MinGW (Minimalist GNU for Windows) which is a minimalist development environment for native Microsoft Windows applications was required. Once the Photran-Eclipse IDE was configured to use the gfortran compiler and debugger, the next task involved eliminating compilation errors. Most of the errors were due to Application Program Interface (API) calls that were not supported by the gfortran compiler. So the API calls used by VAX Fortran were replaced with similar API calls supported by the GCC FORTRAN compiler in accordance with the VAX FORTRAN supporting documentation [55].

4.2 Runtime Errors in GEOTRACK (VAX Version)

After successful compilation and execution of the code, an output file could be generated. However, the resulting output file comprised 'zeros' and 'NaNs' for most of the parameters being calculated. In FORTRAN, although a code executes without displaying errors, runtime errors can still exist. The `-fcheck=all` flag was enabled

to identify and track the runtime errors. Additionally, running the code through a profiling and memory debugging tool 'valgrind' identified the runtime errors. Most of the errors were found to be originating from uninitialized variables. This was due to the default behavior of the gfortran compiler that did not initialize the declared variables and arrays. This was addressed by setting appropriate flags in the gfortran compiler.

Once the FORTRAN legacy code was debugged to prepare a version that could be compiled and executed on modern operating systems, the next task involved verifying the accuracy of the generated output against the output from GEOTRACK for Windows. The primary objective was to ensure that modifications to the code syntax did not adversely affect the calculations performed by different subroutines. The details of the validation are presented in the next section.

4.3 Comparison of Results from the Modified Code with GEOTRACK for WINDOWS

The verification task was accomplished by analyzing different track loading and substructure layer configurations using the modified version of the code as well as GEOTRACK for Windows. This section presents details on the control section analyzed, along with critical track response parameters calculated through the two different versions of the program.

Control Section During the Verification Process: First, a base case was generated to serve as the control section with respect to track substructure layer configuration as well as loading magnitudes. Figure 4.1 presents a schematic of the layer configuration used for this base case.

In Figure 4.1, E is the Young's modulus for each layer, μ is the Poisson's ratio for each layer, and K_0 is the coefficient of lateral earth pressure at rest. Note that the K_0 values for different layers were taken from previously published results using
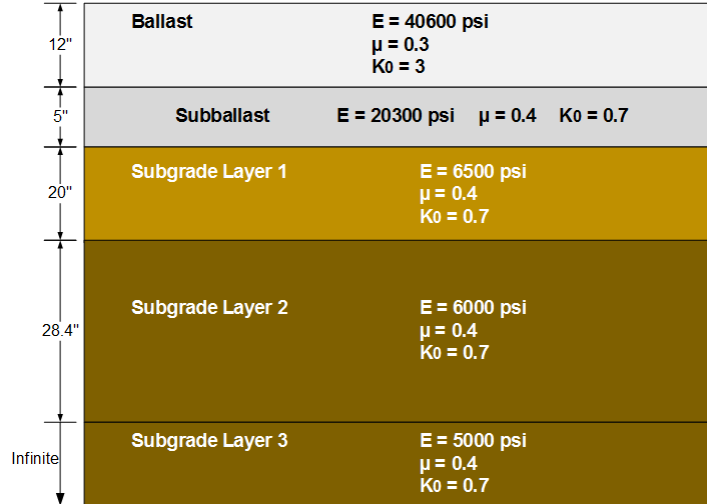
Figure 4.1: Layer Configuration used During Analysis of the Control Section

GEOTRACK. It should be noted that the $K_0 = 3$ value for the ballast layer appears to be significantly larger than those for typical granular layers. To evaluate the effect of such a high K_0 value, further analyses were run to assess the significance of the K_0 value on the analysis results. determine the value of K_0. The coefficient of lateral earth pressure at rest (K_0) can be calculated from the angle of internal friction (ϕ) using the following equation [16].

$$K_0 = 1 - \sin \phi \tag{4.1}$$

The ϕ value calculated from the results by Ngo et al. [57] was 58°, that from Wang et al. [58] was 56°, and that reported by Stark et al. [59] was $48° - 51°$. It could be observed that the typical values of ϕ used for railway ballast lies in the range of $50° - 60°$. When the value of K_0 was calculated using Equation 4.1 with the specified range of ϕ, a range of values between 0.23 and 0.13 was obtained for K_0. Using a value of $K_0 = 0.23$ and $K_0 = 0.13$ in GEOTRACK analysis did not have any significant effect in the output values for track response.

In the GEOTRACK code, the K_0 value is used in calculation of the bulk stress

(θ) at layer (i) using Equation 4.2.

$$\theta(i) = \sigma_v(i) + 2\,K_0(i)\,\sigma_v(i) \tag{4.2}$$

where σ_v is the vertical stress which is calculated using Equation 4.3.

$$\sigma_v(i) = \gamma(i) \times H(i) + Static\,Weight \tag{4.3}$$

where γ is the unit weight of soil and H is the distance to the point from the surface. Analysis of different cases revealed that the value of K_0 would make significant differences in track response values only when it is used in combination with large difference in γ and H values. The base case used the value of $\gamma = 124.1\,pcf$, $H = 12\,in.$ and $K_0 = 3$ for the ballast layer. Different combinations of unrealistically large values of γ and H were used with $K_0 = 0.13$ to track the difference in track responses. The detail of the properties values and track response (only track modulus) are provided in Table 4.1.

Table 4.1: Ballast Unit Weight and Ballast Depth Used for Analysis of K_0

Gamma (pcf)	Ballast Depth ($in.$)	Earth Pressure Coefficient (K_0)	Track Modulus ($kips/in./in.$)
124.1	12	3.00	3.59
124.1	12	0.13	3.63
124.1	30	3.00	3.72
150.0	12	0.13	3.63
150.0	30	0.13	4.97

Table 4.1 shows that the value of K_0 affects the track responses only when used in combination with (unrealistically) high ballast unit weight and depth. Therefore, a value of $K_0 = 3$ (a value used in the past literatures) has been used in this verification process. Table 4.2 lists the Rail and Tie properties used for the base case.

The example analyses illustrated in this document involve modeling the track response under a typical AMTRAK Acela Express locomotive. Recent field instru-

Table 4.2: Rail and Tie Properties Used for Analysis of the Base Case

Tie Parameters	Value	Rail Parameters	Value
Material	Concrete		
Length	103.5 $in.$	Rail gauge	56.5 $in.$
Width	11.2 $in.$	Rail area	13.41 $in.^2$
Area	78.8 $in.^2$	Rail weight	134.7 lbs/yd
Weight	851.1 lbs	Rail EI	2849498.2 $k-in.^2$
EI	1745663 $k-in.^2$	Fastener stiffness	6852000 $lb/in.$
Tie spacing	24 $in.$		

mentation efforts along AMTRAK's Northeast Corridor (NEC) performed by Mishra et al. [60] observed load levels of 27.28 kips and 26 kips on the rail during the passage of the two trailing axles of the locomotive. The spacing between the two axles was 110.24 in. Accordingly, positioning the first wheel on Tie number 1, the second wheel lies in between the fifth and the sixth Ties corresponding to a center to center tie spacing of 24 inch. Simple moment balance equations were used to distribute the second wheel load of 26 kips on to Tie number 5 and Tie number 6. Table 4.3 lists the loading configurations used for the base case. Table 4.4 lists identical values for

Table 4.3: Loading Details Used for the Base Case

Parameter	Value
Number of Axle Loads	3
Axle Loads Applied on Tie Numbers	1, 5, 6
Wheel Load ($kips$)	27.28, 10.58, 15.42

the track response parameters under loading calculated using the modified version of the code and GEOTRACK for Windows. Downward deflections have been reported using negative (-ve) numbers.

Different layer properties and track configuration parameters in the base case were modified to generate alternative track substructure and loading configurations, which were then analyzed using the two versions of the GEOTRACK software. Exactly matching track response values for all the cases were obtained from the modified

code and GEOTRACK for WINDOWS. However, only the results for the control section have been presented in this document.

At this stage, the newly developed program, although now executable on modern operating systems, was identical in features to the older version of GEOTRACK. Using a program without a Graphical User Interface (GUI) is a very tedious task for the user. Therefore, besides incorporating enhanced analysis features, an intuitive GUI was incorporated in GEOTRACK-2016, making the program user-friendly.

Table 4.4: Comparing Results from the Modified Code and GEOTRACK for WINDOWS for the Control Section

Tie No.	Rail deflection (in.)	Reaction Rail Seat (lbs)	Tie deflection (in.)	Tie Center Bending Moment (in.-lbs)	Track Modulus (kips/ in./in.)
Modified Version of GEOTRACK Code					
1	-0.11	11509.00	-0.11	1420.90	
2	-0.11	6114.00	-0.11	10525.00	
3	-0.10	2757.90	-0.10	14045.00	3.59
4	-0.10	3814.20	-0.10	12260.00	
5	-0.11	7722.00	-0.10	6757.30	
6	-0.10	8756.40	-0.10	3747.00	
GEOTRACK for WINDOWS					
1	-0.11	11509.00	-0.11	1420.90	
2	-0.11	6114.00	-0.11	10525.00	
3	-0.10	2757.90	-0.10	14045.00	3.59
4	-0.10	3814.20	-0.10	12260.00	
5	-0.11	7722.00	-0.10	6757.30	
6	-0.10	8756.40	-0.10	3747.00	

GEOTRACK-2016 was then developed in MATLAB$^{\circledR}$ platform. The important functions of GEOTRACK-2016 are discussed in the following section.

4.4 Important Functions in the Underlying Algorithm for GEOTRACK-2016

GEOTRACK_2016: GEOTRACK_2016 is the main routine that starts the Graphical User Interface (GT16_GUI), the details of which is provided in Section 4.5. The

GT16_GUI has several file menu callback functions, which open the Input File, assign the values to the respective variables, and define the global variables. Along with handling the input, the GT16_GUI also manages the outputs except printing the final results. GT16_RUN_ANALYSIS function is the main function for track response analysis where initialization of global variables and constants are also accomplished. The division of a tie into ten segments, surface-interface depth calculations and the initial stress calculations are some of the additional tasks addressed by this function.

SCERJ: The function SCERJ checks if the input values provided by the user conform the permissible limits. The permissible values checked in SCERJ for specific material properties and layer depths are listed as follows.

1. Number of layers (NS): Minimum = 1, Maximum = 5

2. Young's modulus (E) for each layer (psi): Minimum = 100.1, Maximum = 0.1E38

3. Poisson's ratio (VRAT) for each layer: Minimum = 0.05, Maximum = 0.499

4. Layer depth (HH) for each layer (in.): Minimum = 0.0, Maximum = 1000

If any of these values do not conform to the pre-defined permissible range, the program is terminated by displaying an error message. If all the values are acceptable, subroutine CALCUL is invoked.

CALCUL: The function CALCUL sets up the partitions; these partitions span half a tie segment in the transverse direction and half the tie spacing in the longitudinal direction. The function PART is then invoked, which sets up the Gauss constants for the four point Gauss Legendre integration at which the integrals are calculated. These integrals are from the responses that satisfy the equilibrium equations, displacement-strain relationships and Hooke's law in cylindrical coordinates, given by Equations 3.44 through 3.47. The function COEE computes the constants of integration, A_j, B_j, C_j and D_j for the jth layer (these constants are defined in Chapter 3). The function

BESSEL computes either $J_o(m)$ or $J_1(m)$ for the zero or first order Bessel functions. Finally, function CALCIN starts the evaluation of the integrals.

LAC: In the Layered Elastic Theory, all responses are first calculated because of a vertical load $-mJ_0(mrho)$. Subsequently, the boundary conditions are applied, and the Hankel Inverse is performed. All these steps are performed in the LAC function. This function also invokes functions SRAIL and STIE which calculate the Rail deflection and Tie Deflection respectively using the Beam Deflection formula. The function TRIAXL is also invoked by function LAC which calculates the equivalent triaxial stresses.

The use of the above mentioned functions and the subsequent functions (subroutines) invoked by these functions facilitate the calculation of track response under loading using GEOTRACK-2016.

4.5   Graphical User Interface (GUI) in GEOTRACK-2016

An intuitive user-friendly GUI was built into GEOTRACK-2016 as an improvement over the older version of the program. Different modules of the GUI are presented in the following subsections.

4.5.1   Material Properties Tab

Figure 4.2 presents a screenshot of the GUI window incorporated into GEOTRACK-2016. In the first panel of the main window (first vertical tab 'LY' for Layer Properties), a drop-down menu for the "Number of Layers" is present. This menu allows the user to specify the number of layers in the system (upper limit is five). Two text boxes, "Enter title.." and "Number of Iterations" are also part of the first panel. The string entered by the user in the "Enter title.." text box appears as the first line in the Output File. The number of iterations is used to determine the soil moduli used for the final iteration. In most cases, three iterations have been found optimum for reasonable convergence of moduli [17]. In the vertical tabs on the left hand side of
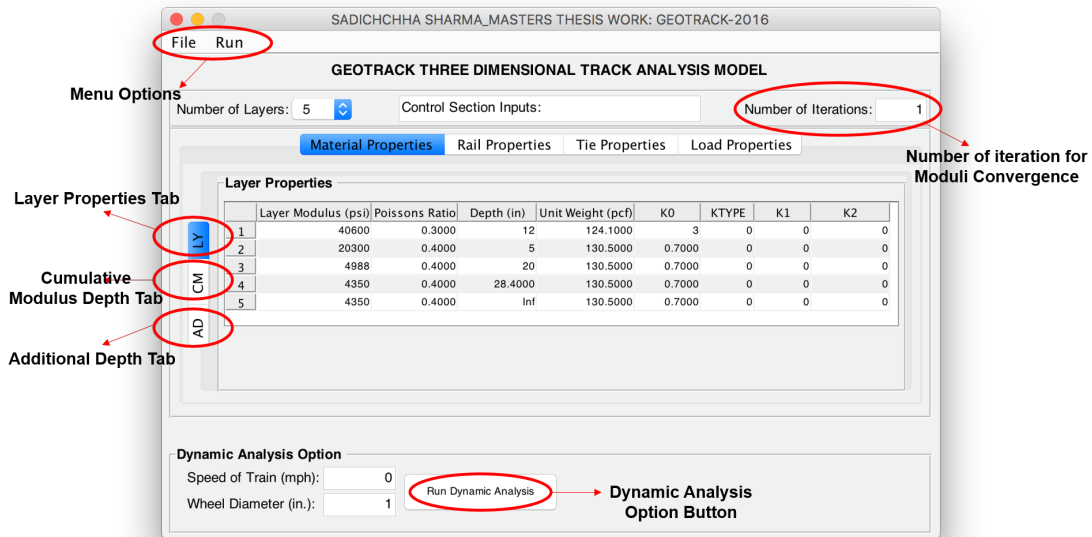
Figure 4.2: A Screenshot of the Graphical User Interface (GUI) Built into GEOTRACK-2016 (Material Properties Tab)

the screen, the "AD" is for providing the additional depths where the responses are desired. The "CM" tab requires the user to input the cumulative modulus depths.

Changing the number of layers option changes the number of rows in the "Layer Properties" table. The material properties of each layer are entered by the user. The "K_0" option is for the coefficient of lateral earth pressure at rest for each layer, "KTYPE" is for determining the type of stress-dependent relationship to use for each layer, "K1" and "K2" are the coefficients for calculation of stress-dependent soil modulus. The "KTYPE" can be entered from 0 to 3; the values represent different stress-dependent relationship described in Table 4.5 [17].

Table 4.5: Type of Stress-Dependent Relationships in GEOTRACK

KTYPE Value	Description
0	No Correction; $[E(new) = E(old)]$
1	Log-log Correction; $[E_r = P_a k_1 \frac{\theta}{P_a}^{k_2}]$
2	Semi-log Correction; $[E_r = P_a[k_1 + k_2 log(\frac{\theta}{P_a})]$
3	Arithmetic Correction; $[E_r = P_a[k_1 + k_2(\frac{\theta}{P_a})]$

P_a is the atmospheric pressure, and θ is the bulk stress or the first stress invariant $(\theta = \sigma_1 + \sigma_2 + \sigma_3)$.

4.5.2 Rail Properties Tab

The "Rail Properties" tab shown in Figure 4.3 requires the user to input the rail properties for analysis. The user can choose whether the analysis is to be run using the default rail sections, RE115, RE132, RE136 or RE140, or choose the "Other" option to enter user defined values. The default rail types are the AREMA recommended rail sections most commonly used in the US (See Table **??** for typical values). The inputs for rail properties are (1) Cross-Sectional Area, (2) Young's Modulus, (3) Moment of Inertia, (4) Rail Weight, (5) Rail Fastener Stiffness, (6) Rail Gage, (7) Number of Tie Segments between Rails and (8) Distance from neutral axis to the farthest point in the rail.
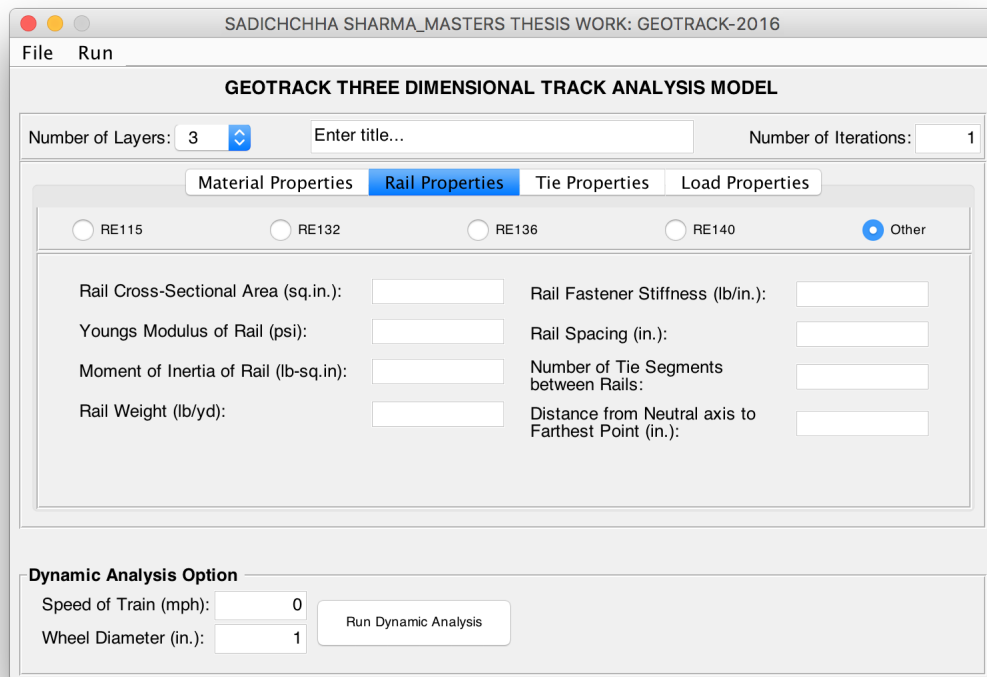
Figure 4.3: A Screenshot of the Graphical User Interface (GUI) Built into GEOTRACK-2016 (Rail Properties Tab)

4.5.3 Tie Properties Tab

The "Tie Properties" tab shown in Figure 4.4 requires the user to input the tie properties for analysis. The user can choose whether the analysis is to be run using the default values of concrete and wood ties, or choose the "Other" option to enter user defined values (the default values set in the program for concrete and wood ties are mentioned in Table 4.6). The inputs for tie properties are (1) Tie Length, (2) Tie Spacing, (3) Tie Width, (4) Tie Area, (5) Young's Modulus of Tie, (6) Tie Moment of Inertia and (7) Tie Weight.
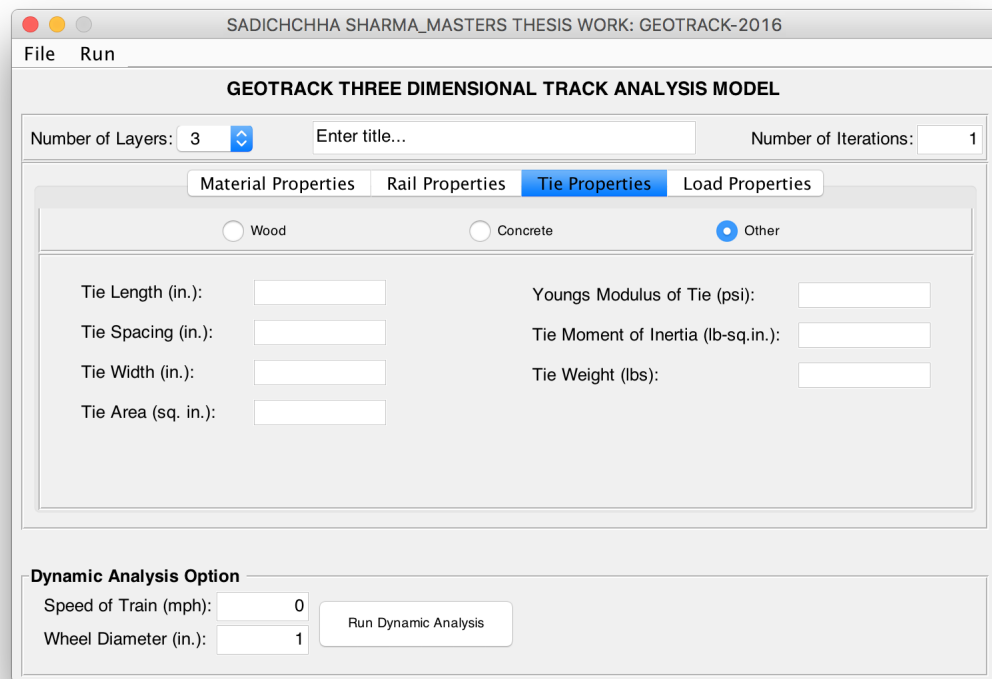
Figure 4.4: A Screenshot of the Graphical User Interface (GUI) Built into GEOTRACK-2016 (Tie Properties Tab)

4.5.4 Load Properties Tab

The "Load Properties" tab shown in Figure 4.5 is for inputing the load properties for analysis. The required load inputs are (1) number of axles to be applied to the track

Table 4.6: Properties for Standard Wood and Concrete Ties Used in the US

	Wood Tie	Concrete Tie
Tie Length ($in.$)	102.0	103.5
Tie Width ($in.$)	9.0	11.2
Tie Area ($in.^2$)	63.0	78.8
Tie spacing ($in.$)	19.5	24.0

(which is done by a pop-up menu that allows upto four axle loads to be applied), and (2) the tie number at which the wheel load is applied along with the magnitude of the corresponding wheel load. This interface also allows the user to input the first segment of the first tie and the last segment of the last tie where the output is desired.

4.5.5   FILE Menu

Figure 4.6 shows a screenshot taken for the "File Menu" in GEOTRACK-2016. The "Open" option allows the user to open an existing input file, which parses the input file and fills in the appropriate values in the GUI. The "Save" and "Save As" options allow the user to save the input file.

4.5.6   RUN Menu

Figure 4.7 shows a screenshot of the "Run Menu" in GEOTRACK-2016. As shown in figure, this menu provides user with four options namely: (1) Analysis, (2) Analysis Using Input File(s), (3) Parametric Analysis, and (4) Query Track Response. The "Analysis" option is for running the analysis in a normal mode by manually inputing all values. "Analysis Using Input File(s)" option allows the user to select an input file and perform the analysis. The "Parametric Analysis" option allows the user to perform a parametric analysis to evaluate the effects of selected track parameter on response under loading. The "Parametric Analysis" option is discussed in Chapter 5 of this thesis document. The "Query Track Response" option allows the user to query the stresses and deflection values at desired points within the track. This option is discussed in detail Chapter 6.
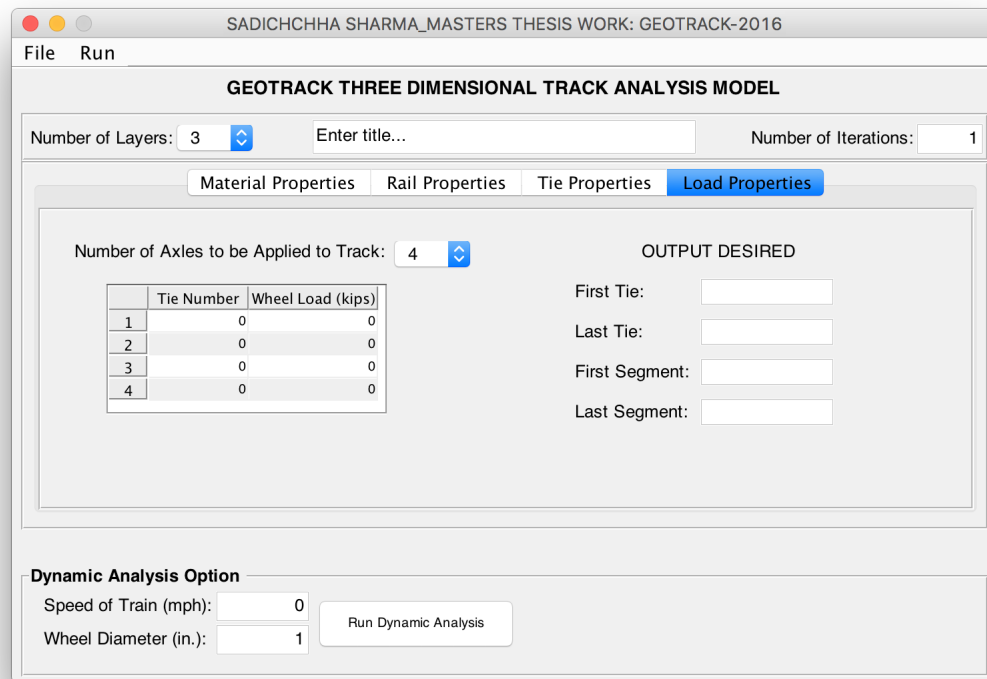
Figure 4.5: A Screenshot of the Graphical User Interface (GUI) Built into GEOTRACK-2016 (Load Properties Tab)

4.6 Summary

This chapter introduced different features of the newly developed GEOTRACK-2016 software program. Challenges associated with compilation and execution of the original VAX FORTRAN version were first explained, and steps followed to address them were detailed. Several representative track structures were analyzed to verify the accuracy of the modified code using GEOTRACK for WINDOWS (the results for the control section have been presented). Subsequently, important functions inherent to the underlying algorithm in GEOTRACK were listed. This was followed by a listing of different modules implemented in the newly developed Graphical User Interface (GUI) in GEOTRACK-2016. The next chapter will present results from a parametric study conducted to evaluate the effects of different track and loading configuration. Different assumptions inherent to the theory of Layered Elastic Analysis are also
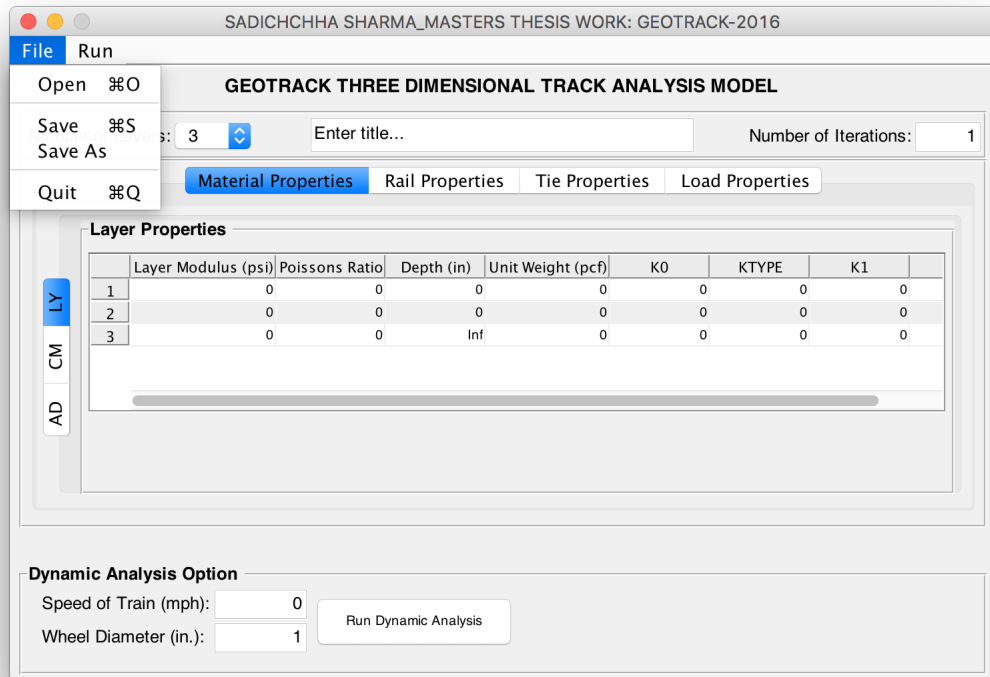
Figure 4.6: A Screenshot of the Graphical User Interface (GUI) Built into GEOTRACK-2016 (File Menu)

evaluated by comparing the results predicted by GEOTRACK-2016 to those obtained from analysis of a typical track structure using a commercially available finite-element based software package.
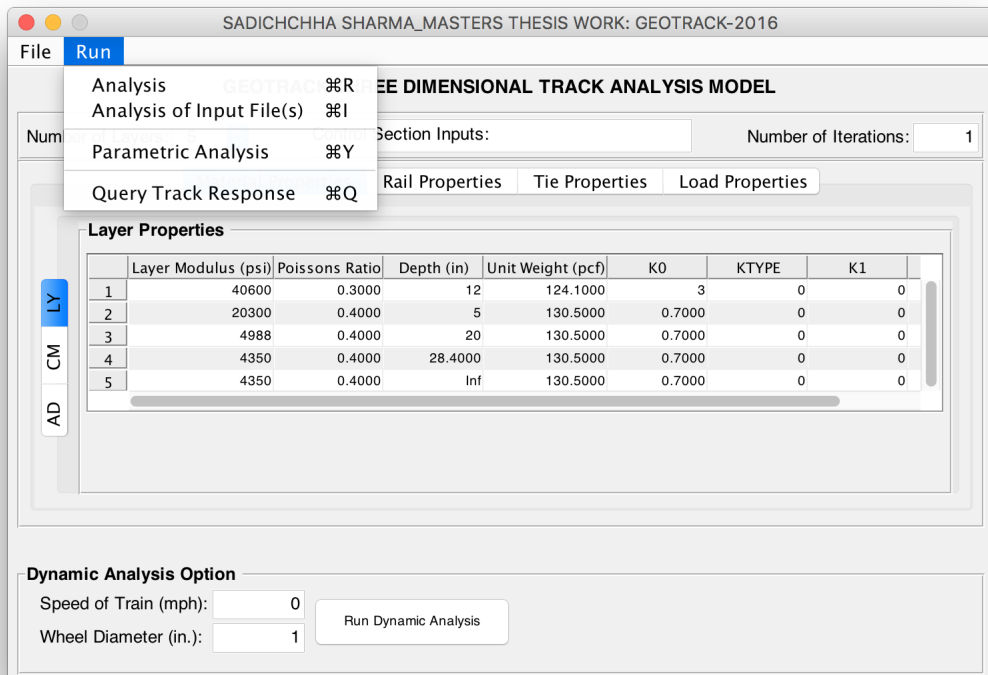
Figure 4.7: Run Menu in GEOTRACK-2016

CHAPTER 5

PARAMETRIC ANALYSIS OF TRACK RESPONSE USING GEOTRACK-2016 AND FINITE ELEMENT VALIDATION

After development of GEOTRACK-2016 as an enhanced, easy-to0use track analysis program, the next task in this research effort was to conduct a parametric study using GEOTRACK-2016 to quantify the effects of different track and loading configurations on track response and overall track modulus. This task was performed by utilizing the "parametric analysis mode" incorporated in GEOTRACK-2016. The results of this study will be discussed in this chapter. Details of this effort have been presented in this chapter. As already mentioned, one of the objectives of this research effort was to evaluate the effect of some of the assumptions inherent to Layered Elastic Theory. This was accomplished by cmparing the GEOTRACK-2016 results with those generated from a commercially available finite-element package, ABAQUS [49].

5.1 Parametric Analysis Mode

Incorporation of a batch-mode in the program facilitating simultaneous parametric analysis of different design alternatives is a salient feature of GEOTRACK-2016. Using this mode, a parametric analysis can be performed by changing only one parameter while keeping all other parameters constant. The program automatically produces different output files with the name `'File Name'_'Parameter Name'_'Parameter Values'`.

Results from the Parametric Analyses Using GEOTRACK-2016

The parametric analysis was accomplished by analyzing different track loading and substructure layer configurations using GEOTRACK-2016. This section presents details on the different sections analyzed, along with critical track response values calculated. The control section illustrated in Figure 4.1 is used as the base case for this parametric study.

5.1.1 Parameters Used in the Analysis

The different track parameters used for the parametric analysis along with the parameter values used are listed below.

1. **Cross-Tie Type**: *Wood*, Concrete
2. **Rail Gauge Length (inch)**: 41.9, *56.5*, 65.7
3. **Subgrade Modulus (psi)** : *6500*, 12000, 25000
4. **Ballast Modulus (psi)**: 20600, 29000, *40600*
5. **Ballast Layer Thickness (inch)**: 6, 10, *12*
6. **Tie Spacing (inch)**: 19.5, *24*, 29.92
7. **Fastener Stiffness (pound/inch)**: 148463.82, 999275.75, *6852000*

*Note that the italicized and underlined parameters are the values used for the Control Section.

5.1.2 Effect of Type of Cross-Tie

The control section used for the analysis comprises concrete ties placed at 24 inch center-to-center. To quantify the effect of different tie types on track response values under loading, a track section similar to that used for the control section was created using wood ties, keeping all other track parameters constant. Note that the tie spacing was changed to 19.5 inch center-to-center for the wood tie case. Table 5.1 shows typical values used in the US for the design and construction of a railroad track comprising wood ties. The standard values of tie properties are set by default in the

Table 5.1: Tie Properties for a standard Wood Tie Track used in the U.S.

Properties	Value
Length	102.0 $in.$
Width	9.0 $in.$
Area	63.0 $in.^2$
Weight	851.1 lbs
EI	1745663 $k - in.^2$
Tie spacing	19.5 $in.$

program. Using the "Parametric Analysis" mode in GEOTRACK-2016 for different tie materials using default pre-defined values for wood and concrete, two different output files were generated. These files were named as 'Parametric_Analysis_Concrete' and 'Parametric_Analysis_Wood'. Relevant track response values for the two cases are listed in Table 5.2.

Table 5.2: Parametric Analysis for Different Tie Materials

Tie No.	Rail deflection (in.)	Reaction Rail Seat (lbs)	Tie deflection (in.)	Tie Center Bending Moment (in.-lbs)	Track Modulus (kips/ in./in.)
Track Response Values for Track Comprising Concrete Ties					
1	-0.11	11512.10	-0.11	1421.50	
2	-0.11	6113.70	-0.11	10528.00	
3	-0.10	2755.70	-0.10	14047.00	3.59
4	-0.10	3813.10	-0.10	12261.00	
5	-0.11	7722.80	-0.10	6759.60	
6	-0.10	8759.00	-0.10	3747.60	
Track Response Values for Track Comprising Wood Ties					
1	-0.11	9869.30	-0.11	3610.50	
2	-0.12	6201.80	-0.12	11301.00	
3	-0.11	3729.80	-0.11	14966.00	3.61
4	-0.11	4459.30	-0.11	13318.00	
5	-0.11	7179.10	-0.11	8146.00	
6	-0.10	7619.60	-0.10	5408.20	

The overall track modulus calculated for the wood-tie case is 3.61 kips/in./in., which is slightly higher (0.5%) than that calculated for the control section, which comprises concrete ties (3.59 kips/in./in.). Although this difference is not significant,

the slight increase in track modulus values may be a result of the closer tie spacings used in the wood-tie case (19.5 in center to center) compared to the control section (24 in center to center). To confirm this, a parametric study for different tie spacing was conducted. The details of this study is presented in the next section.

5.1.3 Effect of Tie Spacing

The control section used for the analysis comprises concrete ties placed at center-to-center spacings of 24 inch. To evaluate the effect of tie spacing on track structure response under loading, response of the control section was calculated under tie spacing of 19.5 in.; corresponding to a commonly used tie spacing for wood ties in U.S. and 29.92 in.; corresponding to a commonly used tie spacing for wood ties in Australia [16]. The tie property were kept constant as concrete ties.

Using the "Parametric Analysis" mode in GEOTRACK-2016 for different tie spacing, three analyses were performed using center-to-center tie spacing of 24 in., 19.5 in., and 29.92 in.

The overall track modulus values calculated for the track with tie spacing 24 in., 19.5 in. and 29.92 in. were 3.59 kips/in./in., 3.64 kips/in./in., and 3.52 kips/in./in. respectively. It can be seen that the track system with the tie spacing of 19.5 in. had higher track modulus value than that of the control section; a decrease of tie spacing by 18.8% increased the overall track modulus by 1.4%. Also, the track system with tie spacing of 29.92 in. had lower track modulus value than that of the control section; an increase of tie spacing by 24.6% decreased the overall track modulus value by 1.9%. It can be concluded from the results that a decreasing tie spacing causes increase in track modulus values. As already discussed in Chapter 2, the track modulus can be calculated using $u = \frac{(P/y_m)^{4/3}}{(64EI)^{1/3}}$, where P is the maximum rail-seat load. Increase in tie spacing leads to low rail-seat loads [15], and thus, low track modulus values.

Table 5.3: Results from Parametric Analysis for Different Tie Spacing

Tie No.	Rail deflection (in.)	Reaction Rail Seat (lbs)	Tie deflection (in.)	Tie Center Bending Moment (in.-lbs)	Track Modulus (kips/ in./in.)
Track Response Values for Track with a Tie Spacing of 24 in.					
1	-0.11	11512.10	-0.11	1421.50	
2	-0.11	6113.70	-0.11	10528.00	
3	-0.10	2755.70	-0.10	14047.00	3.59
4	-0.10	3813.10	-0.10	12261.00	
5	-0.11	7722.80	-0.10	6759.60	
6	-0.10	8759.00	-0.10	3747.60	
Track Response Values for Track with a Tie Spacing of 19.5 in.					
1	-0.10	7683.10	-0.10	3087.52	
2	-0.10	4111.70	-0.10	11583.00	
3	-0.10	2444.00	-0.10	15550.90	3.64
4	-0.10	2723.80	-0.10	13780.70	
5	-0.11	5695.30	-0.11	8033.98	
6	-0.11	9972.20	-0.11	5459.59	
Track Response Values for Track with a Tie Spacing of 29.92 in.					
1	-0.11	13487.90	-0.11	-2341.00	
2	-0.10	5909.60	-0.10	8543.00	
3	-0.08	1614.60	-0.08	11773.00	3.52
4	-0.09	3053.10	-0.09	9957.10	
5	-0.10	8385.50	-0.10	4074.50	
6	-0.09	9998.10	-0.09	993.26	

5.1.4   Effect of Rail Gauge Length

The control section used for the analysis is a track system with rail gage length of 56.5 in. To evaluate the effect of rail gage on track substructure response under loading, response of the control section was calculated under a modified gage length of 65.7 in., corresponding to a commonly used gage length in Europe and 41.9 in., corresponding to a commonly used gage length in South Africa [16]. All other factors were kept unchanged with respect to the control section. The results from the parametric analysis are summarized in Table 5.4.

The overall track modulus values calculated for the track with rail gage length 56.5 in., 65.7 in., and 41.9 in. are 3.59 kips/in./in., 3.72 kips/in./in. (3.6% increase) and

Table 5.4: Results from Parametric Analysis for Different Rail Gauge Lengths

Tie No.	Rail deflection (in.)	Reaction Rail Seat (lbs)	Tie deflection (in.)	Tie Center Bending Moment (in.-lbs)	Track Modulus (kips/ in./in.)
Track Response Values for Track with Rail Gauge Length of 56.5 in.					
1	-0.11	11512.10	-0.11	1421.50	
2	-0.11	6113.70	-0.11	10528.00	
3	-0.10	2755.70	-0.10	14047.00	3.59
4	-0.10	3813.10	-0.10	12261.00	
5	-0.11	7722.80	-0.10	6759.60	
6	-0.10	8759.00	-0.10	3747.60	
Track Response Values for Track with Rail Gauge Length of 65.7 in.					
1	-0.11	11581.00	-0.11	1343.50	
2	-0.10	6124.90	-0.10	12584.68	
3	-0.10	2679.70	-0.10	13115.91	3.72
4	-0.10	3768.30	-0.10	9147.97	
5	-0.10	7739.40	-0.10	7402.39	
6	-0.10	8847.10	-0.09	2338.29	
Track Response Values for Track with Rail Gauge Length of 41.9 in.					
1	-0.12	11401.00	-0.11	2891.00	
2	-0.11	6116.00	-0.11	12574.00	
3	-0.10	2999.50	-0.10	11871.00	3.31
4	-0.11	3073.70	-0.10	3598.50	
5	-0.11	7629.57	-0.11	6033.90	
6	-0.10	8421.00	-0.10	1909.95	

3.31 kips/in./in. (7.8% decrease) respectively. It can be seen that the track system with rail gage length 65.7 in had higher track modulus value than that of the control section. In addition, the track system with rail gage length of 41.9 in. had lower track modulus value than that of the control section. It can be concluded from the results that track systems with higher rail gage lengths have higher track modulus values.

5.1.5 Effect of Subgrade Modulus

The control section used for the analysis is a track system with subgrade modulus value of 6500 psi. Subgrade modulus has been found to have a significant affect on overall track performance under loading [18]. To evaluate the effect of subgrade

modulus on the track response values, two new track configurations comprising high-stiffness (25000 psi) and medium stiffness (12000 psi) subgrade layers respectively, were generated and analyzed using GEOTRACK-2016. The purpose of this effort was to calculate the track response under extreme values of subgrade modulus values that may be encountered for in-service tracks. Figure 5.1 and Figure 5.2 show,

Figure 5.1: Layer Configuration for the Five-Layered System with High Stiffness Subgrade
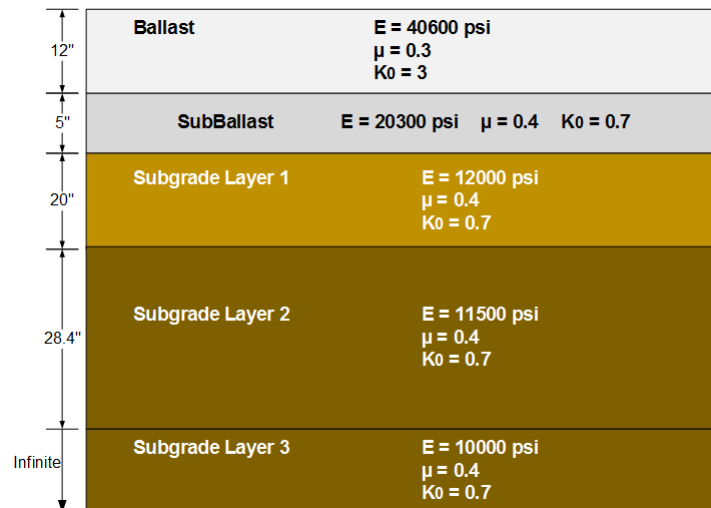
Figure 5.2: Layer Configuration for the Five-Layered System with Medium Stiffness Subgrade

respectively, the Five-Layered Track System with subgrade modulus values used for

the high-stiffness and the medium-stiffness cases. The output from the analyses are summarized in Table 5.5.

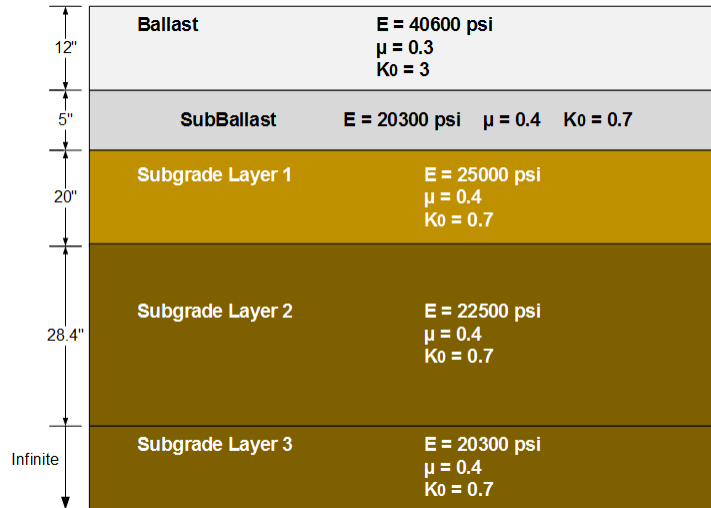**Table 5.5: Results from Parametric Analysis for Different Subgrade Types**

Tie No.	Rail deflection (in.)	Reaction Rail Seat (lbs)	Tie deflection (in.)	Tie Center Bending Moment (in.-lbs)	Track Modulus (kips/ in./in.)
Track Response Values for Track with Subgrade Modulus of 6500 psi					
1	-0.11	11512.10	-0.11	1421.50	
2	-0.11	6113.70	-0.11	10528.00	
3	-0.10	2755.70	-0.10	14047.00	3.59
4	-0.10	3813.10	-0.10	12261.00	
5	-0.11	7722.80	-0.10	6759.60	
6	-0.10	8759.00	-0.10	3747.60	
Track Response Values for Track with Subgrade Modulus of 12000 psi					
1	-0.06	12374.00	-0.06	9910.60	
2	-0.06	6174.60	-0.06	1059.90	
3	-0.05	2065.20	-0.05	6948.00	7.04
4	-0.05	3339.90	-0.05	4705.70	
5	-0.06	8102.40	-0.06	-2967.30	
6	-0.06	9455.60	-0.05	-6026.90	
Track Response Values for Track with Subgrade Modulus of 25000 psi					
1	-0.04	13289.00	-0.04	18554.00	
2	-0.03	6216.80	-0.03	5254.50	
3	-0.03	1335.40	-0.03	3179.80	13.19
4	-0.03	2876.40	-0.03	2846.65	
5	-0.03	8522.50	-0.03	-9918.80	
6	-0.03	10111.00	-0.03	-13253.00	

The overall track modulus values calculated for the track with low, medium, and high subgrade modulus are 3.59 kips/in./in., 7.04 kips/in./in., and 13.19 kips/in./in. respectively. Increase of subgrade modulus from 6500 psi to 12000 psi increased the overall track modulus by 96.10%, and increase to 25000 psi increased the track modulus value by 267%. The most significant effects were observed for the rail and tie deflection and the overall track modulus. From Table 5.5, it is evident that subgrade modulus has the most significant effect on the overall track modulus.

5.1.6 Effect of Ballast Modulus

To evaluate the effect of ballast modulus on track structure response under loading, response of the track structure was calculated under modified ballast moduli of 20600 psi and 29000 psi (the modulus for the base case was 40,600 psi). All other factors were unchanged with respect to the control section.

Table 5.6: Results from Parametric Analysis for Different Ballast Modulus

Tie No.	Rail deflection (in.)	Reaction Rail Seat (lbs)	Tie deflection (in.)	Tie Center Bending Moment (in.-lbs)	Track Modulus (kips/ in./in.)
Track Response Values for Track with Ballast Modulus 40600 psi					
1	-0.11	11512.10	-0.11	1421.50	
2	-0.11	6113.70	-0.11	10528.00	
3	-0.10	2755.70	-0.10	14047.00	3.59
4	-0.10	3813.10	-0.10	12261.00	
5	-0.11	7722.80	-0.10	6759.60	
6	-0.10	8759.00	-0.10	3747.60	
Track Response Values for Track with Ballast Modulus 20600 psi					
1	-0.11	10676.00	-0.11	556.27	
2	-0.11	6288.70	-0.11	8213.90	
3	-0.10	3152.20	-0.10	11853.00	3.37
4	-0.10	4039.00	-0.10	10276.00	
5	-0.11	7535.50	-0.11	5046.00	
6	-0.10	8281.20	-0.10	2573.70	
Track Response Values for Track with Ballast Modulus 29000 psi					
1	-0.09	11407.00	-0.09	-1033.20	
2	-0.08	6228.20	-0.08	5781.80	
3	-0.08	1963.80	-0.08	7376.20	3.49
4	-0.07	393.41	-0.07	4935.70	
5	-0.08	-311.03	-0.08	3097.90	
6	-0.08	-337.81	-0.07	1556.40	

The overall track modulus values calculated for the track with the ballast moduli of 40600 psi, 20600 psi, and 29000 psi are 3.59 kips/in./in., 3.37 kips/in./in., and 3.49 kips/in./in. respectively. Therefore, decreasing the ballast modulus from 40600 psi to 20600 psi (decrease by 49.3%) decreased the track modulus value by 6.1%, and decreasing the value from 40600 psi to 29000 psi (decrease by 28.6%) decreased the

overall track modulus by 2.8%.It can be seen that the track system with the ballast modulus of 40600 psi had highest track modulus value, followed by that with the ballast modulus of 29000 psi. The track system with the reduced ballast modulus of 20600 psi had the lowest track modulus value. It can be concluded from the results that a track system with a high ballast modulus has a high track modulus value but compared with subgrade, the ballast resilient modulus has very less effect on the track modulus. This can be attributed to the fact that thickness of the ballast layer is significantly less than the total thickness of the subgrade.

5.1.7   Effect of Ballast Layer Thickness

To evaluate the effect of ballast layer thickness on track response under loading, the control section was modified to simulate track structures with 6 in. and 10 in. thick ballast layers (the control section comprised ballast layer with a thickness of 12 in.). As with the other cases, other track geometry and loading parameters were kept unchanged with respect to the control section.

The overall track modulus values calculated for the track with the ballast layer thickness of 12 in., 6 in. (decrease by 50%), and 10 in. (decrease by 16.7%) are 3.59 kips/in./in., 3.33 kips/in./in. (decrease by 7.2%), and 3.50 kips/in./in. (decrease by 2.5%) respectively. It can be concluded from the results that reducing the ballast layer thickness reduces the overall track modulus of the system. This can be attributed to the fact that ballast modulus is significantly higher than the modulus values for the other layers. An increase in the depth of the strongest layer would in turn increase the track modulus of the system.

5.1.8   Effect of Fastener System Stiffness

The fastener system stiffness used in the control section was 6852000 lbs/in. To evaluate the effect of rail fastener stiffness on track structure response under loading, the fastener system stiffness was changed to 148463.82 lbs/in. and 999275.75 lbs/in.; these values were in accordance to Li et al. [18].

Table 5.7: Results from Parametric Analysis for Different Ballast Layer Thickness

Tie No.	Rail deflection (in.)	Reaction Rail Seat (lbs)	Tie deflection (in.)	Tie Center Bending Moment (in.-lbs)	Track Modulus (kips/ in./in.)
Track Response Values for Track with Ballast Layer Thickness of 12 in.						
1	-0.11	11512.10	-0.11	1421.50	
2	-0.11	6113.70	-0.11	10528.00	
3	-0.10	2755.70	-0.10	14047.00	3.59
4	-0.10	3813.10	-0.10	12261.00	
5	-0.11	7722.80	-0.10	6759.60	
6	-0.10	8759.00	-0.10	3747.60	
Track Response Values for Track with Ballast Layer Thickness of 6 in.						
1	-0.12	10498.00	-0.11	1833.20	
2	-0.11	6291.80	-0.11	8538.70	
3	-0.10	3290.90	-0.10	11483.00	3.33
4	-0.10	4106.90	-0.10	10187.00	
5	-0.11	7475.00	-0.11	5691.60	
6	-0.10	8155.00	-0.10	3483.10	
Track Response Values for Track with Ballast Layer Thickness of 10 in.						
1	-0.09	11494.00	-0.09	1240.58	
2	-0.08	6179.00	-0.08	6443.10	
3	-0.07	3158.50	-0.07	7553.90	3.50
4	-0.08	4072.8	-0.06	4930.00	
5	-0.08	3091.7	-0.08	3066.70	
6	-0.08	3423.5	-0.08	1539.40	

The overall track modulus values calculated for the track with the rail fastener stiffness of 6852000 lbs/in., 148463.82 lbs/in. (decrease by 97.8%), and 999275.75 lbs/in. (decrease by 85.4%) were 3.59 kips/in./in., 2.10 kips/in./in., and 3.27 kips/in./in., respectively. A decrease of fastening system stiffness ny 97.8% decreased the track modulus value by 41.5%, and a decrease of fastening system stiffness by 85.4% deceased the overall track modulus value by 8.9%. It can be concluded from the results that increasing fastener stiffness causes significant increase in the track modulus values. Considering the significance of this effect, it appears that overall behavior of the track can be significantly improved by modifying the fastening system stiffness

Table 5.8: Results from Parametric Analysis for Different Rail Fastener Stiffness

Tie No.	Rail deflection (in.)	Reaction Rail Seat (lbs)	Tie deflection (in.)	Tie Center Bending Moment (in.-lbs)	Track Modulus (kips/ in./in.)
Track Response Values for Fastener Stiffness of 6852000 lbs/in.					
1	-0.11	11512.10	-0.11	1421.50	
2	-0.11	6113.70	-0.11	10528.00	
3	-0.10	2755.70	-0.10	14047.00	3.59
4	-0.10	3813.10	-0.10	12261.00	
5	-0.11	7722.80	-0.10	6759.60	
6	-0.10	8759.00	-0.10	3747.60	
Track Response Values for Fastener Stiffness of 148463.82 lbs/in.					
1	-0.13	8172.10	-0.08	3765.90	
2	-0.11	6115.10	-0.07	5600.90	
3	-0.08	3184.10	-0.06	6239.10	2.10
4	-0.05	1142.70	-0.04	4951.90	
5	-0.03	-18.22	-0.03	3206.40	
6	-0.01	-869.67	-0.02	2558.90	
Track Response Values for Fastener Stiffness of 999275.75 lbs/in.					
1	-0.10	10644.00	-0.09	960.05	
2	-0.08	6359.20	-0.08	6094.40	
3	-0.06	2218.40	-0.06	7525.80	3.27
4	-0.04	426.08	-0.04	5315.10	
5	-0.03	-271.49	-0.03	3194.80	
6	-0.02	-413.99	-0.02	1714.90	

values without the need for major reconstruction of or modification to individual substructure layers.

5.1.9   Effect of Different Track Properties on Track Modulus

Figure 5.3 presents a graph with the results of the parametric analysis performed. All results of the parametric study of track modulus were observed to comply with the trends reported in published literature [18].
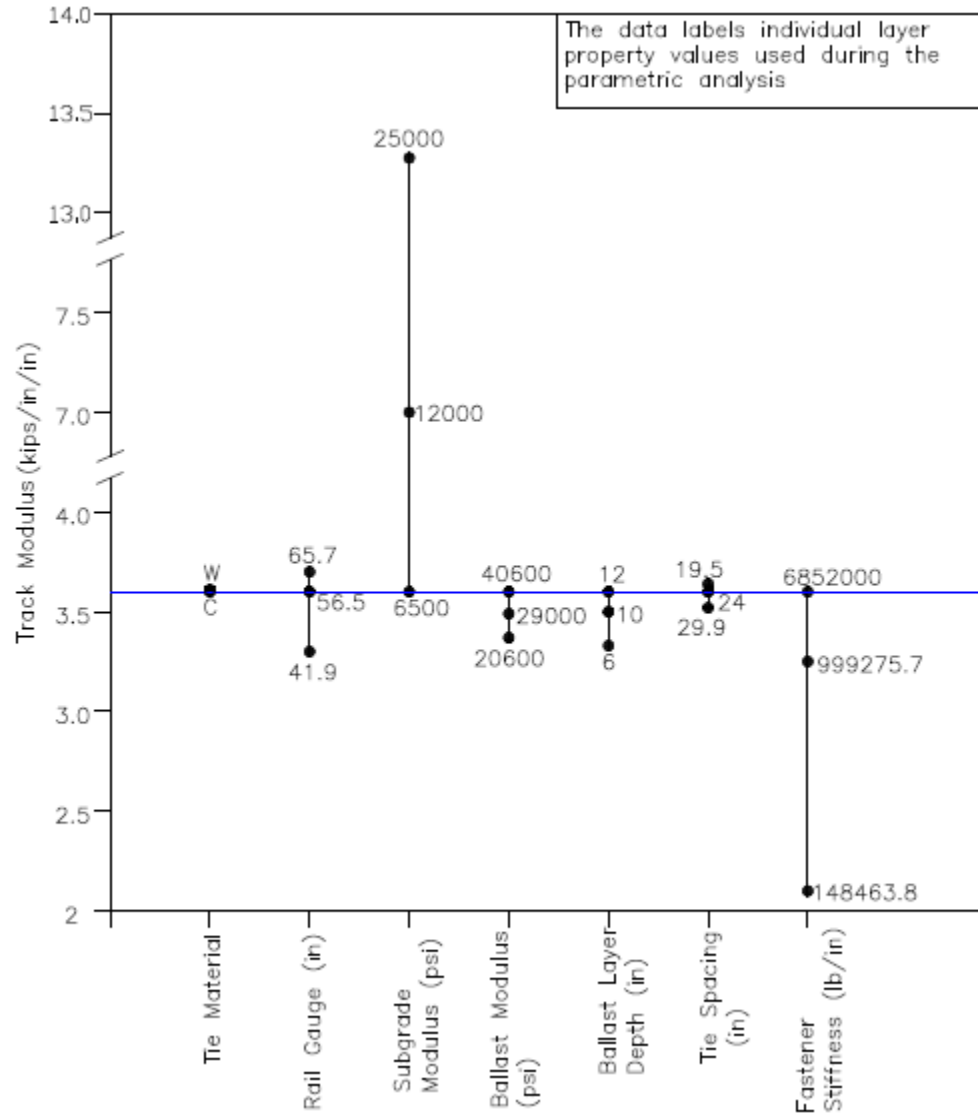
Figure 5.3: Effect of Track Properties on Track Modulus

5.2 Evaluating the Significance of Layered Elastic Analysis Assumptions through Finite-Element Modeling

As already mentioned, one of the primary objectives of this research effort was to evaluate the significance of some of the simplifying assumptions inherent to Layered Elastic analysis. Development of state of art enhanced track analysis methods can significantly improve the accuracy of track response predictions. Accordingly, a software program based on the theory of layered elastic analysis is a viable alternative

only if the analysis results are reasonably close to those predicted from more advanced analysis approaches. The following assumptions in layered elastic analysis were evaluated in this research effort through comparison with results from Finite Element analysis of the control section.

1. The load applied on the substructure is distributed over a circular area.
2. All layers are infinite in the horizontal direction.

This section presents details concerning the use of finite-element modeling to compare some of the response values predicted by GEOTRACK-2016. ABAQUS [61], a commercially available Finite-Element modeling software, was used. The overall finite-element modeling approach can be divided into (1) defining the geometry, (2)defining the material properties, (3) generating a mesh, and (4) defining the boundary condition [5].

5.2.1   Development of the Control Section

To develop a model of the control section, a representative geometry of the section as shown in Figure 4.1 was used. In order to decrease the required computational time, only half of the railway track substructure was modeled. The analysis section comprised 11 ties as is the case in GEOTRACK. The base width of each tie was 11.2 in. and the half length of the tie was 51.75 in. These values correspond to standard tie geometries used in the US. The distance between the centers of the first tie and the eleventh tie was 240 in. The base of each half tie was divided into 5 equal segments. When the tie group was placed in the center of the FE mesh, an additional distance of 224.9 in. was added to both sides of the Z boundary, therefore, the analysis section was 700 in. in the Z direction. Similarly, a distance of 248.25 in. was added to both sides of the X boundary. The schematic of the plan view and the cross sectional view of the model used is shown in Figure 5.4. The model generated using ABAQUS is shown in Figure 5.5. The model consisted of an additional layer

of 17.78 m (700") below Subgrade Layer 3 simulating the infinite bottommost layer in the Layered Elastic Theory, as used by Tutumluer et al. [62].
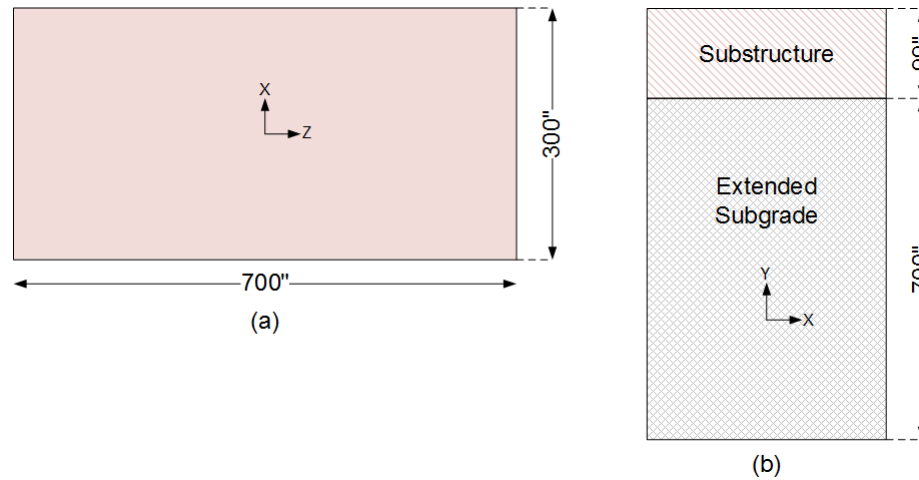
Figure 5.4: (a) Plan View of Half Track Symmetry of the 3D FE Model, (b) Cross Sectional View of the 3D FE Model

5.2.2   Boundary Conditions and Meshing

In the model, the surface-to-surface contact is used to describe the contact between two deformable surfaces (Ballast-Subballast-Subgrade). Boundary conditions were used to specify the values of all the solutions such as displacement/rotation and symmetrical boundary conditions in the X-direction (XSYMM). The positive and negative Z ends of the model were restricted in the Z-direction. Similarly, the positive and negative X ends were restricted in the X-direction and the bottom was restricted in the Y-direction. Referring to the ABAQUS model shown in Figure5.5, it can be seen that the vertical direction of the track is represented as the Y direction in the model.

Initial development of the model in ABAQUS involved several trials for configuring the mesh size within the model. Several trials were conducted until the outcome of the numerical model revealed that the mesh size used was suitable based on displacement and stress contours displayed after model analysis. The element size was fixed at 1.75
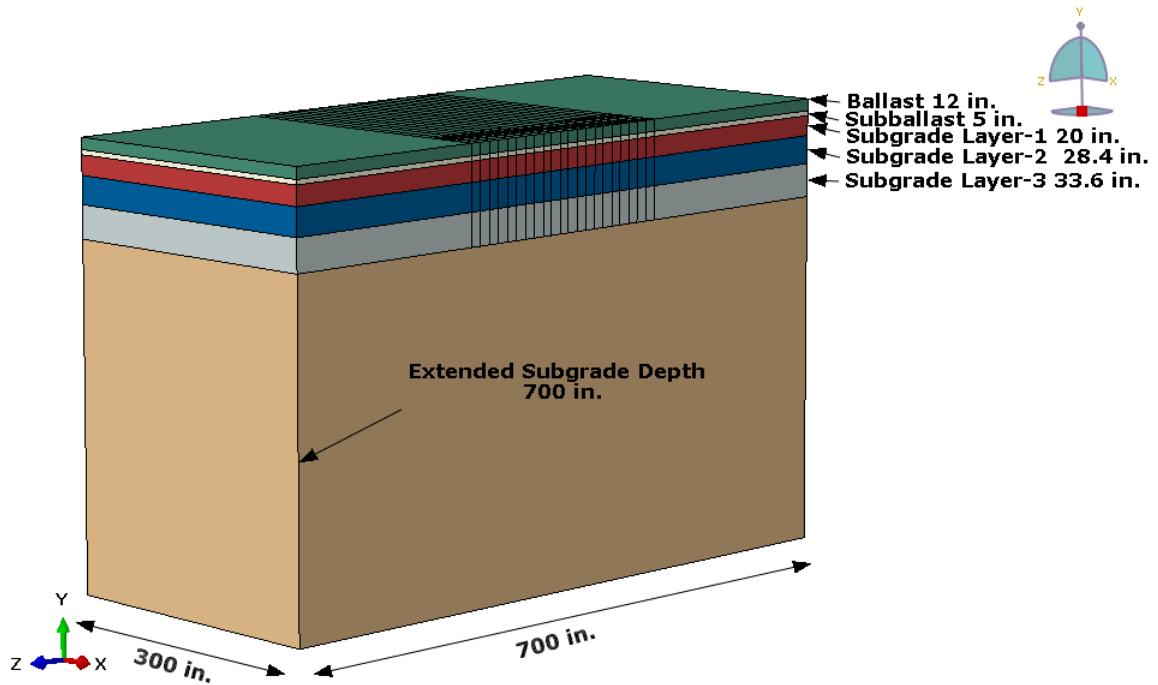
Figure 5.5: Schematic of the Half-Track as Modeled in ABAQUS

in., which falls within the range for ballast grain sizes commonly used according to standard AREMA gradation specifications.

To generate the 3D behavior of the railway track, an elastic model was selected and the model was discretized using a first-order, 3D-stress tetrahedral-element mesh. The discretization chosen consisted of 273,60000 8-noded linear brick hexahedral element with reduced integration and hourglass control finite-elements. The ABAQUS meshing verification tool was used to ensure that no element was distorted. This element type is denoted as C3D8R in Abaqus/CAE [61].

5.2.3 Loading Configurations

The primary objective was to compare the behavior of the substructure layers. Therefore, tie-ballast reaction forces obtained from GEOTRACK-2016 were converted into tie-ballast pressures and were applied directly on top of the ballast layer (the rails and the ties were not modeled during this effort), as listed in Table 5.9. * Downward forces are positive and upward forces are negative. Note that the negative values

Table 5.9: **Tie-Ballast Pressures Obtained from GEOTRACK-2016 Applied on Each Tie Segment in the ABAQUS Model**

Pressure Applied on Each Tie Segment (psi)					
Tie No.	Segment 1	Segment 2	Segment 3	Segment 4	Segment 5
1	23.66	25.63	28.91	23.36	19.08
2	12.41	11.66	13	10.58	8.78
3	4.19	2.22	2.28	1.84	1.59
4	6.68	5.23	5.71	4.63	3.86
5	15.94	16.25	18.24	14.78	12.15
6	18.37	19.40	21.84	17.68	14.50
7	8.27	7.70	8.58	7.00	5.83
8	1.72	0.81	0.81	0.65	0.56
9	-0.09	-0.66	-0.80	-0.68	-0.57
10	-0.22	-0.50	-0.59	-0.50	-0.42
11	0.01	-0.05	-0.06	-0.06	-0.06

obtained for the pressures from GEOTRACK-2016 were applied as negative pressures in the model, simulating an upward force applied on the ballast layer by the ties. It should be noted that ballast layers cannot resist tensile forces and hence such upward forces are not realistic in actual field conditions. However, the objective of this effort was to compare the responses predicted by GEOTRACK-2016 to those from FE analysis. Considering that both approaches (Layered Elastic analysis and Finite-Element analysis in its simplest form) model the ballast layer as a continuum capable of resisting both compression and tensile forces, such simplifications are reasonable.

As already mentioned, in the inherent assumption of Layered Elastic Theory, the loads are applied in form of circles on the substructure. This is implemented in GEOTRACK-2016 by dividing the ties into 10 equal circular segments (based on the principle of equal area) and applying the uniformly distributed pressure over the circular area. However, converting a rectangular area to an equivalent circular area is likely to lead to inaccuracies. For example, a standard tie length is 103.5 in. and the width is 11.2 in. Therefore, dividing a tie into 10 segments will result in rectangular segments that are 10.35 in. X 11.2 in. in dimension. To apply the loading through a

circular area while at the same time not changing the interface pressures significantly, the tie was divided into circles that have equal area as the rectangular segments, using Equation 5.1.

$$R = \sqrt{(L \times B)\frac{1}{\pi}} \tag{5.1}$$

where R is the radius of the circle, L and B are the length and breadth of the tie segment respectively.

This led to circles of radius 6.07 in. However, it should be noted that 10 circles with diameters of 12.14 in. each placed adjacent to each other result in a total length of 121.4 in. This is different from the total length of the tie (103.5 in.). Considering the case of symmetry (as modeled in ABAQUS), the half tie length resulting from 5 adjacent circles is 60.7 in. as compared to 51.75 in. which corresponds to the value in the field (a change of 17.3%). Therefore, it can be said that the loaded area on top of the ballast is modeled to be longer than it is actually in the real track scenario as shown in Figure 5.6. This can potentially change the response of points in the substructure, particularly if the soil element being considered falls at a location that would not be underneath a loaded area in the real track, but is now underneath a loaded area due to the change in dimension of the tie resulting from this simplifying assumption. The comparison of results from GEOTRACK-2016 and ABAQUS for
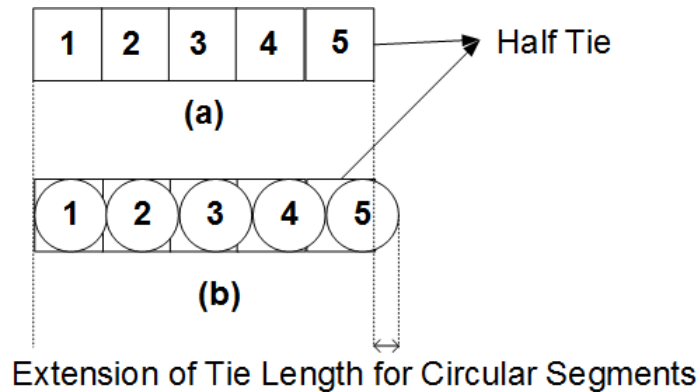
Figure 5.6: (a) Dividing a Half Tie into 5 Rectangular Segments, (b) Dividing a Half Tie into 5 Circular Segments

stresses are presented in Figure 5.7. The points of interest for the GEOTRACK analysis were the midpoints of each substructure layer. These points were chosen under the first segment of the first tie.
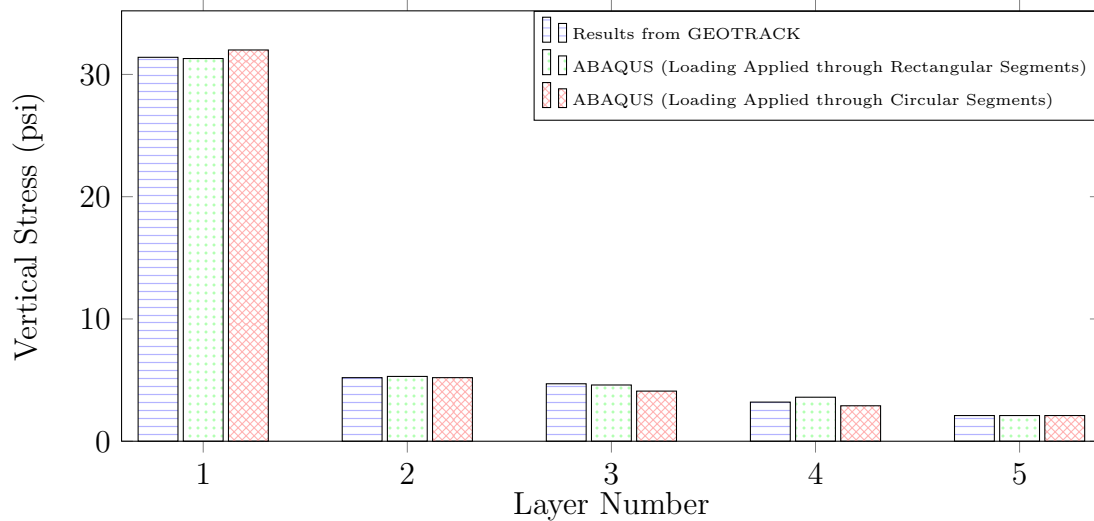
Figure 5.7: Comparing Results from GEOTRACK-2016 and ABAQUS for Vertical Stresses in the Substructure

Figure 5.8 shows the displacement color contours generated by ABAQUS when the loads are applied to the substructure through rectangular and circular segments. The comparison of results from GEOTRACK-2016 and ABAQUS for displacements are presented in Figure 5.9.

The results for stresses and displacements in the substructure from ABAQUS show close match with the ones from GEOTRACK-2016. The maximum difference of the results could be observed as 5.6% for the stresses and 4.05% for the displacements when the pressure to the substructure is applied through circular segments. It can be concluded that the results showed a better match for the model where the pressures are applied in the form of rectangles. Close comparison of stresses and displacements can be observed when pressure is applied through rectangular segments and through circular segments. The response values from the finite-element analysis for both cases are also very close to that of the results obtained from GEOTRACK-2016. Therefore,
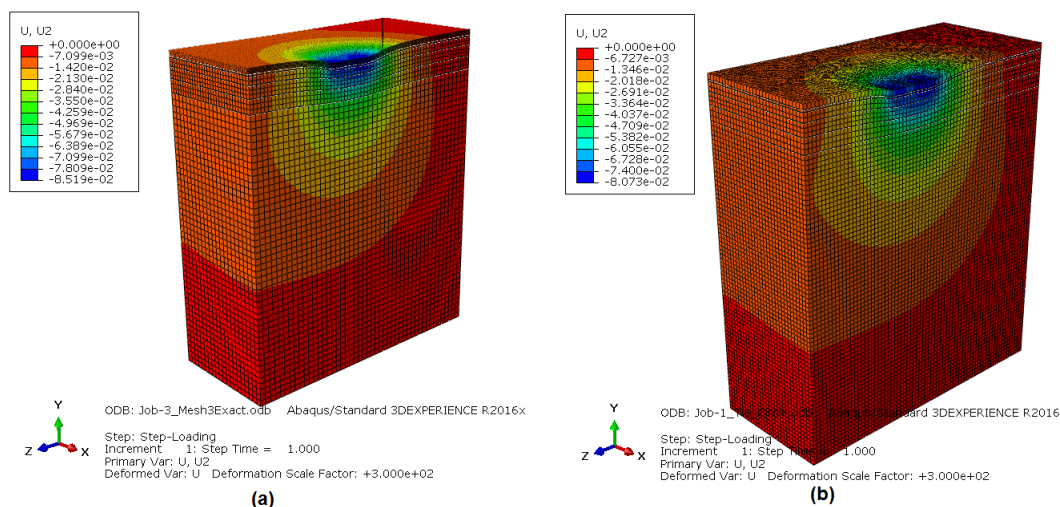
Figure 5.8: Color Contours Showing the Displacement Distribution in the Track Substructure where Load is Applied through (a) Rectangular Segments , (b) Circular Segments

it can be said that when loads are applied to the top of the ballast layer through circular areas (in accordance to the assumption of layered elastic analysis), the effect on track response values are negligible.

5.2.4 Varying Track Geometry

This section addresses the assumption in GEOTRACK-2016 (and Layered Elastic analysis) for infinite length in horizontal extent in all substructure layers. This is significantly different from real track structure that have finite dimensions in the transverse direction. Accordingly, layered elastic analysis prohibits the simulation of actual ballast profile geometries such as the shoulders (ballast material beyond the cross tie slopes down to the bottom of the ballast layer). To quantify the difference in calculated track response values introduced by the assumption of infinite horizontal extent, a realistic railroad track was modeled using ABAQUS with the shoulder as shown in Figure 5.10 and the effects of finite dimensions of the horizontal direction on the deflections and stresses were evaluated. The dimensions used in the figure correspond to a standard railroad track used in the US in accordance to AREMA specifications. Hence, two cases comprising: (1) infinite shoulder (the cases
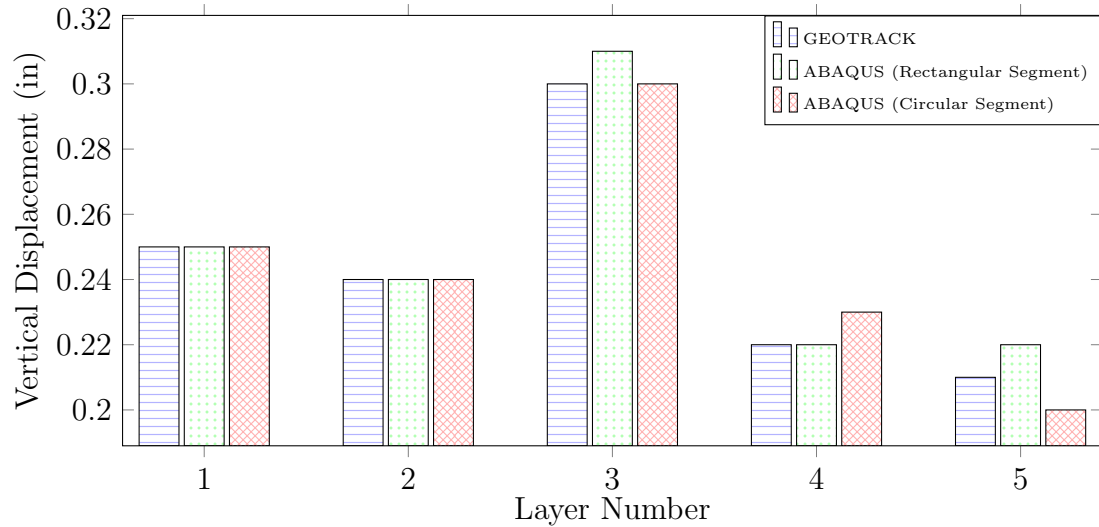
Figure 5.9: Comparing Results from GEOTRACK-2016 and ABAQUS for Vertical Displacements in the Substructure

previously analyzed) and (2) defined shoulder geometry were analyzed and the results from GEOTRACK-2016 and ABAQUS were compared. For the modeling, the load configurations, boundary conditions and meshing were kept the same as before. This means that the ballast shoulder boundary was restricted from movement.

The two cases: (1) loading applied through rectangular segments, and (2) loading applied through circular segments were modeled and analyzed using ABAQUS for comparing the substructure responses with defined shoulder geometry and infinite ballast shoulder. The results obtained for these cases are presented in Figure 5.11 (for stresses) and 5.12 (for displacements).

The comparison of results shows very large differences in the layer displacements obtained from ABAQUS in Layers 3, 4 and 5. This could be because the ballast shoulder is restricted from movement, in other words, all exposed nodes along the shoulder slope are restricted in X, Y and Z direction. However, this is not a realistic simulation of actual track conditions. For instance, the ballast shoulder for an in-service track can undergo significant deformation. To simulate real conditions, the ballast shoulders were kept free and modeled. The comparison of results from
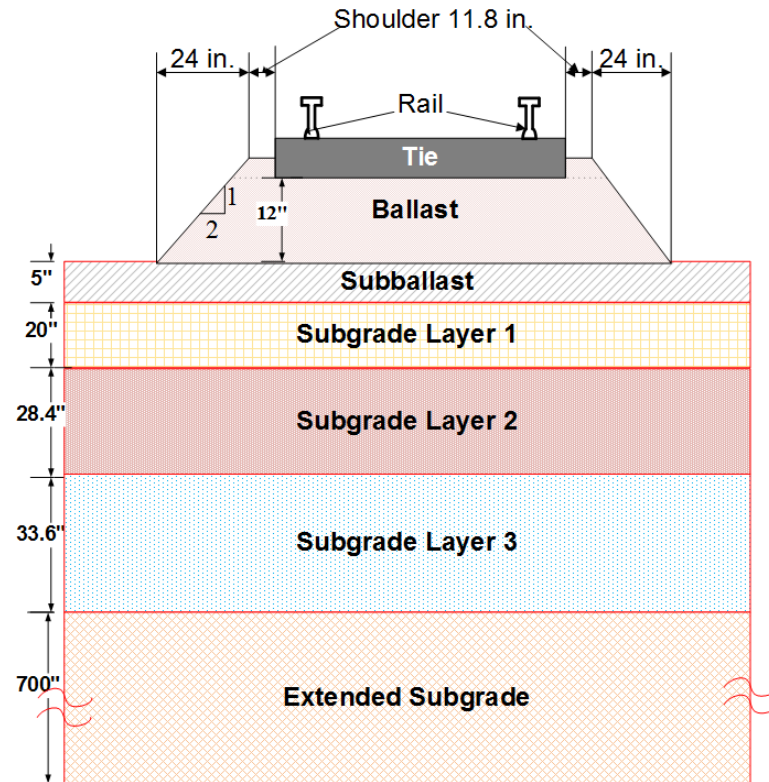
Figure 5.10: Cross-Sectional View of a Track with Shoulders used for Modeling in ABAQUS

GEOTRACK-2016 and ABAQUS for stresses are presented in Figure 5.13, whereas the comparisons for displacements are presented in Figure 5.14.

From Figure 5.13, it can be seen that there is no significant difference for the stress values for all the cases; a maximum difference of 7.6% can be seen for Layer 4. Similarly, from Figure 5.14, a maximum difference of 6.5% can be seen between the displacement values with both simplifying assumptions (infinite shoulders and loading through circular segments) and with no assumptions (defined shoulders and loading through rectangular segments). The results show that no significant difference in the values of stresses and displacements can be seen with infinite shoulder and with defined shoulder geometry in the track (when a realistic track is modeled with unrestricted ballast shoulders). Therefore, it can be concluded that the assumption of infinite dimension of the track in the horizontal direction has negligible effect on the
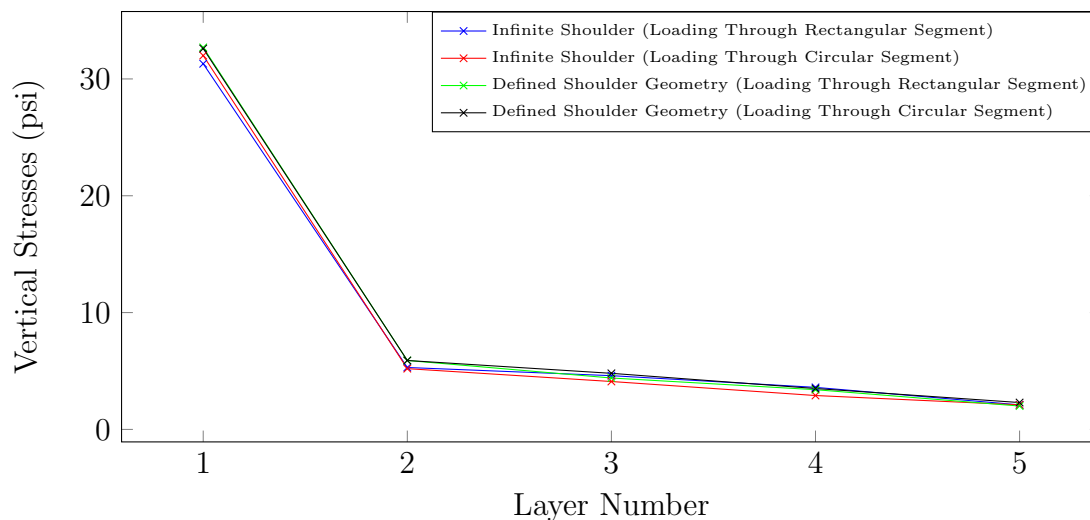
Figure 5.11: Comparing Results from ABAQUS for Vertical Stresses in the Substructure with Infinite and Defined Shoulder Geometry (Preliminary Results for Restricted Ballast Shoulder)

stresses and displacements in the substructure. However, it should be noted that these results reflect inferences about the overall track behavior. If more specific phenomena such as stability of the ballast slope, etc. are of interest, advanced analysis methods such as FEM should be used.

5.3 Comparison of Execution Time between GEOTRACK-2016 and Finite-Element Analysis

As already mentioned, one of the primary advantages of GEOTRACK-2016 concerns its ease of use and speed of execution. The previous section established that the loss of accuracy resulting from different simplifying assumptions in GEOTRACK was not significant. This section compares the time requirements for a standard analysis using GEOTRACK-2016 with that for finite-element analysis using ABAQUS. The elapsed time for the execution part of the GEOTRACK-2016 code was an average of $1.297124\,s$. The performance time was calculated by averaging five executions for a standard case. This time analysis excludes the execution of GUI and providing the input through it. An average of $2\,m$ is required for this process; accordingly, the total

Figure 5.12: Comparing Results from ABAQUS for Vertical Displacements in the Substructure with Infinite and Defined Shoulder Geometry (Preliminary Results for Restricted Ballast Shoulder)

time requirement for analysis using GEOTRACK-2016 is about $121.3\,s$.

For the control section, the execution time required for ABAQUS analysis was found to be about $4794\,s$ ($1\,h\,19\,m\,54\,s$), excluding the time required for modeling the section. An average of about $10800\,s$ - $14400\,s$ (3 - $4\,h$) is required for a user possessing the skill sets on ABAQUS to model the control section; accordingly the total average time requirement is about $17394\,s$ ($4\,h\,49\,m\,54\,s$).

Comparison of the time elapsed for the two cases shows that there is an increase of the execution time by more than $140\times$ when GEOTRACK-2016 is used for analysis instead of finite-element analysis; this corresponds to a reduction of preparation and execution time by 99.3% when GEOTRACK-2016 is used. Considering that the track response values calculated from both the analysis approaches are reasonably close, GEOTRACK-2016 can be considered to be a much efficient method of railroad track analysis as far as adoption by practitioners is concerned.
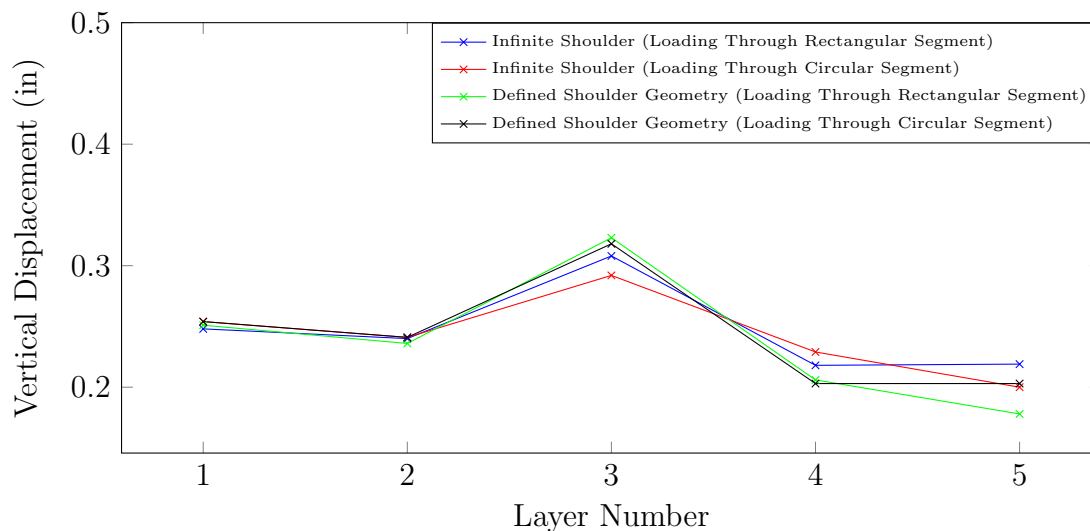
Figure 5.13: Comparing Results from ABAQUS for Vertical Stresses in the Substructure with Infinite and Defined Shoulder Geometry

5.4 Summary

This chapter presented results from a parametric analysis carried out to quantify the effects of different track design and construction parameters on track response under loading. The results from GEOTRACK-2016 were found to comply with the trends observed by past researchers. In an effort to assess the accuracy and identify the limitations of track substructure analysis using a layered elastic approach as in GEOTRACK-2016, a finite-element model of the control section was developed using the commercially available package, ABAQUS. Besides comparing results from the finite-element analysis to those generated using GEOTRACK-2016, an effort was made to assess the limitations of GEOTRACK-2016 as far as simulating realistic track geometries are concerned. Modeling a typical track geometry on ABAQUS and comparing with the results from GEOTRACK-2016, no significant difference in the predicted response values was observed. A comparison of the model preparation and execution times indicated that the time required for analysis can be reduced by 99.3% when GEOTRACK-2016 is used, as opposed to a Finite-Element based analysis package. It is important to note that the purpose of this research effort is
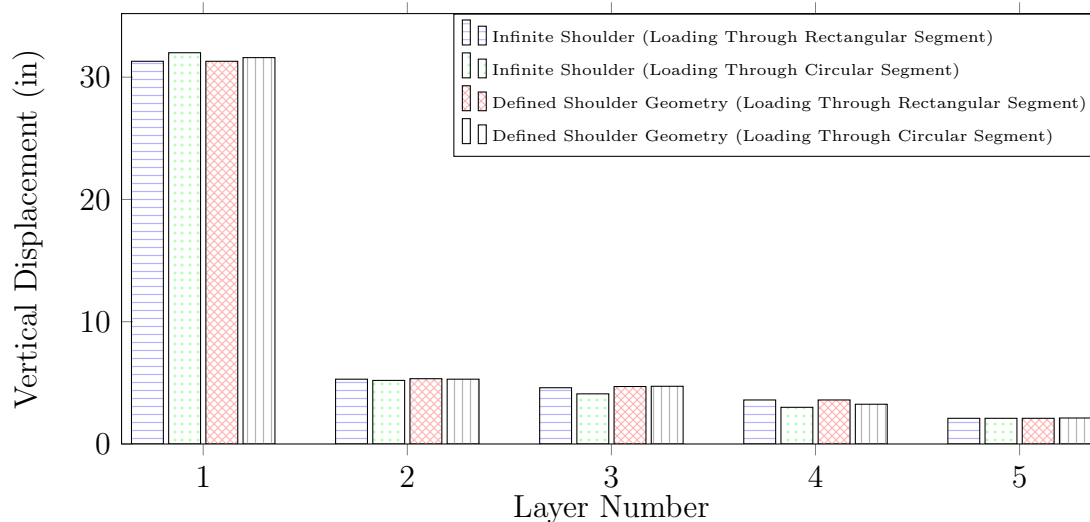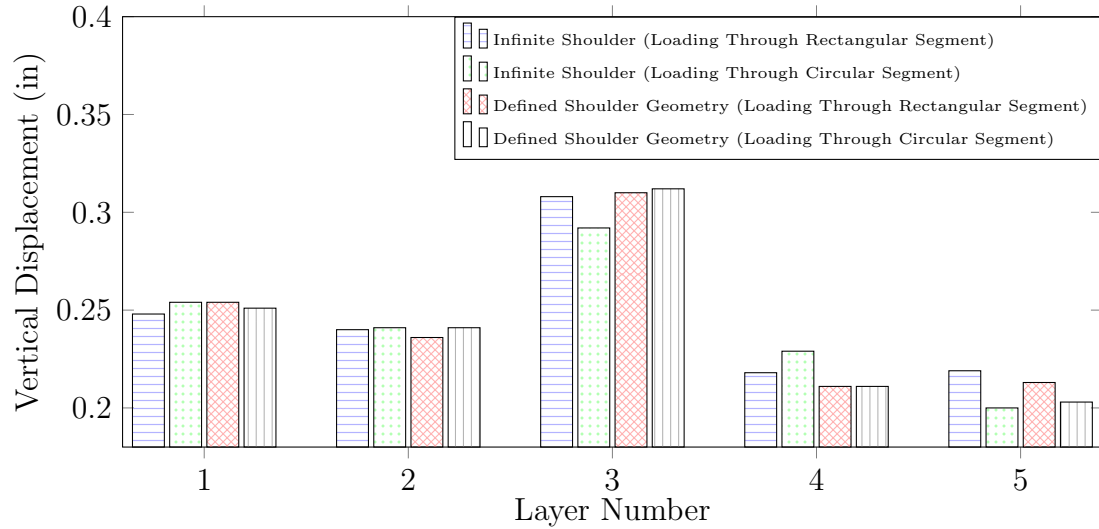
Figure 5.14: Comparing Results from ABAQUS for Vertical Displacements in the Substructure with Infinite and Defined Shoulder Geometry

not to propose GEOTRACK-2016 as an alternative to advanced analysis approaches such as those based on the theory of Finite Element analysis. Rather, the objective is to present GEOTRACK-2016 as an easy to use track analysis approach that can be incorporated into current state of practice in railroad track design and analysis without significantly compromising the accuracy of the results obtained.

CHAPTER 6

ENHANCED ANALYSIS CAPABILITIES IMPLEMENTED IN GEOTRACK-2016

This chapter presents the enhanced analysis capabilities implemented in GEOTRACK-2016 as improvements over GEOTRACK for Windows. Significant enhancements implemented in this newly developed version of the software include: (1) Ability to calculate rail bending stresses for comparison against instrumentation results, (2) Ability to account for train speed and wheel diameter to calculate dynamic amplification factors to be used for magnifying static load levels, and (3) Ability to query track response values at points of interest. Moreover, GEOTRACK-2016 also includes enhanced plotting and data visualization modules. This chapter presents descriptions of these new features.

6.1 Calculation of Bending Stresses within the Rail

Bending stress values help evaluate the resistance of the rail structure to load-induced flexure. GEOTRACK-2016 provides the user with an additional feature of calculating the rail bending stresses. Note that one common approach to measure train-induced wheel loads and identify wheel deflection involves instrumentation of the rail using strain gauges. Rail strains measured using strain gauges can be easily converted to bending stress values. Accordingly, this new feature introduced in GEOTRACK-2016 will help engineers compare the field-measured values with those calculated analytically. The maximum compressive and tensile stresses are developed at the topmost and lowermost edges of the rail, respectively, under a conventional loading

configuration (note that upward bending of the rail away from the load position can reverse the locations of the tensile and compressive stresses). This feature implemented in GEOTRACK-2016 requires the user to provide an additional input for "Distance from Neutral axis to the Farthest Point" as shown in Figure 6.1.
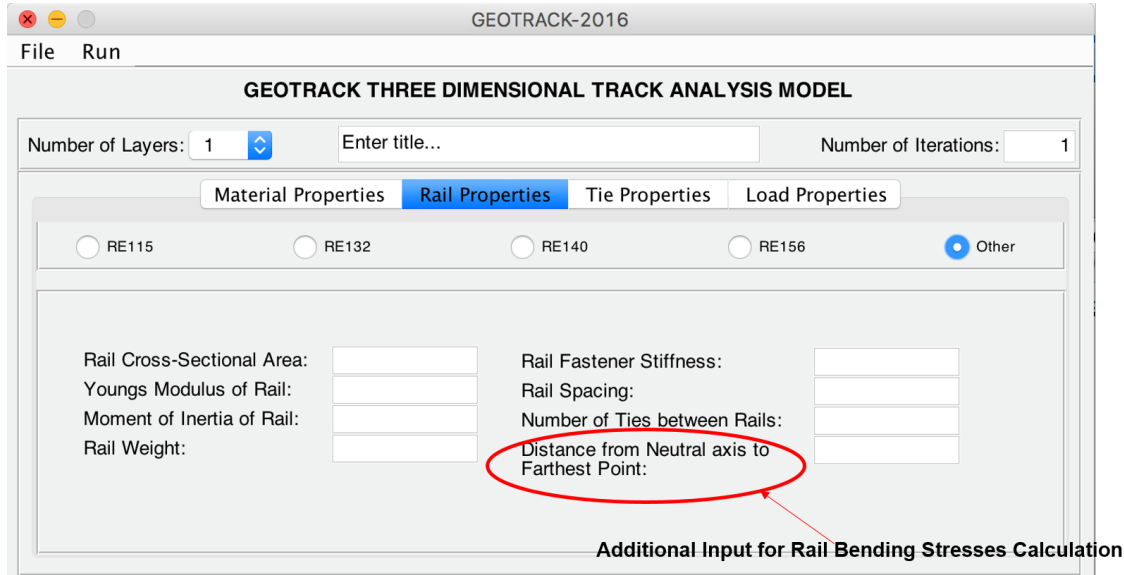
Figure 6.1: Additional Input Requirement for Rail Bending Stress Calculation

Since the rail is considered to be a beam on elastic foundation, from Flexure Formula [63],

$$\sigma = M\frac{c}{I} = \frac{M}{S} \tag{6.1}$$

where σ is the peak rail bending stress in psi, M is the peak rail bending moment in $in. - lb$, c is the distance from the neutral axis to the farthest point in the rail in $in.$, I is the moment of inertia of the rail about neutral axis in $in.^4$ and $S = \frac{I}{c}$ is the section modulus in $in.^3$. The Flexure Formula presented in Equation 6.1 is used to calculate the peak rail bending stress in GEOTRACK-2016. The section modulus of the different rails for default rail sections are presented in Table 6.1 [64]. If the user chooses the 'Other' option to custom-fill the values, the distance from the neutral axis to the farthest point in the rail or the point where the bending stress magnitudes are

desired needs to be manually input. This feature is particularly relevant if bending stress magnitudes at any random location along the rail section is desired. This can correspond to locations where strain gauges are installed.

Table 6.1: Section Geometry Properties for Typical Rail sections Commonly used in North America

Rail Section	Moment of Inertia (in^4)	Base to Neutral Axis Distance (in)	Section Modulus (in^3)
RE 115	65.50	2.99	21.90
RE 132	87.90	3.20	27.40
RE 136	94.20	3.34	28.20
RE 140	95.90	3.36	28.60

Peak bending stress magnitudes calculated for the default rail sections using GEOTRACK-2016 are presented in Figure 6.2. As the rail weight increases, the peak bending stress decreases. In Figure 6.2, the peak rail bending stress has the highest value of 8.06 ksi for rail section RE 115 (for rail weight 114.4 lb/yd) and the lowest value is for RE 140. As expected, the change in bending stress from RE 115 to RE 132 is much more significant compared to that from RE 132 to RE 140.
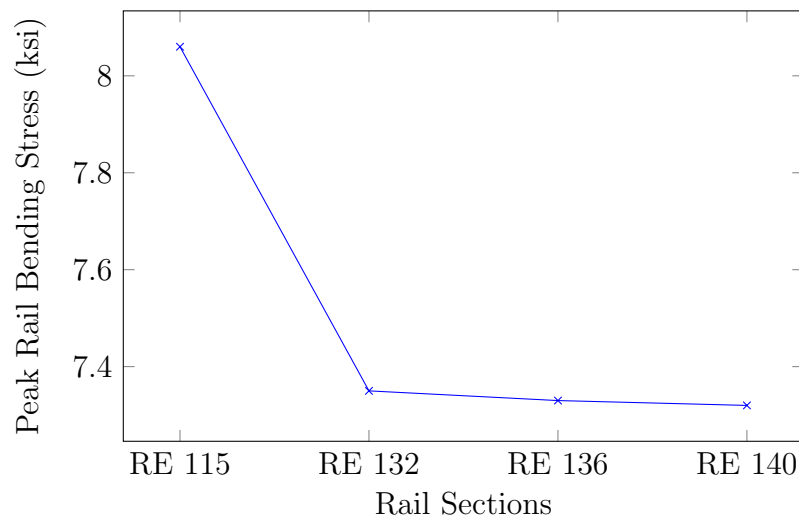
Figure 6.2: Variation of Peak Bending Stress for Different Rail Sections

6.2 Incorporation of Dynamic Amplification Factor into Analysis

In the earlier versions of GEOTRACK, only quasi-static loads were considered; this loading includes the weight of the train at rest and the effect of the static load at a very slow speed. However, in an actual railroad track, irregularities in the track geometry and/or rail wheel defects often lead to dynamic amplification of the load. Thus, the actual load values experienced by the track structure are significantly higher than the corresponding static values [65]. A dynamic factor can be incorporated to the loading to account for this dynamic amplification.

According to Talbot's analysis, the dynamic component of a load can be incorporated using an empirical equation. The Talbot dynamic factor (developed empirically) incorporates wheel diameter and speed of the train, and can be calculated using the Equation 6.2 [65].

$$\phi = 1 + \frac{33V}{100D} \tag{6.2}$$

where ϕ is the dynamic amplification factor, V is the train speed in miles per hour (mph), and D is the wheel diameter in inch ($in.$).

The dynamic load can thus be calculated using Equation 6.3.

$$P_{dyn} = P_{stat} \times \phi \tag{6.3}$$

where P_{dyn} is the dynamic load and P_{stat} is the static load. To quantify the effects of train wheel diameter and operating speed, the wheel diameter and train speed can be input in GEOTRACK-2016 to analyze the track response under amplified load levels. When the speed of the train is zero $\phi = 0$, and Equation 6.3 reduces to $P_{dyn} = P_{stat}$.

In GEOTRACK-2016, when the 'Run Dynamic Analysis' button shown in Figure 6.3 is clicked, two versions of the input file (one for the static loading condition named 'Filename'.txt and the other for the amplified loading condition named

'Filename' dyna.txt) are generated. For a standard freight train, the wheel diameter is $\sim$ 3 ft - 3-ft 9 in. (36 in. - 45 in.), assuming a train speed of $\sim$ 30 mph, the value of ϕ lies between 1.220 to 1.275. Figure 6.3 shows a screen shot of the GUI window where the speed is input as 30 mph and wheel diameter is 36 $in.$
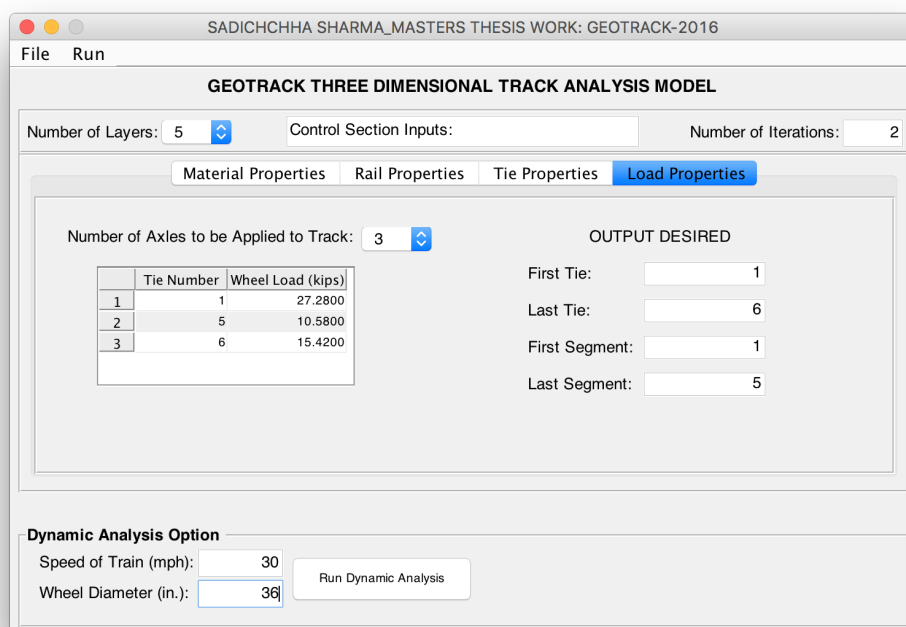
Figure 6.3: Graphical User Interface (GUI) window in GEOTRACK-2016 Showing the Feature to Incorporate Dynamic Load Amplification Factor

The change in magnitude of the dynamic amplification factors with train speeds and a constant wheel diameter of 36 $in.$ has been presented in Figure 6.4. From the figure, it is evident that the amplified load can be as high as 247% of the static load.

As already mentioned in Chapter 1, railroad track components in the US are being designed and constructed for shared-use corridors (for joint use by passenger as well as freight railroads). For such a design, in-depth understanding of the nature of loads being applied and their effects is imperative.

When a maximum load of 27.28 $kips$ is being applied in a railroad track, using the dynamic factors in Figure 6.4 and Equation 6.3, the amplified loads obtained for
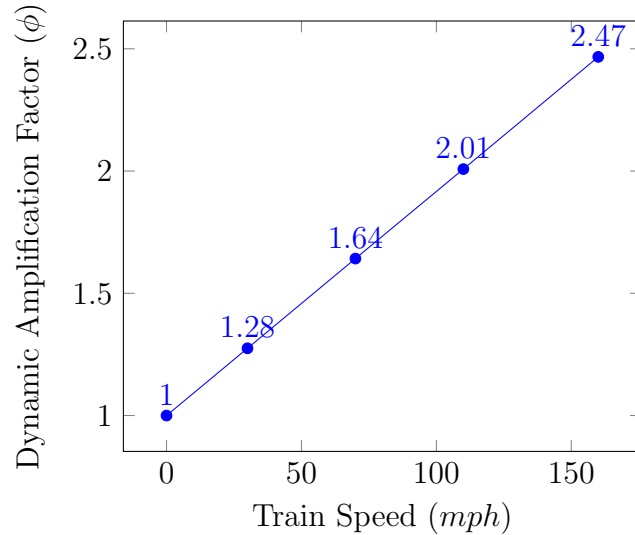
Figure 6.4: Variation of Talbot's Dynamic Factor with Train Speed

different speeds are listed in Table 6.2.

Table 6.2: Variation of Dynamic Loads with Train Speed

Speed (mph)	Dynamic Load ($kips$)
0	27.28
30	34.78
70	44.79
110	54.78
160	67.30

Using the "Dynamic Analysis" option in GEOTRACK-2016, a comparison for the amplified dynamic loading for a typical ACELA Express train moving at 100 mph and a typical freight train moving at 70 mph was performed. This quick comparison revealed that when all other parameters are unchanged, the dynamic load calculated by GEOTRACK-2016 increases from 44.79 $kips$ to 54.78 $kips$, when the static load is 27.28 $kips$, i.e. a dynamic amplification factor increase from 1.64 to 2.01.

6.3 Query Track Response

GEOTRACK-2016 provides the user with the option to query track response values at desired points of interest. This feature makes it easy to track the output values at

desired depth points under desired segment numbers of a specific tie without having to go through more than a thousand lines of an output file.

The "Query Track Response" option under the "Run" menu provides the user with this option. Figure 6.5 shows the 'Query Track Response' window in GEOTRACK-2016 for the control section, where the track response values at a distance of 20 in. from the first tie, at a depth of 15.6 in. is desired. When these three input values are provided, GEOTRACK-2016 is executed where the depth provided by the user is input in the layered elastic analysis as the 'z coordinate'. The length from the first tie provided by the user is used in the program to calculate in which segment (of the input tie number) the desired length falls. The output from the analysis at the required point is then printed out as results.
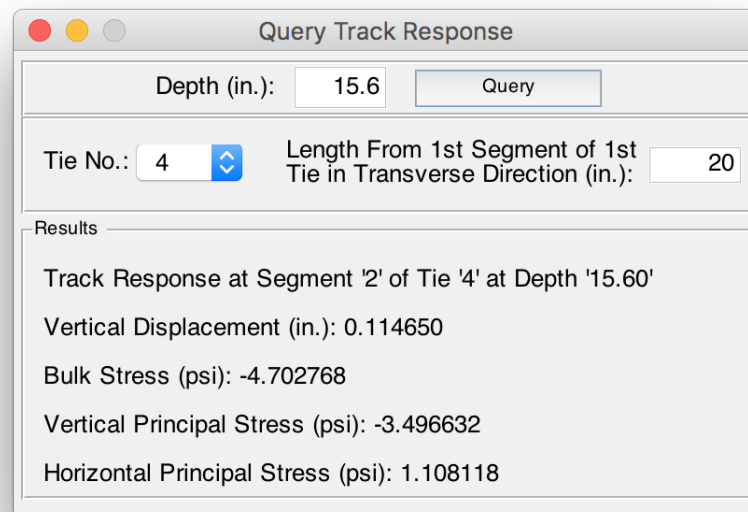
Figure 6.5: Query Track Response Feature in GEOTRACK-2016

*Negative stress values represent compression and downward deflections are represented with positive values.

6.4 Enhanced Visualization Module

One of the major enhancements in GEOTRACK-2016 as far as data processing is concerned, involves the ability to plot trends in the track response values. This is particularly useful for practicing engineers as this eliminates the need for going through the entire output file while seeking one particular response value. GEOTRACK-2016 generates two different windows after execution; these windows are for plots of track response values for the (1) Superstructure and the (2) Substructure.

Output Plots for the Track Superstructure The output plots generated by GEOTRACK-2016 for Superstructure are listed below.

1. Tie Number vs. Rail Deflection
2. Tie Number vs. Tie Deflection
3. Tie Number vs. Rail Bending Moment
4. Tie Number vs. Rail-Seat Reaction

The plots generated by GEOTRACK-2016 for the control section are presented in the following figures. Figure 6.6 shows the output plot with Tie Number along the x-axis and Rail and Tie Deflections along the y-axis. The figure shows close values for rail deflection and tie deflection which is expected because the rail is supported directly on top of the tie, with the stiffness at the point of contact represented by the fastener stiffness. The axle loads are applied at tie numbers 1, 5 and 6 for the control section. Accordingly, the deflection values can be observed to be larger at the points beneath the load application (See Figure 6.6). Also, an analysis segment in GEOTRACK consists of 11 ties (the center tie and 5 ties in each direction). Therefore, the value of rail and tie deflections are higher from the first to the sixth tie, the deflections then decrease when moving further away from the sixth tie. *Note that positive deflections correspond to downward movement.

Figure 6.7 shows the output plot with Tie Number along the x-axis and Rail-Seat Reaction along the y-axis for the control section (refer to Figure 4.1). The axle loads
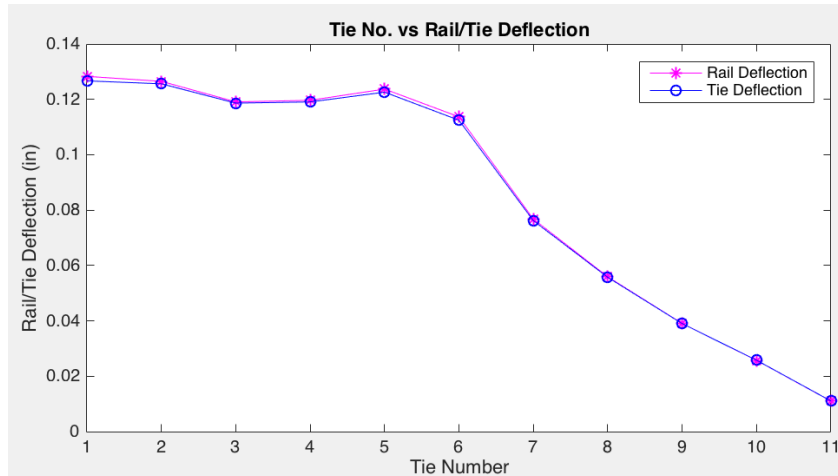
Figure 6.6: Output Plot for Tie No. vs. Rail/Tie Deflection

are applied on tie numbers 1, 5 and 6; and therefore, the values of rail seat reaction are higher at ties 1, 5 and 6. Similar plots for rail and tie bending moments can also be obtained using GEOTRACK-2016.
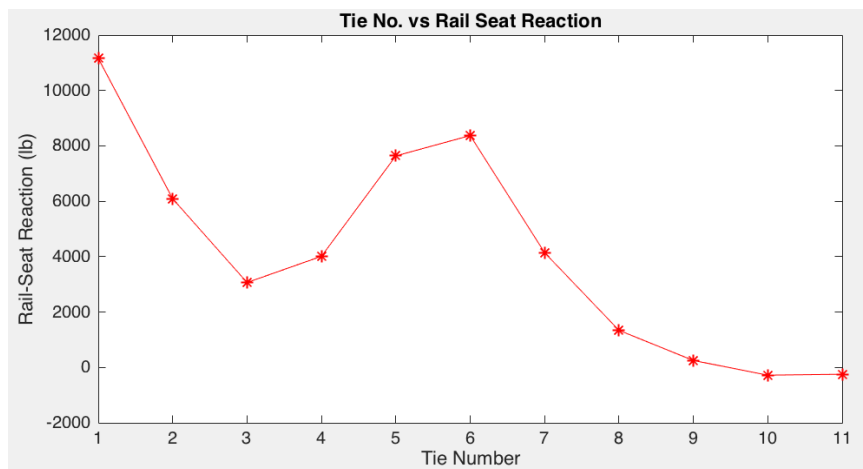
Figure 6.7: Output Plot for Tie No. vs Rail-Seat Reaction

Output Plots for the Track Substructure: The output plots generated by GEOTRACK-2016 for the track Substructure are:

1. Depth vs. Vertical Displacement

2. Depth vs. Bulk Stress

3. Depth vs. Maximum Principal Stress

4. Depth vs. Minimum Principal Stress

After execution of the program, GEOTRACK-2016 presents user with a window with radio-buttons for 'Tie Number' and check boxes for the 'Segment Number(s)'. The user can choose one Tie Number at a time to visually compare the response values under different segments of the tie. A drop-down menu for the 'Plot Type' is also presented. The following figures present the variation of different track response values in substructure with depth. In the case presented below, segments 2, 3 and 4 of Tie Number 1 are selected. Figure 6.8 shows the variation of Vertical Displacements with depth for the three selected segment numbers of the first tie. The graph shows a reduction in vertical displacement with depth. Similar plots for bulk stress, maximum and minimum stress can also be obtained from GEOTRACK-2016. Note that positive deflection values correspond to downward movement.
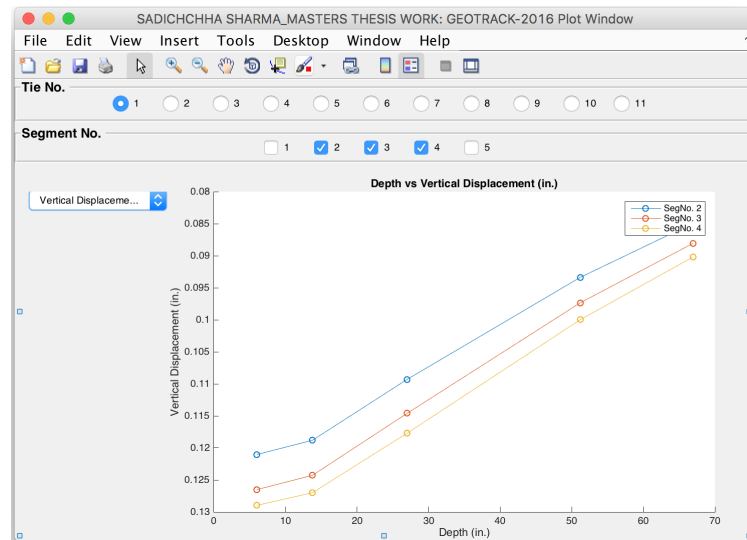

Figure 6.8: Output Plot for Depth vs. Vertical Displacement

6.5   Advantages of Mechanistic Analysis over Current Approach

This section presents some of the advantages that can be realized by practicing rail-road engineers by adopting a mechanistic analysis approach as in GEOTRACK-2016

compared to the currently used empirical design approach.

The average ballast pressure can be calculated using Equation 6.4.

$$P_a = \frac{\left[2\,P(1 + \frac{IF}{100})(\frac{DF}{100})\right]}{A} \tag{6.4}$$

For example, using a 36 $in.$ diameter wheel (D) (36000 lbs load (P)) at speed (V) of 55 mph and 7"×9" ×8'6" ties with a tie spacing of 21 $in.$, calculation of ballast pressure (P_a) can be done as follows.

Impact factor (IF):

$$IF = \frac{33V}{100D} = \frac{33 \times 55}{100 \times 36} = 50$$

Distribution Factor (DF):

For a tie spacing of 21 $in.$, 47% of axle load is assumed applicable to each tie on either side of the applied load [48]. The average ballast pressure at the base of tie calculated using the AREMA method:

$$P_a = \frac{\left[2\,P(1 + \frac{IF}{100})(\frac{DF}{100})\right]}{A} = \frac{\left[2 \times 3600(1 + \frac{50}{100})(\frac{47}{100})\right]}{102 \times 9} = 55\,psi$$

When the same parameters are input in GEOTRACK-2016, and the average ballast pressure is calculated, the value is about 59.33 psi. This difference can be attributed to the difference in analysis method (empirical vs. mechanistic).

The calculation of ballast pressure at the base of tie using Equation 6.4 does not consider the modulus values and Poisson's ratio of the substructure layers, and the size and flexural rigidity of the rail. In addition, the distribution factor also does not consider different kinds of support conditions. This implies that a change in substructure material properties and rail properties would have no effect on the average ballast pressure calculated which is not realistic. From the AREMA method, the ballast depth for design is calculated using Equation 6.5 [48].

$$h = 16.8 \, \frac{P_a{}^{4/5}}{P_c} \tag{6.5}$$

where h is the ballast depth and P_c is the bearing pressure on subgrade.

The ballast depth calculated using this approach by AREMA is empirical in nature, and thus does not account for different parameters which affect the ballast pressure. Therefore, a mechanistic analysis approach is required for accurate and more realistic prediction of track response parameters under loading. Incorporation of an easy-to-use track analysis software into practice is a natural approach to improve the accuracy of response predictions in the field.

6.6   Summary

This chapter presented details of different features implemented in GEOTRACK-2016 incorporated to enhance the analysis capabilities. Calculation of rail bending stresses, incorporation of Talbot's dynamic amplification factor for loading, and the ability to query track response at desired points of interest in the substructure along with the enhanced visualization module are the enhanced analysis capabilities implemented in GEOTRACK-2016. The advantage of a mechanistic analysis over an empirical one was also discussed. The next chapter presents a summary of findings from this Mater's thesis effort and presents recommendations for future research.

CHAPTER 7

SUMMARY OF FINDINGS AND RECOMMENDATIONS FOR FUTURE RESEARCH

7.1   Summary of Findings

Mechanistic analysis of railway track structure response under loading helps to accomplish adequate structural and functional design of track components, and is therefore essential. Mechanistic track analysis programs can serve as a link between the state of art in research and the state of practice in railroad engineering. Therefore, in this research effort, an advanced, easy-to-use track analysis program, GEOTRACK-2016 was developed for use by both researchers and practitioners working in the field of railroad engineering.

Results produced by GEOTRACK-2016 were compared with those from the original version of the software to ensure the accuracy of all modifications. A parametric analysis was subsequently carried out to quantify the effects of different track design parameters on overall track modulus. The results of the parametric study complied with the trends reported in published literature.

The other objective of this Master's thesis was to evaluate the limitations introduced to analysis results when layered elastic theory is used for the analysis of railroad track structures. For this purpose, a commercially available Finite Element package, ABAQUS, was used to model the control section. The track responses under loading were compared under similar loading configurations to those analyzed using GEOTRACK-2016. Careful comparison of the track response values using Layered

Elastic and Finite-Element based analysis approaches revealed close match between the results. Therefore, it was concluded that although Layered Elastic analysis uses several simplifying assumptions, the predicted track response values match reasonably well with those predicted using ore accurate analysis method. These comparisons established GEOTRACK-2016 as an accurate, easy-to-use track analysis tool. An intuitive Graphical user Interface (GUI) was also developed for GEOTRACK-2016 to facilitate easy adoption by practicing engineers. Detailed discussions on different tasks undertaken during this research effort were presented in this Master's thesis document. Incorporation of enhanced data visualization and plotting abilities and incorporation of a parametric analysis mode into the GUI to facilitate side-by-side comparison of different design and construction alternatives are important additional features of GEOTRACK-2016. This newly developed software also includes the ability to query track response values at different points of interest within the track structure and enhanced analysis capabilities such as the option to calculate rail bending stresses and the ability to incorporate dynamic load amplification factors resulting from different train speeds and wheel diameters.

7.2 Recommendations for Future Research

Although this Master's thesis effort evaluated different assumptions inherent to the theory of Layered Elastic analysis through the development of an improved software program for railroad track analysis, there are several avenues for further modifications and enhancements to the software's capabilities. Some of these future research recommendations are enumerated as follows.

1. GEOTRACK-2016 is a software for analysis of railroad track structures under vertical quasi-dynamic loads and does not incorporate the effects of dynamic loads (other than the Talbot's dynamic amplification factor). Incorporation of dynamic loads in the software can be an improvement over the current version.

This can be achieved through the incorporation of time aspect of loading and inertia effects of individual layers.

2. GEOTRACK-2016 can only predict the elastic response of track structures. Incorporation of a permanent deformation model to predict plastic deformations can be incorporated to later versions of this software. Some of the models that relate the cumulative plastic strain with the number of repeated load applications are the Power model, Power-rate model, and Semi-Log model [66], which can be incorporated as additional modules in GEOTRACK-2016. These models will essentially use the elastic strain levels in individual layers to predict the permanent deformation accumulation, which, in turn, can be used to predict the remaining life for a track structure.

3. As a result of the assumptions associated with multilayer elastic theory, GEOTRACK-2016 cannot model spatial variations within a particular substructure layer or geometric variations such as those introduced by track shoulders and/or substructure drainage features. Utilizing the finite-element method for predicting the response of the track substructure can help overcome these limitations. A simple finite-element analysis of the rails and ties (similar to KENTRACK) can also help incorporate the irregularity in the shape of rail and tie materials.

4. Modification of the algorithm of GEOTRACK-2016 code to account for different stress-dependent resilient-modulus models like the Uzan model [67] and Universal model [68] can mark significant further improvements. At present, the software considers only the stress-dependent $k - \theta$ model [69], which relates the resilient modulus of a layer to the bulk stress (first stress invariant; sum of principal stresses), but does not account for stress-softening geomaterial behavior under shear.

REFERENCES

[1] . The 1900s, Railroads In The 20th Century. *http://www.american-rails.com, March 2016.*

[2] Railroading In The 1950s, The Industry In Decline. *http://www.american-rails.com/1950s.html, July 2016.*

[3] Moving the American Auto Industry on Steel Wheels. *AAR State of the Industry 2016 Report 2 C3A2, August 2016.*

[4] 2010 and Beyond: A Vision of America's Transportation Future. *21st Century Freight Mobility*, NCHRP Project 20-24(33) A, August 2004.

[5] Neff J. and Dickens M. *2013 Public Transportation Fact Book.* American Public Transportation Association, 2013.

[6] Freight Railroads Help Reduce Greenhouse Gas Emissions. *Association of American Railroads, April 2016.*

[7] USA Today. *http://www.usatoday.com/story/travel/destinations/2015/11/09/florida-express-train-travel-miami-orlando/75179722/, August 2016.*

[8] Chicago Region Environmental and Transportation Efficiency Program. *http://www.createprogram.org/, August 2016.*

[9] Rose J. G., Liu S. and Souleyrette R.R. KENTRACK 4.0: A Railway Trackbed Structural Design Program. *2014 Joint Rail Conference*, April 2014.

[10] Southgate H. F., Deen R.C, Cain D.H. and Mayes J.G. Modifications To Chevron N-Layer Computer Program. *Kentucky Transportation Research Program, University of Kentucky in cooperation with Transportation Cabinet Commonwealth of Kentucky and Federal Highway Administration U.S. Department of Transportation*, 1987.

[11] Sommer P Claessen A.I.M., Edwards J.M. and Uge P. Asphalt Pavement Design - The Shell Method. *Volume I of proceedings of 4th International Conference on Structural Design of Asphalt Pavements, Ann Arbor, Michigan*, 1977.

[12] Gordon F. Hayhoe. LEAF A New Layered Elastic Computational Program For FAA Pavement Design and Evaluation Procedures. *The 2002 Federal Aviation Administration Airport Technology Transfer Conference*, 2002.

[13] Robnett Q. L., Thompson M.R., Knutson R.M. and Tayabji S.D. Development of a structural model and materials evaluation procedures. *Development of a structural model and materials evaluation procedures*, 1975.

[14] Chang C.S., Clement W. A. and Selig E.T. GEOTRACK Model For Railroad Track Performance. *Journal of the Geotechnical Engineering Division*, pages 1200 – 1218, November 1980.

[15] Kennedy C. J. and Prause R. H. Development of Multilayer Analysis Model for Tie-Ballast Track structures. *Federal Railroad Administration, Report FRA/ORD-77/29*, June 1977.

[16] Selig E.T. and Waters J.M. Track Geotechnology and Substructure Management. *Thomas Telford*, 1994.

[17] Stewart H.E. User's Manual for GEOTRACK Computer Program (VAX Version). 1988.

[18] Li D., Hyslip J., Sussman T., and Chrismer S. *Railway Geotechnics*. 2015.

[19] . Questions About the Railway Association. *http://http://www.rta.org/faqs, September 2016*.

[20] Nicks J.E. The Bump at the End of the Railway Bridge. 2009.

[21] Selig E.T. and Li D. Track Modulus: Its Meaning and Factors Influencing It. *Transportation Research Record 1470*, pages 47–54, 1994.

[22] Cai Z., Raymond G.P. and Bathurst R.J. Estimate of Static Track Modulus Using Elastic Foundation Models. *Transportation Research Record 1470*, pages 65–72, 1994.

[23] Adegoke-Anthony C. W. Elastic and Inelastic Deformation Response of Track Structures under Train Loads. *ProQuest Dissertations and Theses (PQDT)*, 1978.

[24] Sadeghi J. Investigation of Characteristics and Modelling of Railway Track System. *Doctor of Philosophy thesis, Department of Civil and Mining Engineering, University of Wollongong*, 1997.

[25] Timoshenko S. *History of strength of materials*. 1953.

[26] Esveld C. Modern Railway Track. *MRT-Productions*, 2001.

[27] Skoglund A.K. A Study of Some Factors in Mechanistic Railway Track Design. March 2002.

[28] Meleshko V.V. Selected topics in the history of the two-dimensional biharmonic problem. *Department of Theoretical and Applied Mechanics*, 2003.

[29] Vasani P.C. Interactive Analysis Models For Soil and Structures.

[30] Hamarat M.A., Calik K.U.H. and Orakden E. Seismic Analysis of Structures Resting on Two Parameter Elastic Foundation.

[31] Sarvesh Chandra. Modelling of Soil Behavior. *Indian Institute of Technology Kanpur*, 2014.

[32] Burmister D. M. Theory of Stresses and Displacements in Layered Systems and Application to the Design of Airport Runways. *Highway Research Board Proceedings Vol. 23*, pages 126–144, 1943.

[33] Khazanovich L. and Wang Q. MnLayer High-Performance Layered Elastic Analysis Program. *Transportation Research Record: No. 2037, Transportation Research Board of the National Academies, Washington, D.C., 2007*, pages 63–75, 2007.

[34] Liu S. KENTRACK 4.0: Railway trackbed structural design program. 2013.

[35] Rose J. G. and Konduri K.C. KENTRACK: A Railway trackbed structural design and analysis program. 2003.

[36] Thambiratnam D. and Zhuge Y. Dynamic Analysis of Beams on an Elastic Foundation Subjected to Moving Loads. *Journal of Sound and Vibration*, pages 149–169, 1996.

[37] Costa D'Aguiar S. Arlaud E. and Balmes E. Receptance of Railway Tracks at Low Frequency: Numerical and Experimental Approaches. *Transportation Geotechnics*, 2016.

[38] Hall Lars. Simulations and Analysis of Train-Induced Ground Vibrations in Finite Element Models. *Soil Dynamics and Earthquake Engineering 23.5*, pages 403–413, 2003.

[39] Araujo Nuno Miguel Faria. High Speed Trains on Ballasted Railway Track. *PhD Thesis*, 2011.

[40] Verlinden O. Kouroussis G. and Conti C. Free Field Vibrations Caused by High Speed Lines. *Soil Dynamics and Earthquake Engineering 31.4*, pages 692–707, 2011.

[41] Ju S.H. and Li H.C. Dynamic Interaction Analysis of Trains Moving on Embankments During Earthquakes. *Journal of Sound and Vibration 330.22*, pages 5322–5332, 2011.

[42] Banimahd M and Woodward P.K. 3-Dimensional Finite Element Modeling of Railway Transitions. *Proceedings of Ninth International Conference on Railway Engineering*, 2007.

108

[43] Fortunato E. Paixao A. and Calcada R. The effect of Differential Settlements on the Dynamic Response of the Train-Track System: A Numerical Study. *Engineering structures*, pages 216–224, 2015.

[44] Gardien W. and Stuit H.G. Modelling of Soil Vibrations from Railway Tunnels. *Journal of Sound and Vibration 267.3*, pages 605–619, 2003.

[45] Yang Y.B. and Hung H.H. A 2.5 D Finite/Infinite Element Approach for Modelling ViscoElastic Bodies Subjected to Moving Loads. *International Journal for Numerical Methods in Engineering 51.11*, pages 1317–1336, 2001.

[46] Hung H.H. Yang Y.B. and Chang D.W. Train-Induced Wave Propagation in Layered Soils using Finite/Infinite Element Simulation. *Soil Dynamics and Earthquake Engineering 23*, pages 263–278, 2003.

[47] A.G. Correia, J. Cunha, J. Marcelino, J. Varandas, Z. Dimitrovova, A. Antao, and M.G. Silva. Dynamic Analysis of Rail Track for High Speed Trains. 2D Approach. *5th Intl Worksop on Application of Computational Mechanics on Geotechnical Engineering*, 2007.

[48] Manual for Railway Engineering. *Volume 1, Track*, 2010.

[49] Feng H. 3-D models of Railway Track for Dynamic Analysis. 2011.

[50] Ioannides A.M. and Khazanovich L. General Formulation for Multilayered Pavement Systems. *Journal of transportation engineering 124.1*, pages 82–90, 1998.

[51] Warren H. and Dieckmann W.L. Numerical Computation of Stresses and Strains in a Multiple-Layered Asphalt Pavement System. 1963.

[52] Michelow J. Analysis of Stresses and Displacements in an N-Layered Elastic System Under a Load Uniformly Distributed on a Circular Area. *California Research Corporation, Richmond, California*, 1963.

[53] Module 4: Boundary Value Problems in Linear Elasticity. *http://web.mit.edu*, August 2016.

[54] Love Augustus Edward Hough. A Treatise on the Mathematical Theory of Elasticity. *Vol 1. Cambridge University Press*, 2013.

[55] David G Weinman. *VAX FORTRAN*. Boston Boyd And Fraser Publication Co, 1986.

[56] Copyright 2016 The Eclipse Foundation. All Rights Reserved. *http://www.eclipse.org/photran/, April 2016*.

[57] Indraratna B. Ngo T. N. and Rujikiatkamjorn C. DEM Simulation of the Behaviour of Geogrid Stabilised Ballast Fouled with Coal. *Computers and Geotechnics 55*, pages 224–231, 2014.

[58] Yu Q. Wang Z., Jing G. and Yin H. Analysis of ballast Direct Shear Tests by Discrete Element Method under Different Normal Stress. *Measurement 63*, pages 17–24, 2014.

[59] Yuan Z. Stark T.D., Swan R.H. Ballast Direct Shear testing. *Proceedings of the 2014 Joint Rail Conference JRC*, 2014.

[60] Mishra D., Tutumluer E., Boler H., Hyslip J. and Sussman T. Railroad Track Transitions with Multidepth Deflectometers and Strain Gauges. *Transportation Research Record: Journal of the Transportation Research Board 2448*, pages 105–114, 2014.

[61] Simulia. ABAQUS. *"6.10-2, Users manual." Providence, RI, USA: HKS Inc*, 2010.

[62] Hyslip J.H. Boler H. Tutumluer E., Mishra D. and Hou W. Mitigation of Differential Movement at Railway Transitions for US High Speed Rail and Joint Passenger/Freight Corridors. *Final Report, US Department of Transportation Federal Railroad DOT/FRA/ORD-XX/XX*, 2015.

[63] Dupen B. Applied Strength of Materials for Engineering Technology. 2016.

[64] American Railway Engineering and Maintenance of Way Association. 2016 Manual for Railway Engineering. *https://www.arema.org/publications/mre, August 2016*.

[65] Edwards J.R. Conrad J.R. Brandon J.V.D., Dersch M.S. and Barkan C.P.L. Evaluation of Dynamic and Impact Wheel Load Factors and their Application for Design. *Transportation Research Board 93rd Annual Meeting*, 2013.

[66] Li Dingqing. Railway Track Granular Layer Thickness Design Based on Subgrade Performance under Repeated Loading. *ProQuest Dissertations and Theses (PQDT)*, 1994.

[67] Uzan J. Characterization of Granular Materials. *Transportation Research Record 1022*, pages 52–59, 1985.

[68] Witczak M.W. and Uzan J. The universal airport pavement design system. *Report I of V: granular material characterization, Department of Civil Engineering, University of Maryland, College Park, MD*, 1988.

[69] Hicks R.G. and Carl L.M. Factors Influencing the Resilient Response of Granular Materials. *Highway research record 345*, 1971.

[70] Maina J. and Matsui K. Elastic Multi-layered Analysis Using DE-Integration. *Research Institute for Mathematical Sciences, Kyoto University*, 2005.

[71] August 2016 www.math.odu.edu/ jhh/part10.PDF. Continuum Mechanics (Solids). *Old Dominion University*.

APPENDIX A

LAYERED ELASTIC THEORY: DERIVATION OF EQUATIONS

The multilayer theory developed by Burmister uses the equilibrium and compatibility equations from the theory of elasticity. Figure A.1 presents the schematic of a 3-layer track substructure illustrating the important layer properties used in the formulation of layered elastic theory. The equations comprising Layered Elastic Theory for the
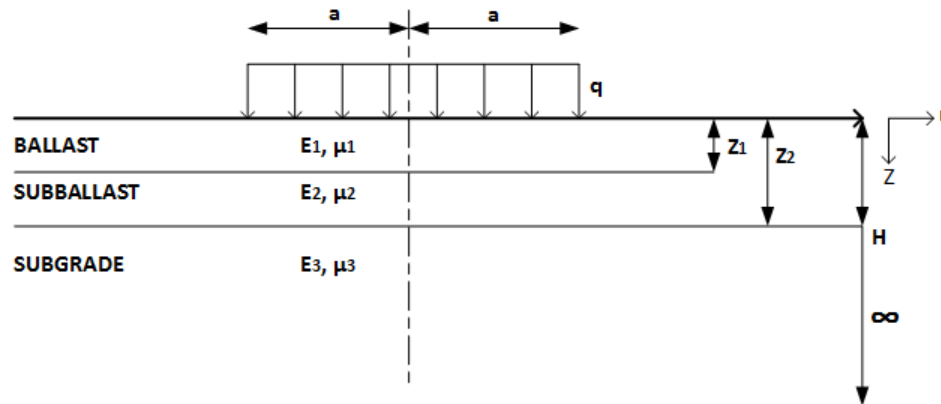
Figure A.1: Schematic of the Cross-Section of Track for Layered Elastic Model

infinitesimal block as shown in Figure A.2 are presented below [51, 52, 50]. In the form of cylindrical coordinates, the equilibrium equations for the infinitesimal block as shown in Figure A.2 can be derived as follows [70] .

Equilibrium Equations   In cylindrical coordinates, the equilibrium in the radial and transverse direction gives,
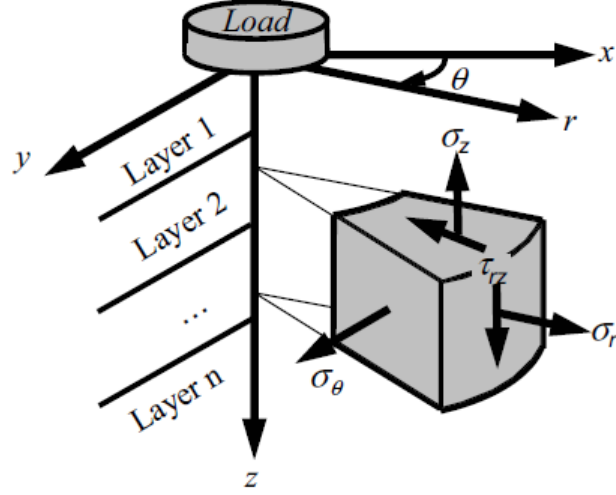
Figure A.2: Stresses Acting on an Element [34]

$$(\sigma_r + \frac{1}{2}\frac{\delta\sigma_r}{\delta r}\delta r)(r + \frac{1}{2}\delta r)\delta\theta\delta z - (\sigma_r - \frac{1}{2}\frac{\delta\sigma_r}{\delta r}\delta r)(r - \frac{1}{2}\delta r)\delta\theta\delta z +$$

$$(\tau_{rz} + \frac{1}{2}\frac{\delta\tau_{rz}}{\delta z}\delta z)\, r\delta r\delta\theta - (\tau_{rz} - \frac{1}{2}\frac{\delta\tau_{rz}}{\delta z}\delta z)r\delta r\delta\theta - \sigma_\theta\delta r\delta z\delta\theta = 0$$

or,

$$\sigma_r\delta r\delta\theta\delta z - \sigma_\theta\delta r\delta\theta\delta z + r\frac{\delta\sigma_r}{\delta r}\delta r\delta\theta\delta z = 0$$

$$\frac{\delta\sigma_r}{\delta r} + \frac{\delta\tau_{rz}}{\delta z} + \frac{\sigma_r - \sigma_\theta}{r} = 0 \tag{A.1}$$

Similarly, the equilibrium in the z-direction gives,

$$\frac{\delta\tau_{rz}}{\delta r} + \frac{\delta\sigma_z}{\delta z} + \frac{\tau_{rz}}{r} = 0 \tag{A.2}$$

Equation A.1 and A.2 are the equilibrium equations in cylindrical coordinates.

Hooke's Law   The Hooke's Law states that the deformation produced is proportional to the load producing it. It applies to any elastic body strained within its elastic limits. Consider the cylinder illustrated in Figure A.3 is in tension because of force F [71]. From Hooke's law, we have,
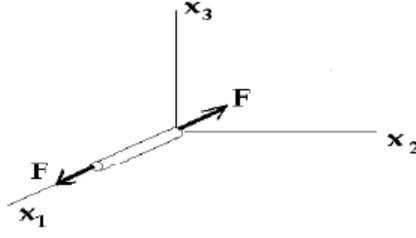
Figure A.3: Stress in a Cylinder [35]

$$\epsilon_{xx} = \frac{\sigma_{xx}}{E}, \ \epsilon_{yy} = \frac{-\nu\sigma_{xx}}{E}, \ \epsilon_{zz} = \frac{-\nu\sigma_{xx}}{E} \tag{A.3}$$

$$\epsilon_{yy} = \frac{\sigma_{yy}}{E}, \ \epsilon_{xx} = \frac{-\nu\sigma_{yy}}{E}, \ \epsilon_{zz} = \frac{-\nu\sigma_{yy}}{E} \tag{A.4}$$

$$\epsilon_{zz} = \frac{\sigma_{zz}}{E}, \ \epsilon_{xx} = \frac{-\nu\sigma_{zz}}{E}, \ \epsilon_{yy} = \frac{-\nu\sigma_{zz}}{E} \tag{A.5}$$

where ϵ represents the strain (the subscripts represent directions), σ is the stress (subscripts represent directions) and ν is the Poisson's ratio; i.e. $\frac{Lateral\ contraction}{Longitudinal\ extension}$. Thus, we have,

$$\epsilon_{xx} = \frac{\sigma_{xx}}{E} - \frac{\nu\sigma_{yy}}{E} - \frac{\nu\sigma_{zz}}{E}$$

$$= \frac{1}{\epsilon}[\sigma_x - \nu\sigma_x + \nu\sigma_x - \nu\sigma_y - \nu\sigma_z]$$

$$= \frac{1}{\epsilon}[\sigma_x + \nu\sigma_x - (\nu\sigma_x + \nu\sigma_y + \nu\sigma_z)] \tag{A.6}$$

$$\epsilon_{xx} = \frac{1}{\epsilon}[\sigma_x + \nu\sigma_x - \nu\phi] \qquad (since\ \phi = \sigma_x + \sigma_y + \sigma_z)$$

$$\&\quad \gamma_{xy} = \frac{\tau_{xy}}{G} = \frac{\tau_{xy}}{E/2(1+\nu)} = \frac{2(1+\nu)}{E}\tau_{xy}$$

So,

$$\epsilon_x = \frac{1}{E}[(1+\nu)\sigma_x - \nu\phi] \tag{A.7}$$

$$\epsilon_y = \frac{1}{E}[(1+\nu)\sigma_y - \nu\phi] \tag{A.8}$$

$$\epsilon_z = \frac{1}{E}[(1+\nu)\sigma_z - \nu\phi] \tag{A.9}$$

$$\gamma_{xy} = \frac{2(1+\nu)}{E}\tau_{xy} \tag{A.10}$$

$$\gamma_{yz} = \frac{2(1+\nu)}{E}\tau_{yz} \tag{A.11}$$

$$\gamma_{zx} = \frac{2(1+\nu)}{E}\tau_{zx} \tag{A.12}$$

Plane strain assumption is applied in situations where there is a cylindrical body with axis parallel to the z axis and loads are applied along the zdirection [71]. In the x-y plane, the body forces are assumed to be independent of z and solutions for the stresses, strains and displacements are assumed to be independent of z.

Compatibility Equations Since literature suggests that deriving the equations of compatibility in Cylindrical coordinates is a cumbersome process, the derivation of compatibility equations is first done for Cartesian coordinates. Because of axial symmetry in the problem, displacements in θ directions are not considered. Therefore, in Cartesian coordinates, the normal strains (ϵ_x, ϵ_y and ϵ_z) and shearing strains (γ_{xy}, γ_{yz} and γ_{zx}) can be written as Equation A.8 through Equation A.10. the three normal strains ϵ_x, ϵ_y, and ϵ_z and the shearing strains γ_{xy}, γ_{yz}, and γ_{zx} can be written as,

$$\begin{aligned}
\epsilon_x &= \frac{\delta u_x}{\delta x} \\
\epsilon_y &= \frac{\delta v_y}{\delta y} \\
\epsilon_z &= \frac{\delta w_z}{\delta z}
\end{aligned} \tag{A.13}$$

$$\begin{aligned}
\gamma_{xy} &= \frac{\delta u_x}{\delta y} + \frac{\delta v_y}{\delta x} \\
\gamma_{yz} &= \frac{\delta v_y}{\delta z} + \frac{\delta w_z}{\delta y} \\
\gamma_{zx} &= \frac{\delta u_x}{\delta z} + \frac{\delta w_z}{\delta x}
\end{aligned} \tag{A.14}$$

which gives, Differentiating the first equation of equation A.13 with respect to y and the second with respect to x and differentiating first equation of equation A.14 with respect to x,

$$\frac{\delta \epsilon_x}{\delta_y} = \frac{\delta^2 u_x}{\delta x \, \delta y} \Rightarrow \frac{\delta^2 \epsilon_x}{\delta y^2} = \frac{\delta^3 u_x}{\delta x \, \delta y^2}$$

$$\frac{\delta \epsilon_y}{\delta_x} = \frac{\delta^2 v_y}{\delta x \, \delta y} \Rightarrow \frac{\delta^2 \epsilon_y}{\delta x^2} = \frac{\delta^3 v_y}{\delta x^2 \, \delta y}$$

$$\frac{\delta \gamma_{xy}}{\delta x} = \frac{\delta^2 u_x}{\delta x \, \delta y} + \frac{\delta^2 v_y}{\delta x^2} \Rightarrow \frac{\delta^2 \gamma_{xy}}{\delta x \, \delta y} = \frac{\delta^3 u_x}{\delta x \, \delta y^2} + \frac{\delta^3 v_y}{\delta x^2 \, \delta y}$$

which means,

$$\frac{\delta^2 \gamma_{xy}}{\delta x \, \delta y} = \frac{\delta^2 \epsilon_x}{\delta y^2} + \frac{\delta^2 \epsilon_y}{\delta x^2} \tag{A.15}$$

Similarly,

$$\frac{\delta^2 \epsilon_x}{\delta y^2} + \frac{\delta^2 \epsilon_y}{\delta x^2} = \frac{\delta^2 \gamma_{xy}}{\delta x \, \delta y} \tag{A.16}$$

$$\frac{\delta^2 \epsilon_y}{\delta z^2} + \frac{\delta^2 \epsilon_z}{\delta y^2} = \frac{\delta^2 \gamma_{yz}}{\delta y \, \delta z} \tag{A.17}$$

$$\frac{\delta^2 \epsilon_z}{\delta x^2} + \frac{\delta^2 \epsilon_x}{\delta z^2} = \frac{\delta^2 \gamma_{zx}}{\delta z \, \delta x} \tag{A.18}$$

Similar differentiation and manipulation of variable gives,

$$\frac{\delta^2 \epsilon_x}{\delta y \, \delta z} = \frac{\delta^3 u_x}{\delta x \, \delta y \, \delta z}$$

$$\frac{\delta \gamma_{yz}}{\delta x} = \frac{\delta^2 v_y}{\delta z \, \delta x} + \frac{\delta^2 w_z}{\delta y \, \delta x}$$

Differentiating the equation with respect to x,

$$\frac{\delta}{\delta x} \left(\frac{\delta \gamma_{yz}}{\delta x} \right) = \frac{\delta^2 \gamma_{yz}}{\delta x^2} = \frac{\delta^3 v_y}{\delta x^2 \, \delta z} + \frac{\delta^3 w_z}{\delta x^2 \, \delta y}$$

So,

$$\frac{\delta}{\delta x} \left(\frac{\delta \gamma_{xz}}{\delta y} \right) = \frac{\delta^3 u_x}{\delta x \, \delta y \, \delta z} + \frac{\delta^3 w_z}{\delta x^2 \, \delta y}$$

$$\frac{\delta}{\delta x}\left(\frac{\delta \gamma_{xy}}{\delta y}\right) = \frac{\delta^3 v_x}{\delta x\, \delta y\, \delta z} + \frac{\delta^3 v_y}{\delta x^2\, \delta z}$$

Then,

$$-\frac{\delta}{\delta x}\left(\frac{\delta \gamma_{yz}}{\delta x}\right) + \frac{\delta}{\delta x}\left(\frac{\delta \nu_{xz}}{\delta y}\right) + \frac{\delta}{\delta x}\left(\frac{\delta \nu_{xy}}{\delta z}\right) = \frac{2\delta^3 v_x}{\delta x\, \delta y\, \delta z} + 0 + 0$$

and,

$$\frac{2\delta^2 \epsilon_x}{\delta y\, \delta z} = \frac{2\delta^3 u_x}{\delta x\, \delta y\, \delta z}$$

Similarly,

$$\frac{2\delta^2 \epsilon_x}{\delta y\, \delta z} = \frac{\delta}{\delta x}\left(-\frac{\delta \gamma_{yz}}{\delta x} + \frac{\delta \gamma_{xz}}{\delta y} + \frac{\delta \gamma_{xy}}{\delta z}\right) \tag{A.19}$$

$$\frac{2\delta^2 \epsilon_y}{\delta x\, \delta z} = \frac{\delta}{\delta y}\left(\frac{\delta \gamma_{yz}}{\delta x} - \frac{\delta \gamma_{xz}}{\delta y} + \frac{\delta \gamma_{xy}}{\delta z}\right) \tag{A.20}$$

$$\frac{2\delta^2 \epsilon_z}{\delta x\, \delta y} = \frac{\delta}{\delta z}\left(\frac{\delta \gamma_{yz}}{\delta x} + \frac{\delta \gamma_{xz}}{\delta y} - \frac{\delta \gamma_{xy}}{\delta z}\right) \tag{A.21}$$

Replace $\epsilon_x, \epsilon_y, \epsilon_z, \nu_{xy}$ from Equation A.16,

$$\frac{\delta^2}{\delta y^2}\left[\frac{1}{E}(1+\nu)\sigma_x - \nu\phi\right] + \frac{\delta^2}{\delta x^2}\left[\frac{1}{E}(1+\nu)\sigma_y - \nu\phi\right] = \frac{\delta^2}{\delta x\, \delta y}[\gamma_{xy}]$$

or,

$$\frac{1}{E}(1+\nu)\frac{\delta^2\, \sigma_x}{\delta y^2} - \frac{\nu\delta^2\phi}{\delta y^2} + \frac{1}{E}(1+\nu)\frac{\delta^2\sigma_y}{\delta x^2} - \frac{\nu\delta^2\phi}{\delta x^2} = \frac{\delta^2}{\delta x\delta y}\left[\frac{2(1+\nu)}{E}\tau_{xy}\right]$$

or,

$$\frac{1}{E}(1+\nu)\frac{\delta^2\sigma_x}{\delta y^2} + \frac{1}{E}(1+\nu)\frac{\delta^2\sigma_y}{\delta x^2} - \frac{\nu\delta^2\phi}{\delta y^2} - \frac{\nu\delta^2\phi}{\delta x^2} = \frac{2(1+\nu)}{E}\frac{\delta^2}{\delta x\, \delta y}\tau_{xy}$$

Therefore,

$$(1+\nu)\left(\frac{\delta^2\sigma_x}{\delta y^2} + \frac{\delta^2\sigma_y}{\delta x^2}\right) - \nu\left(\frac{\delta^2\phi}{\delta y^2} + \frac{\delta^2\phi}{\delta x^2}\right) = 2(1+\nu)\frac{\delta^2\tau_{xy}}{\delta x\delta y} \tag{A.22}$$

We have,

$$\frac{\delta \tau_{xy}}{\delta x} + \frac{\delta \tau_{yz}}{\delta z} = -\frac{\delta \sigma_y}{\delta y} \tag{A.23}$$

$$\frac{\delta \tau_{yz}}{\delta y} + \frac{\delta \tau_{zx}}{\delta x} = -\frac{\delta \sigma_z}{\delta z} \tag{A.24}$$

$$\frac{\delta\tau_{xy}}{\delta y} + \frac{\delta\tau_{xz}}{\delta z} = -\frac{\delta\sigma_x}{\delta x} \tag{A.25}$$

Differentiating Equation A.23 with respect to y,

$$\frac{\delta^2\tau_{xy}}{\delta x\,\delta y} = -\frac{\delta^2\sigma_y}{\delta y^2} - \frac{\delta^2\tau_{yz}}{\delta y\,\delta z} \tag{A.26}$$

Differentiating Equation A.25 with respect to x,

$$\frac{\delta^2\tau_{xy}}{\delta x\,\delta y} = -\frac{\delta^2\sigma_x}{\delta x^2} - \frac{\delta^2\tau_{xz}}{\delta z\,\delta x} \tag{A.27}$$

Adding Equation A.23 and Equation A.25,

$$2\frac{\delta^2\tau_{xy}}{\delta x\,\delta y} = -\frac{\delta^2\sigma_y}{\delta y^2} - \frac{\delta^2\sigma_x}{\delta x^2} - \frac{\delta}{\delta z}\Big(\frac{\delta\tau_{yz}}{\delta y} + \frac{\delta\tau_{xz}}{\delta z}\Big) \tag{A.28}$$

From Equation A.24,

$$2\frac{\delta^2\tau_{xy}}{\delta x\,\delta y} = -\Big[\frac{\delta^2\sigma_x}{\delta x^2} + \frac{\delta^2\sigma_y}{\delta y^2} - \frac{\delta^2\sigma_z}{\delta z^2}\Big] \tag{A.29}$$

Replace Equation A.28 in Equation A.22,

$$\begin{aligned}
&(1+\nu)\Big(\frac{\delta^2\sigma_x}{\delta x^2} + \frac{\delta^2\sigma_y}{\delta y^2}\Big) - \nu\Big(\frac{\delta^2\phi}{\delta x^2} + \frac{\delta^2\phi}{\delta y^2}\Big) - (1+\nu)\Big[-\frac{\delta^2\sigma_x}{\delta x^2} + \frac{\delta^2\sigma_y}{\delta y^2} - \frac{\delta^2\sigma_z}{\delta z^2}\Big] \\
&(1+\nu)\Big(\frac{\delta^2\sigma_x}{\delta x^2} + \frac{\delta^2\sigma_y}{\delta y^2} + \frac{\delta^2\sigma_x}{\delta x^2} + \frac{\delta^2\sigma_y}{\delta y^2} - \frac{\delta^2\sigma_z}{\delta z^2}\Big) - \nu\Big(\frac{\delta^2\phi}{\delta x^2} + \frac{\delta^2\phi}{\delta y^2}\Big) = 0
\end{aligned} \tag{A.30}$$

$$\begin{aligned}
(1+\nu)\Big[\frac{\delta^2\sigma_x}{\delta x^2} + \frac{\delta^2\sigma_y}{\delta x^2} + \frac{\delta^2\sigma_z}{\delta x^2} - \frac{\delta^2\sigma_z}{\delta x^2} + \frac{\delta^2\sigma_y}{\delta y^2} + \frac{\delta^2\sigma_z}{\delta y^2} - \frac{\delta^2\sigma_z}{\delta y^2} + \frac{\delta^2\sigma_x}{\delta y^2} - \frac{\delta^2\sigma_z}{\delta z^2}\Big] - \nu\Big(\frac{\delta^2\phi}{\delta x^2} + \\
\frac{\delta^2\phi}{\delta y^2} + \frac{\delta^2\phi}{\delta z^2} - \frac{\delta^2\phi}{\delta z^2}\Big) = 0
\end{aligned}$$

By mathematical manipulation in the equation above,

$$(1+\nu)\Big[\nabla^2\phi - \nabla^2\sigma_z - \frac{\delta^2\phi}{\delta z^2}\Big] - \nu\Big[\nabla^2\phi - \frac{\delta^2\phi}{\delta z^2}\Big] = 0 \tag{A.31}$$

From Equation A.31,

$$\nabla^2\phi - \nabla^2\sigma_z - \frac{\delta^2\phi}{\delta z^2} - \nu\nabla^2\sigma_z = 0 \tag{A.32}$$

where, ∇^2 is the Laplace Operator represented as $\nabla^2 = (\frac{\delta^2}{\delta x^2} + \frac{\delta^2}{\delta y^2} + \frac{\delta^2}{\delta z^2})$ and ϕ is the bulk stress represented as $\phi = \sigma_x + \sigma_y + \sigma_z$.

$$\nabla^2 = (\frac{\delta^2}{\delta x^2} + \frac{\delta^2}{\delta y^2} + \frac{\delta^2}{\delta z^2})$$

and

$$\phi = \sigma_x + \sigma_y + \sigma_z$$

Similarly replace $\epsilon_x, \epsilon_y, \epsilon_z$ ... in Equation A.17,

$$\frac{\delta^2\epsilon_y}{\delta z^2} + \frac{\delta^2\epsilon_z}{\delta y^2} = \frac{\delta^2\gamma_{yz}}{\delta y.\delta z}$$

$$\frac{\delta^2}{\delta z^2}[\frac{1}{E}(1+\nu)\sigma_y - \nu\phi] + \frac{\delta^2}{\delta y^2}[\frac{1}{E}(1+\nu)\sigma_z - \nu\phi] = \frac{\delta^2}{\delta y.\delta z}[\frac{2(1+\nu)}{E}\tau_{yz}]$$

or,

$$\frac{1}{E}(1+\nu)\frac{\delta^2\sigma_y}{\delta z^2} + \frac{1}{E}(1+\nu)\frac{\delta^2\sigma_z}{\delta Y^2} - \frac{1}{E}\nu\frac{\delta^2\phi}{\delta z^2} - \frac{1}{E}\nu\frac{\delta^2\phi}{\delta y^2} = \frac{2(1+\nu)}{E}\frac{\delta^2}{\delta y.\delta z}\tau_{yz}$$

or,

$$(1+\nu)(\frac{\delta^2\sigma_y}{\delta z^2} + \frac{\delta^2\sigma_z}{\delta Y^2}) - \nu(\frac{\delta^2\phi}{\delta z^2} + \frac{\delta^2\phi}{\delta y^2}) = 2(1+\nu)\frac{\delta^2\tau_{yz}}{\delta y.\delta z}$$

Similarly,

$$\nabla^2\phi - \nabla^2\sigma_x - \frac{\delta^2\phi}{\delta x^2} - \nu\nabla^2\sigma_x = 0 \tag{A.33}$$

and

$$\nabla^2\phi - \nabla^2\sigma_y - \frac{\delta^2\phi}{\delta y^2} - \nu\nabla^2\sigma_y = 0 \tag{A.34}$$

Adding equations Equation A.32, Equation A.33 and Equation A.34, gives

$$\nabla^2\phi - \nabla^2\sigma_z - \frac{\delta^2\phi}{\delta z^2} - \nu\nabla^2\sigma_z + \nabla^2\phi - \nabla^2\sigma_x - \frac{\delta^2\phi}{\delta x^2} - \nu\nabla^2\sigma_x + \nabla^2\phi -$$

$$\nabla^2\sigma_y - \frac{\delta^2\phi}{\delta y^2} - \nu\nabla^2\sigma_y = 0$$

$$3\nabla^2\phi - \nabla^2\sigma_z - \nabla^2\sigma_x - \nabla^2\sigma_y - \frac{\delta^2\phi}{\delta z^2} - \frac{\delta^2\phi}{\delta y^2} - \frac{\delta^2\phi}{\delta x^2} - \nu\nabla^2\sigma_z - \nu\nabla^2\sigma_x - \nu\nabla^2\sigma_y = 0$$

$$3\nabla^2\phi - \nabla^2\phi - \nabla^2\phi - \nu\nabla^2\phi = 0$$

$$\nabla^2\phi - \nu\nabla^2\phi = 0$$

$$(1 - \nu)\nabla^2\phi = 0$$

Since ν (Poisson's ratio) can never be equal to 1,

$$\nabla^2\phi = 0 \tag{A.35}$$

Beltrami-Mitchell Equations   For the body considered in Figure A.2, the Beltrami-Mitchell equation [53] can be derived as follows. Using Equation A.35 in Equation A.32,

$$\nabla^2\sigma_z + \frac{\delta^2\phi}{\delta z^2} + \nu\nabla^2\sigma_z = 0$$

$$(1 + \nu)\nabla^2\sigma_z + \frac{\delta^2\phi}{\delta z^2} = 0 \tag{A.36}$$

Similarly, we get,

$$(1 + \nu)\nabla^2\sigma_x + \frac{\delta^2\phi}{\delta x^2} = 0 \tag{A.37}$$

$$(1 + \nu)\nabla^2\sigma_y + \frac{\delta^2\phi}{\delta y^2} = 0 \tag{A.38}$$

Substitute Equation A.7 through Equation A.12 in Equation A.19 through Equation A.21,

$$\frac{2\delta^2 \epsilon_x}{\delta y \, \delta z} = \frac{\delta}{\delta x}(-\frac{\delta \nu_{yz}}{\delta x} + \frac{\delta \nu_{xz}}{\delta y} + \frac{\delta \nu_{xy}}{\delta z})$$

which results in,

$$\frac{2\delta^2 \epsilon_x}{\delta y \delta z}[\frac{1}{E}[(1+\nu)\sigma_x - \nu\phi]] = -\frac{2\delta^2}{\delta x^2}(1+\nu)\tau_{yz} + \frac{2\delta^2}{\delta x \delta y}(1+\nu)\tau_{zx} - \frac{2\delta^2}{\delta x \delta z}(1+\nu)\tau_{xy}$$

$$(1+\nu)\frac{\delta^2 \sigma_x}{\delta y \delta z} - \frac{\nu \delta^2 \phi}{\delta y \delta z} = (1+\nu)[-\frac{\delta^2}{\delta x^2}\tau_{yz} + \frac{\delta^2}{\delta x.\delta y}\tau_{zx} + \frac{\delta^2}{\delta x \delta z}\tau_{xy}]$$

$$(1+\nu)\frac{\delta^2 \sigma_x}{\delta y \delta z} - \nu\frac{\delta^2 \phi}{\delta y \delta z} = (1+\nu)[-\frac{\delta^2 \tau_{yz}}{\delta x^2} - \frac{\delta^2 \tau_{yz}}{\delta y^2} - \frac{\delta^2 \sigma_z}{\delta z \delta y} - \frac{\delta^2 \tau_{yz}}{\delta z^2} - \frac{\delta^2 \sigma_y}{\delta y \delta z}]$$

$$(1+\nu)\frac{\delta^2 \sigma_x}{\delta y \delta z} - \nu\frac{\delta^2 \phi}{\delta y \delta z} + (1+\nu)\frac{\delta^2 \tau_{yz}}{\delta x^2} + (1+\nu)\frac{\delta^2 \tau_{yz}}{\delta y^2} + (1+\nu)\frac{\delta^2 \sigma_z}{\delta y \delta z} +$$

$$(1+\nu)\frac{\delta^2 \tau_{yz}}{\delta z^2} + (1+\nu)\frac{\delta^2 \sigma_y}{\delta y \delta z} = 0$$

$$(1+\nu)\frac{\delta^2 \phi}{\delta y \, \delta z} - \frac{\nu \delta^2 \phi}{\delta y \, \delta z} + (1+\nu)\nabla^2 \tau_{yz} = 0$$

$$\frac{\delta^2 \phi}{\delta y \, \delta z} + (1+\nu)\nabla^2 \tau_{yz} = 0$$

Similarly the following equations are obtained,

$$\frac{\delta^2 \phi}{\delta x \, \delta y} + (1+\nu)\nabla^2 \tau_{xy} = 0 \tag{A.39}$$

$$\frac{\delta^2 \phi}{\delta y \, \delta z} + (1+\nu)\nabla^2 \tau_{yz} = 0 \tag{A.40}$$

$$\frac{\delta^2 \phi}{\delta z \, \delta x} + (1+\nu)\nabla^2 \tau_{xz} = 0 \tag{A.41}$$

Equations Equation A.39 through Equation A.41 are the Beltrami-Mitchell equations. The concept of stress functions are used to further simplify and reduce the equations. The Beltrami-Mitchell equations are used to convert the compatibility equations from Cartesian coordinates to Cylindrical coordinates.
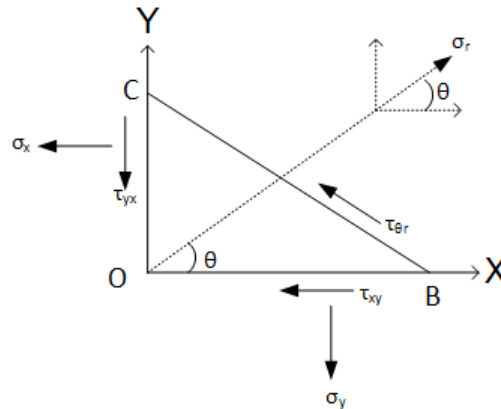

Figure A.4: Stresses in an Element

Compatibility Equations in Cylindrical Coordinates Components of normal stress and shear stress on OC and OB in Figure A.4 are,

$$\sigma_x BC cos\theta \qquad \& \qquad \sigma_y BC sin\theta$$

$$\tau_{xy} BC cos\theta \qquad \& \qquad \tau_{xy} BC sin\theta$$

$$\sigma_r - \sigma_x \, cos\theta \, cos\theta - \sigma_y \, sin\theta sin\theta - \tau_{xy} \, cos\theta \, sin\theta - \tau_{xy} \, sin\theta \, cos\theta = 0$$

or,

$$\sigma_r = \sigma_x cos^2\theta + \sigma_y sin^2\theta + 2\tau_{xy} sin\theta \, cos\theta$$

Also,

$$\tau_{r\theta} + \sigma_x \, cos\theta \, sin\theta - \sigma_y \, sin\theta \, cos\theta + \tau_{xy} \, sin\theta \, sin\theta - \tau_{xy} \, cos\theta \, cos\theta = 0$$

$$\tau_{r\theta} = (\sigma_y - \sigma_x) \, sin\theta \, cos\theta + (cos^2\theta - sin^2\theta) \, \tau_{xy}$$

Since $\tau_{r\theta} = 0$,

$$\tau_{xy}\left(cos^2\theta - sin^2\theta\right) = -(\sigma_y - \sigma_x)\,sin\theta\,cos\theta$$

$$\tau_{xy} = \frac{(\sigma_x - \sigma_y)\,2\,sin\theta\,cos\theta}{(cos^2\theta - sin^2\theta)} \tag{A.42}$$

So,

$$\sigma_r = \sigma_x\,cos^2\theta + \sigma_y\,sin^2\theta + (\sigma_x - \sigma_y)\frac{2sin\theta\,cos\theta}{(cos^2\theta - sin^2\theta)} \tag{A.43}$$

Since σ_θ makes $(\theta + 90°)$ angle with x axis. Using Equation A.43,

$$\sigma_\theta = \sigma_x cos^2(\theta + 90°) + \sigma_y sin^2(\theta + 90°) + (\sigma_x - \sigma_y)\frac{2sin(\theta + 90°)\,cos(\theta + 90°)}{cos^2(\theta + 90°) - sin^2(\theta + 90°)}$$

$$\sigma_\theta = \sigma_x sin^2\theta + \sigma_y cos^2\theta - (\sigma_x - \sigma_y)\frac{2sin\theta\,cos\theta}{(cos^2\theta - sin^2\theta)} \tag{A.44}$$

From Equation A.43,

$$\sigma_r(cos^2\theta - sin^2\theta) = \sigma_x cos^2\theta$$

$$\sigma_x = \sigma_r cos^2\theta + \sigma_\theta sin^2\theta \tag{A.45}$$

$$\sigma_y = \sigma_r sin^2\theta + \sigma_\theta cos^2\theta \tag{A.46}$$

So, from Equation A.42, we obtain,

$$\tau_{xy} = \frac{[\sigma_r cos^2\theta + \sigma_\theta sin^2\theta - \sigma_r sin^2\theta - \sigma_\theta cos^2\theta]sin\theta\,cos\theta}{(cos^2\theta - sin^2\theta)}$$

$$= \frac{(\sigma_r - \sigma_\theta)(cos^2\theta - sin^2\theta)sin\theta\,cos\theta}{(cos^2\theta - sin^2\theta)}$$

$$\tau_{xy} = \frac{1}{2}(\sigma_r - \sigma_\theta)\,sin\,2\theta \tag{A.47}$$

When converting to cylindrical co-ordinates, $r^2 = x^2 + y^2$, $\theta = \tan^{-1}\frac{y}{x}$

$$\frac{\delta r}{\delta x} = \frac{x}{r} = \cos\theta \quad , \qquad \frac{\delta r}{\delta y} = \frac{y}{r} = \sin\theta$$

$$\frac{\delta\theta}{\delta x} = -\frac{y}{r^2} = \frac{-\sin\theta}{r} \quad , \qquad \frac{\delta\theta}{\delta y} = \frac{x}{r^2} = \frac{\cos\theta}{r} \tag{A.48}$$

$$\frac{\delta\phi}{\delta x} = \frac{\delta\phi}{\delta r}\frac{\delta r}{\delta x} + \frac{\delta\phi}{\delta\theta}\frac{\delta\theta}{\delta x}$$

$$= \frac{\delta\phi}{\delta r}\cos\theta - \frac{1}{r}\frac{\delta\phi}{\delta\theta}\sin\theta$$

When ϕ is a function of r & θ and [from Equation A.48].

$$\frac{\delta^2\phi}{\delta x^2} = \left(\cos\theta\frac{\delta}{\delta r} - \frac{\sin\theta}{r}\frac{\delta}{\delta\theta}\right)\left(\cos\theta\frac{\delta\phi}{\delta r} - \frac{\sin\theta}{r}\frac{\delta\phi}{\delta\theta}\right)$$

$$\frac{\delta^2\phi}{\delta x^2} = \frac{\delta^2\phi}{\delta r^2}\cos^2\theta + \frac{\delta^2\phi}{\delta\theta^2}\frac{\sin^2\theta}{r^2} - 2\frac{\delta^2\phi}{\delta r\,\delta\theta}\frac{\sin\theta\cos\theta}{r} + \frac{\delta\phi}{\delta r}\frac{\sin^2\theta}{r} + 2\frac{\delta\phi}{\delta\theta}\frac{\sin\theta\cos\theta}{r^2} \tag{A.49}$$

As it is axisymmetry, σ_r, σ_θ and σ_z are dependent on θ which means $\frac{\delta\phi}{\delta\theta} = 0$,

From Equation A.49,
$$\frac{\delta^2\phi}{\delta x^2} = \frac{\delta^2\phi}{\delta r^2}\cos^2\theta + \frac{\delta\phi}{\delta r}\frac{\sin^2\theta}{r} \tag{A.50}$$

Similarly we can obtain,

$$\frac{\delta^2\phi}{\delta y^2} = \frac{\delta^2\phi}{\delta r^2}\sin^2\theta + \frac{\delta\phi}{\delta r}\frac{\cos^2\theta}{r} + 2\frac{\sin\theta\cos\theta}{r\delta r} + \frac{\delta^2\phi}{\delta\theta^2}\frac{\cos^2\theta}{r^2} - 2\frac{\delta\phi}{\delta\theta}\frac{\sin\theta\cos\theta}{r^2} \tag{A.51}$$

Now we have,
$$\nabla^2\phi = \frac{\delta^2\phi}{\delta x^2} + \frac{\delta^2\phi}{\delta y^2} + \frac{\delta^2\phi}{\delta z^2}$$

From, Equation A.49 and Equation A.51,

$$\nabla^2\theta = \frac{\delta^2\phi}{\delta r^2}\cos^2\theta + \frac{\delta^2\phi}{\delta\theta^2}\frac{\sin^2\theta}{r^2} - 2\frac{\delta^2\phi}{\delta r\,\delta\theta}\frac{\sin\theta\cos\theta}{r} + \frac{\delta\phi}{\delta r}\frac{\sin^2\theta}{r} + 2\frac{\delta\phi}{\delta\theta}\frac{\sin\theta\cos\theta}{r^2} +$$

$$\frac{\delta^2\phi}{\delta r^2}\sin^2\theta + \frac{\delta\phi}{\delta r}\frac{\cos^2\theta}{r} + 2\frac{\delta^2\phi}{\delta r\,\delta\theta}\frac{\sin\theta\cos\theta}{r} + \frac{\delta^2\phi}{\delta\theta^2}\frac{\cos^2\theta}{r} - 2\frac{\delta\phi}{\delta\theta}\frac{\sin\theta\cos\theta}{r^2} + \frac{\delta^2\phi}{\delta z^2}$$

$$= \frac{\delta^2\phi}{\delta r^2} + \frac{1}{r^2}\frac{\delta^2\theta}{\delta\theta^2} + \frac{1}{r}\frac{\delta\phi}{\delta r} + \frac{\delta^2\phi}{\delta z^2}$$

$$\nabla^2\phi = \frac{\delta^2\phi}{\delta r^2} + \frac{1}{r}\frac{\delta\phi}{\delta r} + \frac{1}{r^2}\frac{\delta^2\phi}{\delta\theta^2} + \frac{\delta^2\phi}{\delta z^2} \tag{A.52}$$

Using Equation A.52 with Equation A.45 and Equation A.46,

$$\nabla^2\sigma_x = \left(\frac{\delta^2}{\delta r^2} + \frac{1}{r}\frac{\delta}{\delta r} + \frac{1}{r^2}\frac{\delta^2}{\delta\theta^2} + \frac{\delta^2}{\delta z^2}\right)(\sigma_r\cos^2\theta + \sigma_\theta\sin^2\theta)$$

$$\nabla^2\sigma_x = \left(\frac{\delta^2}{\delta r^2} + \frac{1}{r}\frac{\delta}{\delta r} + \frac{\delta^2}{\delta z^2}\right)(\sigma_r\cos^2\theta + \sigma_\theta\sin^2\theta) - \frac{2}{r^2}\sin\theta\cos\theta(\sigma_r - \sigma_\theta) \tag{A.53}$$

$$\phi = \sigma_r + \sigma_\theta + \sigma_z$$

Using Equation A.53 and Equation A.50 in Equation A.37,

$$(1+\nu)\nabla^2\sigma_x + \frac{\delta^2\phi}{\delta x^2} = 0$$

$$\nabla^2\sigma_x + \frac{1}{1+\nu}\frac{\delta^2\phi}{\delta x^2} = 0$$

$$\left(\frac{\delta^2}{\delta r^2} + \frac{1}{r}\frac{\delta}{\delta r} + \frac{\delta^2}{\delta z^2}\right)(\sigma_r\cos^2\theta + \sigma_\theta\sin^2\theta) - \frac{2}{r^2}\sin\theta\cos\theta(\sigma_r - \sigma_\theta) +$$

$$\frac{1}{1+\nu}\frac{\delta^2\phi}{\delta r^2}\cos^2\theta + \frac{1}{1+\nu}\frac{\delta\phi}{\delta r}\sin^2\theta\frac{1}{r} = 0$$

$$\left(\frac{\delta^2}{\delta r^2} + \frac{1}{r}\frac{\delta}{\delta r} + \frac{\delta^2}{\delta z^2}\right)\sigma_r\cos^2\theta + \left(\frac{\delta^2}{\delta r^2} + \frac{1}{r}\frac{\delta}{\delta r} + \frac{\delta^2}{\delta z^2}\right)\sigma_\theta\sin^2\theta -$$

$$\frac{2}{r^2}\sin\theta\cos\theta(\sigma_r - \sigma_\theta) + \frac{1}{1+\nu}\frac{\delta^2\phi}{\delta r^2}\cos^2\theta + \frac{1}{1+\nu}\frac{\delta\phi}{\delta r}\frac{1}{r}\sin^2\theta = 0$$

$$\begin{aligned}
&[(\frac{\delta^2}{\delta r^2} + \frac{1}{r}\frac{\delta}{\delta r} + \frac{\delta^2}{\delta z^2})\sigma_r + \frac{1}{1+\nu}\frac{\delta^2\phi}{\delta r^2}]\cos^2\theta + [(\frac{\delta^2}{\delta r^2} + \frac{1}{r}\frac{\delta}{\delta r} \\
&+\frac{\delta^2}{\delta z^2})\sigma_\theta + \frac{1}{1+\nu}\frac{\delta\phi}{\delta r}\frac{1}{r}]\sin^2\theta - \frac{2}{r^2}(\sigma_r - \sigma_\theta)\cos^2\theta + \frac{2}{r^2}(\sigma_r - \sigma_\theta)\sin^2\theta = 0
\end{aligned}$$

(A.54)

Equation A.54 is satisfied for all values of θ when, (eliminating θ)

$$(\frac{\delta^2}{\delta r^2} + \frac{1}{r}\frac{\delta}{\delta r} + \frac{\delta^2}{\delta z^2})\,\sigma_r - \frac{2}{r^2}(\sigma_r - \sigma_\theta) + \frac{1}{1+\nu}\frac{\delta^2\phi}{\delta r^2} = 0 \qquad (A.55)$$

&

$$(\frac{\delta^2}{\delta r^2} + \frac{1}{r}\frac{\delta}{\delta r} + \frac{\delta^2}{\delta z^2})\,\sigma_\theta + \frac{2}{r^2}(\sigma_r - \sigma_\theta) + \frac{1}{1+\nu}\frac{1}{r}\frac{\delta\phi}{\delta r} = 0 \qquad (A.56)$$

This was performed for Equation A.37, if Equation A.38 is solved for, the same equations as Equation A.53 and Equation A.56 can be achieved. Equation A.36 does not change since "z" is the same for cartesian and cylindrical coordinates.

To convert Equation A.39 through Equation A.41 from the Cartesian to Cylindrical coordinates,

$$u_x = u\cos\theta \quad , \quad v_y = u\sin\theta$$

$$u = \frac{u_x}{\cos\theta} \quad , \quad u = \frac{v_y}{\sin\theta}$$

$$\frac{\delta u}{\delta z} = \frac{\delta u_x}{\delta z}\frac{1}{\cos\theta} \quad , \quad \frac{\delta u}{\delta z} = \frac{\delta v_y}{\delta z}\frac{1}{\sin\theta}$$

Also, $\frac{\delta w}{\delta r} = (\frac{\delta w_z}{\delta x})(\frac{\delta x}{\delta r})$ & $\frac{\delta w}{\delta r} = (\frac{\delta w_z}{\delta y})(\frac{\delta y}{\delta r})$ & $\frac{\delta\phi}{\delta r} = \frac{\delta\theta}{\delta r}\cos\theta$

$$\tau_{rz} = \mu\left(\frac{\delta u}{\delta z} + \frac{\delta w}{\delta r}\right)$$

$$\tau_{rz} = \mu\left(\frac{\delta u_x}{\delta z} + \frac{\delta w_z}{\delta x}\right)\frac{1}{\cos\theta}$$

$$\tau_{rz} = \mu\left(\frac{\delta v_y}{\delta z} + \frac{\delta w_z}{\delta y}\right)\frac{1}{\sin\theta}$$

Differentiating $\frac{\delta \phi}{\delta x} = \frac{\delta \phi}{\delta r} \cos \theta$ with respect to z,

$$\frac{\delta^2 \phi}{\delta x \, \delta z} = \frac{\delta^2 \phi}{\delta r \, \delta z} \cos \theta \tag{A.57}$$

Similarly,

$$\nabla^2 \tau_{xz} = \nabla^2 (\tau_{rz} \cos \theta)$$

From rule of differentiation ($\frac{\delta AB}{\delta x} = A \frac{\delta B}{\delta x}$),

$$\nabla^2 \tau_{xz} = \cos \theta \, \nabla^2(\tau_{rz}) + \tau_{rz} \, \nabla^2(\cos \theta)$$
$$= \cos \theta \, \nabla^2(\tau_{rz}) - \tau_{rz} \frac{1}{r^2} \frac{\delta^2}{\delta \theta^2} \cos \theta \tag{A.58}$$
$$\therefore \nabla^2 \tau_{xz} = (\nabla^2 \tau_{rz} - \frac{\tau_{rz}}{r^2}) \cos \theta$$

Using Equation A.57 and Equation A.58 in Equation A.41,

$$\frac{\delta^2 \phi}{\delta z \, \delta x} + (1 + \nu) \nabla^2 \tau_{xz} = 0$$
$$\frac{\delta^2 \phi}{\delta r \, \delta z} \cos \theta + (1 + \nu)[\nabla^2 \tau_{rz} - \frac{\tau_{rz}}{r^2}] \cos \theta = 0$$

$$\nabla^2 \tau_{rz} - \frac{1}{r^2} \tau_{rz} + \frac{1}{1 + \nu} \frac{\delta^2 \phi}{\delta r \, \delta z} = 0 \tag{A.59}$$

The compatibility equations in Cylindrical coordinates can be written as the following equations.

$$\nabla^2 \sigma_r - \frac{2}{r^2}(\sigma_r - \sigma_\theta) + \frac{1}{1 + \nu} \frac{\delta^2 \phi}{\delta r^2} = 0$$

$$\nabla^2 \sigma_\theta + \frac{2}{r^2}(\sigma_r - \sigma_\theta) + \frac{1}{1 + \nu} \frac{1}{r} \frac{\delta \phi}{\delta r} = 0$$

$$\nabla^2 \sigma_z + \frac{1}{1 + \nu} \frac{\delta^2 \phi}{\delta z^2} = 0$$

$$\nabla^2 \tau_{rz} - \frac{1}{r^2} \tau_{rz} + \frac{1}{1 + \nu} \frac{\delta^2 \phi}{\delta r \, \delta z} = 0$$

where σ_r, σ_θ and σ_z are radial, circumferential and vertical

General Differential Equations Derivation To derive the differential equations, the equilibrium equations are to be solved and the state of stress are to be expressed in terms of surface forces [54]. However, Equation A.1 and Equation A.2 are not sufficient to find the stresses. The equilibrium equations and compatibility equations should be used together to develop equations, which can be used to determine the stresses. Similar to plane strain theory (since the z-coordinate is very large in comparison to the other two directions) when S is an arbitrary function,

$$\tau_{rz} = -\frac{\delta^2 S}{\delta r\, \delta z} \tag{A.60}$$

When replaced in Equation A.2, Equation A.23 transforms to Equation A.24.

$$-\frac{\delta^3 S}{\delta r^2\, \delta z} + \frac{\delta \sigma_z}{\delta z} - \frac{1}{r}\frac{\delta^2 S}{\delta r\, \delta z} \tag{A.61}$$

Integrating Equation A.61 with respect to z,

$$\int \left(\frac{\delta^3 S}{\delta r^2 \delta z} + \frac{1}{r}\frac{\delta^2 S}{\delta r\, \delta z} \right) \delta z = \int \frac{\delta \sigma_z}{\delta z}\, \delta z$$

$$\sigma_z = \frac{\delta^2 S}{\delta r^2} + \frac{1}{r}\frac{\delta S}{\delta r} \tag{A.62}$$

Now,

$$\epsilon_r = \frac{\delta u}{\delta r} = \frac{\delta}{\delta r}(r\epsilon_\theta)$$

From Hooke's law,

$$\begin{aligned}
\epsilon_r &= \frac{1}{E}(\sigma_r - \nu(\sigma_\theta + \sigma_z)) \\
\epsilon_\theta &= \frac{1}{E}(\sigma_\theta - \nu(\sigma_r + \sigma_z)) \\
\epsilon_z &= \frac{1}{E}(\sigma_z - \nu(\sigma_\theta + \sigma_r))
\end{aligned} \tag{A.63}$$

$$\epsilon_r = \frac{1}{E}[\sigma_r - \nu(\sigma_\theta + \sigma_z)]$$

$$\frac{\delta}{\delta r}(r\epsilon_\theta) = \frac{1}{E}[\sigma_r - \nu(\sigma_\theta + \sigma_z)]$$

$$\frac{\delta}{\delta r} r \left[\frac{1}{E}(\sigma_\theta - \nu(\sigma_r + \sigma_z))\right] = \frac{1}{E}[\sigma_r - \nu(\sigma_\theta + \sigma_z)]$$

$$(1+\nu)(\sigma_r - \sigma_\theta) = r\frac{\delta}{\delta r}[\sigma_\theta - \nu(\sigma_r + \sigma_z)] \tag{A.64}$$

Introducing a new function R defined ,

$$\sigma_r = \frac{\delta^2 S}{\delta z^2} + R \tag{A.65}$$

Replace Equation A.28, Equation A.64 and Equation A.65 in Equation A.1,

$$\frac{\delta\sigma_r}{\delta r} + \frac{\delta\tau_{rz}}{\delta z} + \frac{\sigma_r - \sigma_\theta}{r} = 0$$

$$\frac{\delta^3 S}{\delta z^2 \delta r} + \frac{\delta R}{\delta r} - \frac{\delta^3 S}{\delta z^2 \delta r} + \frac{1}{1+\nu}\frac{\delta}{\delta r}[\sigma_\theta - \nu(\sigma_r + \sigma_z)] = 0$$

$$(1+\nu)\frac{\delta R}{\delta r} + \frac{\delta}{\delta r}[\sigma_\theta - \nu(\sigma_r + \sigma_z)] = 0 \tag{A.66}$$

Let S include any arbitrary function of z, independent of θ such that,

$$\sigma_\theta = \nu\nabla^2 S - R \tag{A.67}$$

$$\nabla^2 S = \frac{\delta^2 S}{\delta r^2} + \frac{1}{r}\frac{\delta S}{\delta r} + \frac{\delta^2 S}{\delta z^2} \tag{A.68}$$

Adding Equation A.62, Equation A.65 and Equation A.67,

$$\phi = \sigma_r + \sigma_\theta + \sigma_z$$

$$\phi = \frac{\delta^2 S}{\delta r^2} + \frac{1}{r}\frac{\delta S}{\delta r} + \nu\nabla^2 S - R + \frac{\delta^2 S}{\delta z^2} + R$$

From Equation A.68,

$$\phi = \nabla^2 S + \nu \nabla^2 S$$

$$\phi = (1+\nu)\nabla^2 S$$

We have,

$$u = \frac{r}{E}\left[\sigma_\theta - \nu(\sigma_r + \sigma_z)\right] \tag{A.69}$$

$$\because \epsilon_\theta = \frac{u}{r}$$

Replace Equation A.62, Equation A.65 and Equation A.67 in Equation A.69,

$$u = \frac{r}{E}[\nu\nabla^2 S - R - \nu(\frac{\delta^2 S}{\delta z^2} + R) - \nu(\frac{\delta^2 S}{\delta r^2} + 1/r\frac{\delta S}{\delta r})]$$
$$= \frac{r}{E}[\nu\nabla^2 S - R - \nu\frac{\delta^2 S}{\delta z^2} - \nu R - \nu\frac{\delta^2 S}{\delta r^2} - \frac{\nu}{r}\frac{\delta S}{\delta r}$$
$$= \frac{r}{E}[-R - \nu R + \nu[\nabla^2 S - \frac{\delta^2 S}{\delta r^2} - \frac{1}{r}\frac{\delta S}{\delta r} - \frac{\delta^2 S}{\delta z^2}]]$$

$$\therefore u = -\frac{r}{E}(1+\nu)R \tag{A.70}$$

We have from Hooke's law,

$$\gamma_{rz} = \frac{2(1+\nu)}{E}\tau_{rz} \tag{A.71}$$

Replace $\gamma_{rz} = \frac{\delta u}{\delta z} + \frac{\delta w}{\delta r}$ and Equation A.60 in such a way,

$$\frac{2(1+\nu)}{E}\tau_{rz} = \frac{\delta u}{\delta z} + \frac{\delta w}{\delta r}$$
$$\tau_{rz} = \frac{E}{2(1+\nu)}(\frac{\delta u}{\delta z} + \frac{\delta w}{\delta r})$$
$$-\frac{\delta^2 S}{\delta r\delta z} = \frac{E}{2(1+\nu)}(\frac{\delta u}{\delta z} + \frac{\delta w}{\delta r})$$

$$\frac{\delta w}{\delta r} = -\frac{2(1+\nu)}{E}(\frac{\delta^2 S}{\delta r\,\delta z}) - \frac{\delta u}{\delta z} \tag{A.72}$$

Differentiating Equation A.70, with respect to z,

$$\frac{\delta u}{\delta z} = -\frac{r}{E}(1+\nu)\frac{\delta R}{\delta z} \tag{A.73}$$

Substituting Equation A.73 in Equation A.72,

$$\frac{\delta w}{\delta r} = -\frac{2(1+\nu)}{E}\frac{\delta^2 S}{\delta r\,\delta z} + \frac{r}{E}(1+\nu)\frac{\delta R}{\delta z} \tag{A.74}$$

From Hooke's law,

$$\epsilon_z = \frac{\delta w}{\delta z} = \frac{1}{E}(\sigma_z - \nu(\sigma_\theta + \sigma_r))$$

$$= \frac{1}{E}\left[\frac{\delta^2 S}{\delta r^2} + \frac{1}{r}\frac{\delta S}{\delta r} - \nu\left(\frac{\delta^2 S}{\delta z^2} + \nu\nabla^2 S\right)\right]$$

$$= \frac{1}{E}\left[(1-\nu^2)\left(\frac{\delta^2 S}{\delta r^2} + \frac{1}{r}\frac{\delta S}{\delta r}\right) - \nu(1+\nu)\frac{\delta^2 S}{\delta z^2}\right]$$

$$\therefore \epsilon_z = \frac{1}{E}(1+\nu)\left[(1-\nu)\nabla^2 S - \frac{\delta^2 S}{\delta z^2}\right] \tag{A.75}$$

For Equation A.74 and Equation A.75 to be compatible,

$$\frac{\delta}{\delta z}(1.74) = \frac{\delta}{\delta r}(1.75)$$

$$-\frac{2(1+\nu)}{E}\left(\frac{\delta^3 S}{\delta r\,\delta z^2}\right) + \frac{r}{E}(1+\nu)\frac{\delta^2 R}{\delta z^2} = \frac{1}{E}(1+\nu)\left[(1-\nu)\frac{\delta}{\delta r}\nabla^2 S - \frac{\delta^3 S}{\delta r\,\delta z^2}\right]$$

$$-2\frac{\delta^3 S}{\delta r\,\delta z^2} + \frac{r\delta^2 R}{\delta z^2} = (1-\nu)\frac{\delta\nabla^2 S}{\delta r} - \frac{\delta^3 S}{\delta r\,\delta z^2}$$

$$\frac{r\delta^2 R}{\delta z^2} = (1-\nu)\frac{\delta}{\delta r}\nabla^2 S + \frac{\delta^3 S}{\delta r\,\delta z^2} \tag{A.76}$$

Let's introduce a function N in Equation A.76 such that,

$$rR = \frac{\delta S}{\delta r} + \frac{\delta N}{\delta r} \tag{A.77}$$

$$r\frac{\delta R}{\delta z} = \frac{\delta^2 S}{\delta r\,\delta z} + \frac{\delta^2 N}{\delta r\,\delta z} \tag{A.78}$$

Differentiating Equation A.78 with respect to z,

$$r\frac{\delta^2 R}{\delta z^2} = \frac{\delta^3 S}{\delta r\,\delta z^2} + \frac{\delta^2 N}{\delta z^2} \tag{A.79}$$

From Equation A.76 and Equation A.79 we have,

$$\frac{\delta^2 N}{\delta z^2} = (1-\nu)\frac{\delta}{\delta r}\nabla^2 S \tag{A.80}$$

Substituting $r\frac{\delta R}{\delta z}$ from Equation A.78 in Equation A.75,

$$\frac{\delta w}{\delta r} = \frac{(1+\nu)}{E}[-2\frac{\delta^2 S}{\delta r\,\delta z} + r\frac{\delta R}{\delta z}]$$
$$= \frac{(1+\nu)}{E}[-2\frac{\delta^2 S}{\delta r\,\delta z} + \frac{\delta^2 S}{\delta r\,\delta z} + \frac{\delta^2 N}{\delta r\,\delta z}]$$

$$\frac{\delta w}{\delta r} = -\frac{(1+\nu)}{E}\frac{\delta^2 S}{\delta r\,\delta z} + \frac{(1+\nu)}{E}\frac{\delta^2 N}{\delta r\,\delta z} \tag{A.81}$$

Substituting Equation A.80 in Equation A.75,

$$\frac{\delta w}{\delta z} = \frac{1}{E}(1+\nu)[(1-\nu)\nabla^2 S - \frac{\delta^2 S}{\delta z^2}]$$

$$\frac{\delta w}{\delta z} = \frac{1}{E}(1+\nu)[\frac{\delta^2 N}{\delta z^2} - \frac{\delta^2 S}{\delta z^2}] \tag{A.82}$$

Integrating Equation A.81 with respect to r,

$$w = -\frac{(1+\nu)}{E}[\frac{\delta S}{\delta z} - \frac{\delta N}{\delta z}] \tag{A.83}$$

For u, from Equation A.70,

$$u \quad = -\frac{r}{E}(1+\nu)R \quad = -\frac{(1+\nu)}{E}rR$$

From Equation A.77,

$$u = -\frac{(1+\nu)}{E}(\frac{\delta S}{\delta r} + \frac{\delta N}{\delta r}) \tag{A.84}$$

Also,

$$\epsilon = \epsilon_r + \epsilon_\theta + \epsilon_z = \frac{\delta u}{\delta r} + \frac{u}{r} + \frac{\delta w}{\delta z}$$

$$\epsilon = -\frac{(1+\nu)}{E}[\frac{\delta^2 N}{\delta r^2} + \frac{\delta^2 S}{\delta r^2}] + \frac{u}{r} + \frac{(1+\nu)}{E}[\frac{\delta^2 N}{\delta z^2} - \frac{\delta^2 S}{\delta z^2}]$$

From Equation A.70,

$$\epsilon = -\frac{(1+\nu)}{E}[\frac{\delta^2 N}{\delta r^2} + \frac{\delta^2 S}{\delta r^2}] - \frac{(1+\nu)}{E}R + \frac{(1+\nu)}{E}[\frac{\delta^2 N}{\delta z^2} - \frac{\delta^2 S}{\delta z^2}]$$

$$= -\frac{(1+\nu)}{E}[\frac{\delta^2 S}{\delta r^2} + \frac{\delta^2 N}{\delta r^2} + R + \frac{\delta^2 S}{\delta z^2} - \frac{\delta^2 N}{\delta z^2}]$$

From Equation A.77, $R = \frac{1}{r}(\frac{\delta S}{\delta r} + \frac{\delta N}{\delta r})$. Substituting this in the equation above,

$$\epsilon = -\frac{(1+\nu)}{E}[\frac{\delta^2 S}{\delta r^2} + \frac{\delta^2 S}{\delta z^2} + \frac{1}{r}\frac{\delta S}{\delta r} + \frac{\delta^2 N}{\delta r^2} - \frac{\delta^2 N}{\delta z^2} + \frac{1}{r}\frac{\delta N}{\delta r}]$$

$$= -\frac{(1+\nu)}{E}[\nabla^2 S + \frac{\delta^2 N}{\delta r^2} + \frac{1}{r}\frac{\delta N}{\delta r} + \frac{\delta^2 N}{\delta z^2} - \frac{\delta^2 N}{\delta z^2} - \frac{\delta^2 N}{\delta z^2}]$$

$$= -\frac{(1+\nu)}{E}[\nabla^2 S + \nabla^2 N - 2\frac{\delta^2 N}{\delta z^2}]$$

Substituting $\frac{\delta^2 N}{\delta z^2}$ from Equation A.80,

$$\epsilon = -\frac{(1+\nu)}{E}[\nabla^2 S + \nabla^2 N - 2(1-\nu)\nabla^2 S]$$

$$\epsilon = \frac{(1+\nu)}{E}[(1-2\nu)\nabla^2 S - \nabla^2 N] \tag{A.85}$$

From Equation A.65,

$$\epsilon = \epsilon_r + \epsilon_\theta + \epsilon_z$$

$$= \frac{1}{E}[\sigma_r - \nu\sigma_\theta - \nu\sigma_z + \sigma_\theta - \nu\sigma_r - \nu\sigma_z + \sigma_z - \nu\sigma_\theta - \nu\sigma_r]$$

$$= \frac{1}{E}[\sigma_r + \sigma_\theta + \sigma_z - 2\nu(\sigma_\theta + \sigma_r + \sigma_z)]$$

$$= \frac{1}{E}(\phi - 2\nu\theta)$$

$$\epsilon = \frac{1}{E}\phi(1 - 2\nu) \tag{A.86}$$

Adding Equation A.62, Equation A.65 and Equation A.67,

$$\phi = \frac{\delta^2 S}{\delta r^2} + \frac{1}{r}\frac{\delta S}{\delta r} + \frac{\delta^2 S}{\delta z^2} + R + \nu\nabla^2 S - R$$

$$= \nabla^2 S + \nu\nabla^2 S$$

$$\phi = (1 + \nu)\nabla^2 S \tag{A.87}$$

Substituting Equation A.87 in Equation A.86,

$$\epsilon = \frac{1 - 2\nu}{E}(1 + \nu)\nabla^2 S$$

This shows that ϵ is independent of N and hence, $\nabla^2 N = 0$ for ϵ. Let $x' = S + N$ and substitute Equation A.77 in Equation A.65,

$$\sigma_r = \frac{\delta^2 S}{\delta z^2} + R = \frac{\delta^2 S}{\delta z^2} + \frac{1}{r}\left(\frac{\delta S}{\delta r} + \frac{\delta N}{\delta r}\right)$$

$$= \frac{\delta^2 S}{\delta z^2} + \frac{1}{r}\frac{\delta S}{\delta r} + \frac{1}{r}\frac{\delta N}{\delta r}$$

$$= \frac{\delta^2 S}{\delta z^2} + \frac{1}{r}\frac{\delta S}{\delta r} + \frac{\delta^2 S}{\delta r^2} - \frac{\delta^2 S}{\delta r^2} + \frac{1}{N}\frac{\delta N}{\delta r} + \frac{\delta^2 N}{\delta r^2} - \frac{\delta^2 N}{\delta r^2} + \frac{\delta^2 N}{\delta z^2} - \frac{\delta^2 N}{\delta z^2}$$

$$= \nabla^2 S - \frac{\delta^2 S}{\delta r^2} + \nabla^2 N - \frac{\delta^2 N}{\delta r^2} - \frac{\delta^2 N}{\delta z^2}$$

$$= \nabla^2 x' - \frac{\delta^2 S}{\delta r^2} - \frac{\delta^2 N}{\delta z^2} - \frac{\delta^2 N}{\delta r^2}$$

From Equation A.80,

$$\sigma_r = \nabla^2 x' - \frac{\delta^2 S}{\delta r^2} - (1 - \nu)\nabla^2 S - \frac{\delta^2 N}{\delta r^2}$$

$$= \nabla^2 x' - \frac{\delta^2}{\delta r^2}(S + N) - (1 - \nu)\nabla^2 S$$

$$= \nabla^2 x' - \frac{\delta^2 x'}{\delta r^2} - (1 - \nu)\nabla^2 S$$

$$= \nabla^2 x' - \frac{\delta^2 x'}{\delta r^2} - \nabla^2 S + \nu\nabla^2 S - \nabla^2 N + \nu\nabla^2 N$$

$$(\because \nabla^2 N = 0)$$

$$\sigma_r = \nabla^2 x' - \nabla^2 x' - \frac{\delta^2 x'}{\delta r^2} + \nu \nabla^2 x'$$

$$\sigma_r = \nu \nabla^2 x' - \frac{\delta^2 x'}{\delta r^2} \tag{A.88}$$

From Equation A.67,

$$\sigma_\theta = \nu \nabla^2 S - R$$

$$= \nu \nabla^2 S - \frac{1}{r}\left(\frac{\delta S}{\delta r} - \frac{\delta N}{\delta r}\right) \tag{A.89}$$

$$\sigma_\theta = \nu \nabla^2 x' - \frac{1}{r}\frac{\delta x'}{\delta r}$$

From Equation A.62,

$$\sigma_z = \frac{\delta^2 S}{\delta r^2} + \frac{1}{r}\frac{\delta S}{\delta r}$$

$$= \frac{\delta^2 S}{\delta r^2} + \frac{1}{r}\frac{\delta S}{\delta r} + \frac{\delta^2 S}{\delta z^2} - \frac{\delta^2 S}{\delta z^2}$$

$$= \nabla^2 S - \frac{\delta^2 S}{\delta z^2}$$

$$= \nabla^2 S - \frac{\delta^2 S}{\delta z^2} - \frac{\delta^2 N}{\delta z^2} + \frac{\delta^2 N}{\delta z^2}$$

$$= \nabla^2 S - \frac{\delta^2 x'}{\delta z^2} + (1-\nu)\nabla^2 S$$

$$\sigma_z = (2-\nu)\nabla^2 x' - \frac{\delta^2 x'}{\delta z^2} \tag{A.90}$$

Let $x' = \frac{\delta X_0}{\delta z}$,

$$\sigma_r = \frac{\delta}{\delta z}\left[\nu \nabla^2 X_0 - \frac{\delta^2 X_0}{\delta r^2}\right] \tag{A.91}$$

$$\sigma_\theta = \frac{\delta}{\delta z}\left[\nu \nabla^2 X_0 - \frac{1}{r}\frac{\delta X_0}{\delta r}\right] \tag{A.92}$$

$$\sigma_z = \frac{\delta}{\delta z}\left[(2-\nu)\nabla^2 X_0 - \frac{\delta^2 X_0}{\delta z^2}\right] \tag{A.93}$$

Substituting these values in Equation A.2,

$$\frac{\delta \tau_{rz}}{\delta r} + \frac{\delta \sigma_z}{\delta z} + \frac{\tau_{rz}}{r} = 0$$

$$\frac{\delta}{\delta r}\frac{\delta}{\delta r}[(1-\nu)\nabla^2 X_0 - \frac{\delta^2 X_0}{\delta z^2}] + \frac{\delta}{\delta z}\frac{\delta}{\delta z}[(2-\nu)\nabla^2 X_0 - \frac{\delta^2 X_0}{\delta z^2}] + \frac{1}{r}\frac{\delta}{\delta r}[(1-\nu)\nabla^2 X_0 -$$

$$\frac{\delta^2 X_0}{\delta z^2}] = 0$$

which is in the form $\frac{\delta^2 A}{\delta r^2} + \frac{1}{r}\frac{\delta A}{\delta r} + \frac{\delta^2 A}{\delta z^2}$ which equals to $\nabla^2 A$. So,

$$(1-\nu)\nabla^4 X_0 = 0$$

Since $\nu \neq 1$,

$$\nabla^4 X_0 = 0 \tag{A.94}$$

Substituting Equation A.91, Equation A.92 and Equation A.93 in Equation A.63 gives,

$$\epsilon_z = \frac{\delta w}{\delta z} = \frac{1}{E}[\sigma_z - \nu(\sigma_\theta + \sigma_r)]$$

$$\frac{\delta w}{\delta z} = \frac{1}{E}[\frac{\delta}{\delta z}[(2-\nu)\nabla^2 X_0 - \frac{\delta^2 X_0}{\delta z^2}] - \nu(\frac{\delta}{\delta z}[\nu\nabla^2 X_0 - \frac{1}{r}\frac{\delta X_0}{\delta r}] + \frac{\delta}{\delta z}[\nu\nabla^2 X_0 - \frac{\delta^2 X_0}{\delta r^2}])$$

$$= \frac{1}{E}\frac{\delta}{\delta z}[(2-\nu)\nabla^2 X_0 - \frac{\delta^2 X_0}{\delta z^2} - \nu^2\nabla^2 X_0 + \frac{\nu}{r}\frac{\delta X_0}{\delta r} + \nu\nabla^2 X_0 - \frac{\delta^2 X_0}{\delta r^2}]$$

$$= \frac{1}{E}[2\nabla^2 X_0 - \nu\nabla^2 X_0 - \frac{\delta^2 X_0}{\delta z^2} - \nu^2\nabla^2 X_0 + \frac{\nu}{r}\frac{\delta X_0}{\delta r} - \nu^2\nabla^2 X_0 + \nu\frac{\delta^2 X_0}{\delta r^2}]$$

$$= \frac{1}{E}[-2\nu^2\nabla^2 X_0 + \nabla^2 X_0 + \nabla^2 X_0 - \nu\nabla^2 X_0 + \nu\frac{\delta^2 X_0}{\delta r^2} + \frac{\nu}{r}\frac{\delta X_0}{\delta r} - \frac{\delta^2 X_0}{\delta z^2}]$$

$$= \frac{1}{E}[(1-\nu-2\nu^2)\nabla^2 X_0 + \frac{\delta^2 X_0}{\delta r^2} + \frac{1}{r}\frac{\delta X_0}{\delta r} + \frac{\delta^2 X_0}{\delta z^2} + \nu\frac{\delta^2 X_0}{\delta r^2} + \frac{\nu}{r}\frac{\delta X_0}{\delta r} - \frac{\delta^2 X_0}{\delta z^2}]$$

$$= \frac{1}{E}[(1+\nu)(1-2\nu)\nabla^2 X_0 + (1+\nu)\frac{\delta^2 X_0}{\delta r^2} + \frac{1}{r}(1+\nu)\frac{\delta X_0}{\delta r}]$$

$$= \frac{1}{E}(1+\nu)[(1-2\nu)\nabla^2 X_0 + \frac{\delta^2 X_0}{\delta r^2} + \frac{1}{r}\frac{\delta X_0}{\delta r}]$$

$$w = \frac{1}{E}(1+\nu)[(1-2\nu)\nabla^2 X_0 + \frac{\delta^2 X_0}{\delta r^2} + \frac{1}{r}\frac{\delta X_0}{\delta r}] \tag{A.95}$$

Substituting in Equation A.63 gives,

$$\epsilon_r = \frac{\delta u}{\delta r} = \frac{1}{E}[\sigma_r - \nu(\sigma_\theta + \sigma_z)]$$

$$\frac{\delta u}{\delta r} = \frac{1}{E}[\frac{\delta}{\delta z}(\nu\nabla^2 X_0 - \frac{\delta^2 X_0}{\delta r^2} - \nu^2\nabla^2 X_0 + \frac{\nu}{r}\frac{\delta X_0}{\delta r} - \nu(2-\nu)\nabla^2 X_0 + \nu\frac{\delta^2 X_0}{\delta z^2})]$$

$$= \frac{1}{E}\frac{\delta}{\delta z}[-\nu\nabla^2 X_0 - \frac{\delta^2 X_0}{\delta r^2} + \frac{\nu}{r}\frac{\delta X_0}{\delta r} + \nu\frac{\delta^2 X_0}{\delta z^2}]$$

$$= \frac{1}{E}\frac{\delta}{\delta z}[-\nu\nabla^2 X_0 - \frac{\delta^2 X_0}{\delta r^2} + \nu\frac{\delta^2 X_0}{\delta r^2} - \nu\frac{\delta^2 X_0}{\delta r^2} + \frac{\nu}{r}\frac{\delta X_0}{\delta r} + \nu\frac{\delta^2 X_0}{\delta z^2}]$$

$$= \frac{1}{E}\frac{\delta}{\delta z}[-\nu\nabla^2 X_0 - \frac{\delta^2 X_0}{\delta r^2} - \nu\frac{\delta^2 X_0}{\delta r^2} + \nu\nabla^2 X_0]$$

$$= \frac{1}{E}\frac{\delta}{\delta z}[-(1+\nu)\frac{\delta^2 X_0}{\delta r^2}]$$

$$\frac{\delta u}{\delta r} = -\frac{(1+\nu)}{E}\frac{\delta^3 X_0}{\delta z\delta r^2}$$

$$u = -\frac{(1+\nu)}{E}\frac{\delta^2 X_0}{\delta r\delta z} \tag{A.96}$$

where E is the modulus of elasticity of the material in the substructure layer. Let $X = kX_0$, where k is a constant. In addition, let $k = \frac{1}{2(\lambda+\mu)}$, where λ and μ are Lame's constants, such that

$$\nabla^4 X = 0 \tag{A.97}$$

The normal and shear stresses can be expressed in terms of the Lame's constant using Equation A.29 and Equation A.30. Expressing Equation A.91 through Equation A.96 in terms of X and $\nu = k\lambda$, Then Equation A.92 and Equation A.93 become,

$$\sigma_z = \frac{\delta}{\delta z}[(3\lambda + 4\mu)\nabla^2 X - 2(\lambda + \mu)\frac{\delta^2 X}{\delta z^2}] \tag{A.98}$$

$$\tau_{rz} = \frac{\delta}{\delta r}[(\lambda + 2\mu)\nabla^2 X - 2(\lambda + \mu)\frac{\delta^2 X}{\delta z^2}] \tag{A.99}$$

Application of Boundary and Interface Conditions For layered elastic analysis, there is the assumption of continuous surface of contact in the layer interface.

The following equations should satisfy equation Equation A.97. At upper surface when $z = 0$,

$$\tau_{rz} = 0 \qquad (A.100)$$

Also, for radius (r) < radius of load (a),

$$\sigma_z = p[1 - (\frac{r}{a})^2] \qquad (A.101)$$

For $r > a$,

$$\sigma_z = 0 \qquad (A.102)$$

At interface, there is continuity of vertical stress (σ_z), vertical displacement (w) and shear stress (τ_{rz}), which gives,

$$(\sigma_z)_j = (\sigma_z)_{j+1} \qquad (A.103)$$

$$(w_z)_j = (w_z)_{j+1} \qquad (A.104)$$

$$(\tau_{rz})_j = (\tau_{rz})_{j+1} \qquad (A.105)$$

As z approaches infinity, the stresses and displacements (represented by function X) approach zero. At $z \to \infty$,

$$X \to 0 \qquad (A.106)$$

Using Hankel Transform to Find the Solution of the Biharmonic Function

The Biharmonic equation can be transformed to a differential equation using Hankel transform. The Hankel transform of $F_n(H)$ is defined as,

$$F_n(H) = \int_0^\infty f(r) J_n(Hr) r \delta r$$

and using the Hankel inverse when f(r) satisfies the requisite conditions,

$$f(r) = \int_0^\infty F_n(H) J_n(Hr) H \delta H$$

where H is the variable of integration introduced by Hankel transformation and J_n is the Bessel function of the first kind with order n.

The biharmonic function can be represented as,

$$\nabla^4 X = \left(\frac{\delta^2}{\delta r^2} + \frac{1}{r}\frac{\delta}{\delta r} + \frac{\delta^2}{\delta z^2}\right)\left(\frac{\delta^2}{\delta r^2} + \frac{1}{r}\frac{\delta}{\delta r} + \frac{\delta^2}{\delta z^2}\right)X = 0 \qquad (A.107)$$

Multiplying Equation A.107 by $J_o(Hr)r$,

$$\left(\frac{\delta^2 \eta}{\delta r^2} + \frac{1}{r}\frac{\delta \eta}{\delta r} + \frac{\delta^2 \eta}{\delta z^2}\right)r J_o(H_r) = 0$$

$$\int_0^\infty \left(\frac{\delta^2 \eta}{\delta r^2} + \frac{1}{r}\frac{\delta \eta}{\delta r} + \frac{\delta^2 \eta}{\delta z^2}\right)r J_o(H_r)\delta r = 0$$

where,

$$\eta = \frac{\delta^2 X}{\delta r^2} + \frac{1}{r}\frac{\delta X}{\delta r} + \frac{\delta^2 X}{\delta z^2}$$

$$\int_0^\infty \frac{\delta^2}{\delta z^2}\eta r J_o(H_r)\delta r + \int_0^\infty \frac{1}{r}\frac{\delta \eta}{\delta r} r J_o(H_r)\delta r + \int_0^\infty \frac{\delta^2}{\delta z^2}\eta J_o(H_r)r\delta r = 0$$

$$\frac{\delta^2}{\delta z^2}\int_0^\infty \eta J_o(H_r)r\delta r + \int_0^\infty \frac{\delta}{\delta r}\left[r\frac{\delta \eta}{\delta r}\right]J_o(H_r)\delta r = 0$$

$$\frac{\delta^2}{\delta z^2}\bar{\eta} + \left[r\frac{\delta \eta}{\delta r}J_o(H_r)\right]_0^\infty - \int_0^\infty r\frac{\delta \eta}{\delta r}\frac{\delta}{\delta r}[J_o(H_r)]\delta r = 0$$

where,

$$\bar{\eta} = \int_0^\infty \eta J_o(Hr)r\delta r$$

$$\because \int uv\delta x = u\int v\delta x - \int u'\left(\int v\delta x\right)\delta x$$

Here,

$$u = J_o(Hr)$$

$$v = \frac{\delta}{\delta r}[r\frac{\delta\eta}{\delta r}]$$

Since $\frac{\delta\eta}{\delta r}$ is assumed to be finite for all values of r, So,

$$[r\frac{\delta}{\delta r}\eta J_o(Hr)]_0^\infty = 0$$

Since the first derivative of zero order Bessel function is first order Bessel function,

$$\frac{\delta}{\delta r}J_o(Y) = -J_1(r)$$

$$\frac{\delta}{\delta r}[J_o(Hr)] = -H[J_1(Hr)]$$

$$\frac{\delta}{\delta r}[rJ_1(Hr)] = (Hr)J_o(Hr)$$

The equation becomes,

$$\frac{\delta^2\bar{\eta}}{\delta z^2} - 0 - \int_0^\infty r\frac{\delta}{\delta r}\eta[-HJ_1(Hr)]\delta r = 0$$

$$\frac{\delta^2\bar{\eta}}{\delta z^2} + H\int_0^\infty r\frac{\delta\eta}{\delta r}J_1(Hr)\delta r = 0$$

$$\frac{\delta^2\bar{\eta}}{\delta z^2} + [\eta HJ_1(Hr)]_0^\infty - H\int_0^\infty \eta\frac{\delta}{\delta r}[rJ_1(Hr)]\delta r = 0$$

$$\frac{\delta^2\bar{\eta}}{\delta z^2} - H\int_0^\infty \eta(Hr)J_o(Hr)\delta r = 0$$

$$\frac{\delta^2\bar{\eta}}{\delta z^2} - H^2\int_0^\infty \eta J_o(Hr)r\delta r = 0$$

$$(\frac{\delta^2}{\delta z^2} - H^2)\int_0^\infty \eta J_o(Hr)r\delta r = 0$$

$$(\frac{\delta^2}{\delta z^2} - H^2)^2\int_0^\infty (\frac{\delta^2 X}{\delta r^2} + \frac{1}{r}\frac{\delta X}{\delta r} + \frac{\delta^2 X}{\delta z^2})J_o(Hr)r\delta r = 0$$

When the operations are performed again,

$$\int_0^\infty r\nabla^4 X J_0(Hr)\delta r = (\frac{\delta^2}{\delta z^2} - H^2)^2 \int_0^\infty rX J_o(Hr)\delta r = 0$$

Using G for the zero order Hankel transform which is a function of H & z, $G(H,z)$ can be expressed as,

$$G(H,z) = \int_0^\infty rX J_o(H_r)\delta r \tag{A.108}$$

$$(\frac{\delta^2}{\delta z^2} - H^2)^2 G(H,z) = 0$$

The solution of which is,

$$G(H,z) = (A + B_z)e^{-Hz} + (C + D_z)e^{Hz} \tag{A.109}$$

where A, B, C and D are the integration constants.

Now Equation A.98 becomes,

$$\sigma_z = \frac{\delta}{\delta z}[(3\lambda + 4\mu)\nabla^2 X - 2(\lambda + \mu)\frac{\delta^2 X}{\delta z^2}]$$

When Equation A.98 is multiplied by $rJ_0(Hr)$ and integrated with respect to r,

$$\int_0^\infty r\sigma_z J_o(Hr)\delta r = (3\lambda + 4\mu)\frac{\delta}{\delta z}\int_0^\infty r\nabla^2 X J_o(Hr)\delta r - 2(\lambda + \mu)\frac{\delta}{\delta z}\int_0^\infty r\frac{\delta^2 X}{\delta z^2}J_o(Hr)\delta r$$

From Equation A.108,

$$\bar{\sigma}_z = (3\lambda + 4\mu)\frac{\delta}{\delta z}[(\frac{\delta^2}{\delta z^2} - H^2)G] - 2(\lambda + \mu)\frac{\delta}{\delta z}[\frac{\delta^2 G}{\delta z^2}]$$

$$= (3\lambda + 4\mu)\frac{\delta^3 G}{\delta z^3} - (3\lambda + 4\mu)H^2\frac{\delta G}{\delta z} - 2(\lambda + \mu)\frac{\delta^3 G}{\delta z^3}$$

$$\bar{\sigma}_z = (\lambda + 2\mu)\frac{\delta^3 G}{\delta z^3} - (3\lambda + 4\mu)H^2\frac{\delta G}{\delta z} \tag{A.110}$$

which gives,

$$\sigma_z = \int_0^\infty H[(\lambda + 2\mu)\frac{\delta^3 G}{\delta z^3} - (3\lambda + 4\mu)H^2\frac{\delta^3 G}{\delta z^3}]J_o(Hr)\delta H \tag{A.111}$$

From Equation A.99,

$$\tau_{rz} = \frac{\delta}{\delta r}[(\lambda + 2\mu)\nabla^2 X - 2(\lambda + \mu)\frac{\delta^2 X}{\delta z^2}]$$

$$\int_0^\infty r\tau_{rz}J_1(Hr)\delta r = (\lambda + 2\mu)\int_0^\infty r\frac{\delta}{\delta r}\nabla^2 X J_1(Hr)\delta r - 2(\lambda + \mu)$$

$$\int_0^\infty r\frac{\delta^3 X}{\delta r\delta z^2}J_1(Hr)\delta r$$

$$\bar{\tau}_{rz} = (\lambda + 2\mu)[(rJ_1(H_r)\nabla^2 X)_0^\infty - \int_0^\infty \nabla^2 X\frac{\delta}{\delta r}[rJ_1(H_r)]\delta r] - 2(\lambda + \mu)\frac{\delta^2}{\delta z^2}$$

$$\int_0^\infty r\frac{\delta X}{\delta r}J_1(H_r)\delta r$$

$$= -(\lambda + 2\mu)H\int_0^\infty \nabla^2 X rJ_o(H_r)\delta r + 2(\lambda + \mu)\frac{\delta^2}{\delta z^2}$$

$$[[H\int_0^\infty rXJ_o(H_r)\delta r] - [XrJ_1(H_r)]_0^\infty]$$

$$= -(\lambda + 2\mu)H(\frac{\delta^2}{\delta z^2} - H^2)G + 2(\lambda + \mu)H\frac{\delta^2 G}{\delta z^2}$$

$$\bar{\tau}_{rz} = \lambda H\frac{\delta^2 G}{\delta z^2} + (\lambda + 2\mu)H^3 G \tag{A.112}$$

$$\tau_{rz} = \int_0^\infty H^2[\lambda\frac{\delta^2 G}{\delta z^2} + (\lambda + 2\mu)H^2 G]J_1(Hr)\delta H \tag{A.113}$$

$$w = \frac{\lambda + 2\mu}{\mu}\nabla^2 X - \frac{\lambda + \mu}{\mu}\frac{\delta^2 X}{\delta z^2}$$

$$\int_0^\infty rwJ_o(H_r)\delta r = \frac{\lambda + 2\mu}{\mu}\int_0^\infty r\nabla^2 X J_o(Hr)\delta r - \frac{\lambda + \mu}{\mu}\int_0^\infty r\frac{\delta^2 X}{\delta z^2}J_o(Hr)\delta r$$

$$\bar{w} = \frac{\lambda + 2\mu}{\mu}(\frac{\delta^2}{\delta z^2} - H^2)\int_0^\infty rXJ_o(H_r)\delta r - \frac{\lambda + \mu}{\mu}\frac{\delta^2}{\delta z^2}\int_0^\infty rXJ_o(Hr)\delta r$$

$$= \frac{\lambda + 2\mu}{\mu}(\frac{\delta^2}{\delta z^2} - H^2)G - \frac{\lambda + \mu}{\mu}\frac{\delta^2 G}{\delta z^2}$$

$$\bar{w} = \frac{\delta^2 G}{\delta z^2} - \frac{\lambda + 2\mu}{\mu}H^2 G \tag{A.114}$$

$$w = \int_0^\infty H[\frac{\delta^2 G}{\delta z^2} - \frac{\lambda + 2\mu}{\mu}H^2 G]J_o(Hr)\delta H \tag{A.115}$$

We have,

$$u = -\frac{\lambda + \mu}{\mu}\frac{\delta^2 X}{\delta z \delta r}$$

$$\int_0^\infty ruJ_1(Hr)\delta r = -\frac{\lambda + \mu}{\mu}\frac{\delta}{\delta z}\int_0^\infty \frac{\delta X}{\delta r}rJ_1(Hr)\delta r$$

$$\bar{u} = -\frac{\lambda + \mu}{\mu}[[XrJ_1(H_r)]_0^\infty - \frac{\delta}{\delta r}\int_0^\infty X\frac{\delta}{\delta r}[rJ_1(Hr)]\delta r]$$

$$= \frac{\lambda + \mu}{\mu}H\frac{\delta}{\delta z}\int_0^\infty XrJ_o(H_r)\delta r$$

$$\bar{u} = \frac{\lambda + \mu}{\mu}H\int_0^\infty \frac{\delta G}{\delta z} \tag{A.116}$$

$$u = \frac{\lambda + \mu}{\mu}\int_0^\infty H^2\frac{\delta G}{\delta z}J_1(Hr)\delta H \tag{A.117}$$

Hankel transform of X (for multi-layered media) for j^{th} layer is,

$$G_j = (A_j + B_{jz})e^{-Hz} + (C_j + D_{jz})e^{Hz} \tag{A.118}$$

For the jth layer, Equation A.110 through Equation A.117 will have a 'j' subscript for $\bar{\sigma}_z$, σ_z, $\bar{\tau}_{rz}$, τ_{rz}, $\bar{w}$, w, $\bar{u}$, u, λ, μ, G, which are,

$$\bar{\sigma}_{zj} = (\lambda_j + 2\mu_j)\frac{\delta^3 G_j}{\delta z^3} - (3\lambda + 4\mu)H^2\frac{\delta G_j}{\delta z} \tag{A.119}$$

$$\sigma_{zj} = \int_0^\infty H[(\lambda_j + 2\mu_j)\frac{\delta^3 G_j}{\delta z^3} - (3\lambda_j + 4\mu_j)H^2\frac{\delta^3 G_j}{\delta z^3}]J_o(Hr)\delta H \tag{A.120}$$

$$\bar{\tau}_{rzj} = \lambda_j H\frac{\delta^2 G_j}{\delta z^2} + (\lambda_j + 2\mu_j)H^3 G_j \tag{A.121}$$

$$\tau_{rzj} = \int_0^\infty H^2[\lambda_j \frac{\delta^2 G_j}{\delta z^2} + (\lambda_j + 2\mu_j)H^2 G_j]J_1(Hr)\delta H \tag{A.122}$$

$$\bar{w}_j = \frac{\delta^2 G_j}{\delta z^2} - \frac{\lambda_j + 2\mu_j}{\mu_j}H^2 G_j \tag{A.123}$$

$$w_j = \int_0^\infty H[\frac{\delta^2 G_j}{\delta z^2} - \frac{\lambda_j + 2\mu_j}{\mu_j}H^2 G_j]J_o(Hr)\delta H \tag{A.124}$$

$$\bar{u} = \frac{\lambda_j + \mu_j}{\mu_j}H\int_0^\infty \frac{\delta G_j}{\delta z} \tag{A.125}$$

$$u_j = \frac{\lambda_j + \mu_j}{\mu_j}\int_0^\infty H^2 \frac{\delta G_j}{\delta z}J_1(Hr)\delta H \tag{A.126}$$

And the boundary conditions are,

At $z = 0$,

$$(\bar{\tau}_{rz})_1 = 0 \tag{A.127}$$

$$(\bar{\sigma}_{z1}) = F(H) \tag{A.128}$$

where F(H) is the Hankel transform of σ_z.

For $0 < r < a$,

$$\sigma_z = p[1 - (\frac{r}{a})^2]$$

For $a < r < \infty$

$$\sigma_z = 0$$

At interface,

$$(\bar{\sigma}_z)_j = (\bar{\sigma}_z)_{j+1} \tag{A.129}$$

$$(\bar{w})_j = (\bar{w})_{j+1} \tag{A.130}$$

$$(\bar{\tau}_{rz})_j = (\bar{\tau}_{rz})_{j+1} \tag{A.131}$$

$$(\bar{\tau}_{rz})_j = \beta[(\bar{u})_j - (\bar{u})_{j+1}] \tag{A.132}$$

At $z \to \infty$,

$$G_n \to 0 \qquad (\text{A}.133)$$

where n is the number of layers.

Calculation of the Constants of Integration   Using Equation A.127 in Equation A.121 (with $z = 0$ & $j = 1$),

$$(\bar{\tau_{rz}})_j = \lambda_j H \frac{\delta^2 G_j}{\delta z^2} + (\lambda_j + 2\mu_j) H^3 G_j$$

$$0 = H[\lambda_1 \frac{\delta^2 G_1}{\delta z^2} + (\lambda_1 + 2\mu_1) H^2 G_1] \qquad (\text{A}.134)$$

We know,

$$G_j = (A_j + B_j z)e^{-Hz} + (C_j + D_j z)e^{Hz} \qquad (\text{A}.135)$$

$$\frac{\delta G_j}{\delta z} = (A_j + B_j z)(-He^{-Hz}) + e^{-Hz}(0 + B_j) + (C_j + D_j z)(He^{Hz}) + e^{Hz}(0 + D_j)$$

For $z = 0$ & $j = 1$,

$$\frac{\delta G_j}{\delta z} = (A_j + B_j z)(-He^{-Hz}) + e^{-Hz}B_j + (C_j + D_j z)(He^{Hz}) + D_j e^{Hz}$$

$$\frac{\delta G_j}{\delta z} = -HA_1 + B_1 + HC_1 + D_1 \qquad (\text{A}.136)$$

$$\frac{\delta^2 G_j}{\delta z^2} = (A_j + B_j z)[-H * -He^{-Hz}] + (-He^{-Hz})[0 + B_j] +$$

$$B_j(-He^{-Hz}) + (C_j + D_{jz})[H * He^{Hz}] + (He^{Hz})[0 + D_j] + D_j(He^{Hz})$$

$$= (A_j + B_j z)H^2 e^{-Hz} - B_j He^{-Hz} - B_j He^{-Hz} + (C_j + D_j z)H^2 e^{Hz} + D_j He^{Hz}$$

$$+ D_j He^{Hz}$$

For $z = 0$ & $j = 1$,

$$\frac{\delta^2 G_j}{\delta z^2} = (A_j + B_j z)H^2 e^{-Hz} - B_j H e^{-Hz} - B_j H e^{-Hz} + (C_j + D_j z)H^2 e^{Hz} + D_j H e^{Hz} +$$

$$D_j H e^{Hz}$$

$$\frac{\delta^2 G_j}{\delta z^2} = (A_1 H - 2B_1 + C_1 H + 2D_1)H \tag{A.137}$$

For $z = 0$ and $j = 1$,

$$\frac{\delta^3 G_j}{\delta z^3} = (-A_1 H + 3B_1 + C_1 H + 3D_1)H^2 \tag{A.138}$$

Replacing these equations in Equation A.134 gives,

$$\lambda_1 \frac{\delta^2 G_j}{\delta z^2} + (\lambda_1 + 2\mu_1)H^2 G_1 = 0$$

$$\lambda_1 [A_1 H - 2B_1 + C_1 H + 2D_1]H + (\lambda 1 + 2\mu_1)H^2[A_1 + C_1] = 0$$

$$\lambda_1 (A_1 H^2 - 2B_1 H + C_1 H^2 + 2D_1 H) + (\lambda_1 + 2\mu)H^2(A_1 + C_1) = 0$$

$$A_1 H \lambda_1 - 2B_1 \lambda_1 + C_1 H \lambda_1 + 2D_1 \lambda_1 + A_1 H \lambda_1 + C_1 H \lambda_1 + 2A_1 \mu_1 H + 2C_1 \mu_1 H = 0$$

$$2A_1 H \lambda_1 + 2A_1 H \mu_1 + 2C_1 H \lambda_1 + 2C_1 H \mu_1 = 2B_1 \lambda_1 - 2D_1 \lambda_1$$

$$H\lambda_1(A_1 + C_1) + H\mu_1(A_1 + C_1) = \lambda_1(B_1 - D_1)$$

$$(A_1 + C_1)(H\lambda_1 + H\mu_1) = \lambda_1(B_1 - D_1) \tag{A.139}$$

Substituting the boundary conditions in Equation A.119,

$$(\bar{\sigma_z})_j = (\lambda_j + 2\mu_j)\frac{\delta^3 G_j}{\delta z^3} - (3\lambda_j + 4\mu_j)H^2\frac{\delta G_j}{\delta z}$$

$$F(H) = (\lambda_1 + 2\mu_1)[-A_1H + 3B_1 + C_1H + 3D_1]H^2 -$$

$$(3\lambda_1 + 4\mu_1)H^2[-HA_1 + B_1 + HC_1 + D_1]$$

$$= -A_1H^3\lambda_1 + 3B_1\lambda_1H^2 + C_1H^3\lambda_1 + 3D_1H^2\lambda_1 - 2A_1H^3\mu_1 + 6B_1H^2\mu_1 + 2C_1H^3\mu_1 +$$

$$6D_1\mu_1H^2 + 3A_1H^3\lambda_1 - 3B_1\lambda_1H^2 - 3C_1H^3\lambda_1 - 3D_1\lambda_1H^2 + 4A_1H^3\mu_1 - 4B_1H^2\mu_1$$

$$-4H^3C_1\mu_1 - 4H^2D_1\mu$$

$$F(H) = 2A_1H^3\mu_1 + 2A_1H^3\lambda_1 - 2C_1H^3\lambda_1 - 2C_1H^3\mu_1 + B_1\mu_1H^2 + 2D_1\mu_1H^2$$

$$F(H) = 2H^3(A_1 - C_1)(\lambda_1 + \mu_1) + 2H^2\mu_1(B_1 + D_1) \tag{A.140}$$

Using Equation A.129 in Equation A.119,

$$(\bar{\sigma_z})_j = (\bar{\sigma_z})_{j+1}$$

$$(\lambda_j + 2\mu_j)\frac{\delta^3 G_j}{\delta z^3} - (3\lambda_j + 4\mu_j)H^2\frac{\delta G_j}{\delta z} = (\lambda_{j+1} + 2\mu_{j+1})\frac{\delta^3 G_{j+1}}{\delta z^3} -$$
$$(3\lambda_{j+1} + 4\mu_{j+1})H^2\frac{\delta G_{j+1}}{\delta z}$$

Replacing $\frac{\delta^3 G_j}{\delta z^3}$ and $\frac{\delta G_j}{\delta z}$ in the equation,

$$A_je^{-Hz}H^3(2\lambda_j + 2\mu_j) + 2B_jH^2e^{-Hz}H^2[\mu_j + 2\mu_j + Hz(\lambda_j + \mu_j)] -$$

$$C_je^{Hz}H^3(2\lambda_j + 2\mu_j) + 2D_jH^2e^{-Hz}H^2[\mu_j + 2\mu_j + Hz(\lambda_j + \mu_j)] =$$

$$A_{j+1}e^{-Hz}H^3(2\lambda_{j+1} + 2\mu_{j+1}) + 2B_{j+1}H^2e^{-Hz}H^2[\mu_{j+1} + 2\mu_{j+1} + Hz(\lambda_{j+1} + \mu_{j+1})] -$$

$$C_{j+1}e^{Hz}H^3(2\lambda_{j+1} + 2\mu_{j+1}) + 2D_{j+1}H^2e^{-Hz}H^2[\mu_{j+1} + 2\mu_{j+1} + Hz(\lambda_{j+1} + \mu_{j+1})]$$

$$\tag{A.141}$$

Using the boundary conditions for interface DD gives,

$$\frac{\delta^2 G_j}{\delta z^2} - \frac{\lambda_j + 2\mu_j}{\mu_j}H^2G_j = \frac{\delta^2 G_{j+1}}{\delta z^2} - \frac{\lambda_{j+1} + 2\mu_{j+1}}{\mu_{j+1}}H^2G_{j+1}$$

$$A_j e^{-HDD} H^2 (\frac{-\lambda_j + \mu_j}{\mu_j}) - B_j e^{-HDD} H[2 + \frac{HDD}{\mu_j}(\lambda_j + \mu_j)]+$$

$$C_j e^{HDD} H^2 (\frac{-\lambda_j + \mu_j}{\mu_j}) - D_j e^{HDD} H[-2 + \frac{HDD}{\mu_j}(\lambda_j + \mu_j)] =$$

$$A_{j+1} e^{-HDD} H^2 (\frac{-\lambda_{j+1} + \mu_{j+1}}{\mu_{j+1}}) - B_{j+1} e^{-HDD} H[2 + \frac{HDD}{\mu_{j+1}}(\lambda_{j+1} + \mu_{j+1})]$$

$$+C_{j+1} e^{HDD} H^2 (\frac{-\lambda_{j+1} + \mu_{j+1}}{\mu_{j+1}}) - D_{j+1} e^{HDD} H[-2 + \frac{HDD}{\mu_{j+1}}(\lambda_{j+1} + \mu_{j+1})]$$

$$(A.142)$$

Substituting Equation A.131 in Equation A.121,

$$\lambda_j H \frac{\delta^2 G_j}{\delta z^2} + (\lambda_j + 2\mu_j) H^3 G_j = \lambda_{j+1} H \frac{\delta^2 G_{j+1}}{\delta z^2} + (\lambda_{j+1} + 2\mu_{j+1}) H^3 G_{j+1}$$

$$\lambda_j \frac{\delta^2 G_j}{\delta z^2} + (\lambda_j + 2\mu_j) H^2 G_j = \lambda_{j+1} \frac{\delta^2 G_{j+1}}{\delta z^2} + (\lambda_{j+1} + 2\mu_{j+1}) H^2 G_{j+1}$$

$$\lambda_j [(A_j H - 2B_j + B_j HDD) H e^{-HDD} + (C_j H + 2D_j - D_j HDD) H e^{HDD}]+$$

$$(\lambda_j + 2\mu_j) H^3 [(A_j + B_j DD) e^{-HDD} + (C_j + D_j DD) e^{HDD}] =$$

$$\lambda_{j+1} [(A_{j+1} H -$$

$$2B_{j+1} + B_{j+1} HDD) H e^{-HDD} + (C_{j+1} H + 2D_{j+1} - D_{j+1} HDD) H e^{HDD}]$$

$$+(\lambda_{j+1} + 2\mu_{j+1}) H^3 [(A_{j+1} + B_{j+1} DD) e^{-HDD} + (C_{j+1} + D_{j+1} DD) e^{HDD}]$$

$$A_j H^2 e^{-HDD} (\lambda_j + \mu_j) + B_j H e^{-HDD} [-\lambda_j + HDD(\lambda_j + \mu_j)]+$$

$$C_j H^2 e^{HDD} (\lambda_j + \mu_j) + D_j H e^{HDD} [\lambda_j + HDD(\lambda_j + \mu_j)] =$$

$$A_{j+1} H^2 e^{-HDD} (\lambda_{j+1} + \mu_{j+1})+ \quad (A.143)$$

$$B_{j+1} H e^{-HDD} [-\lambda_{j+1} + HDD(\lambda_{j+1} + \mu_{j+1})] + C_{j+1} H^2 e^{HDD} (\lambda_{j+1} + \mu_{j+1})+$$

$$D_{j+1} H e^{HDD} [\lambda_{j+1} + HDD(\lambda_{j+1} + \mu_{j+1})]$$

Similarly, using Equation A.132 in Equations A.121 and A.125 gives,

$$A_j H e^{-HDD}[(\lambda_j + \mu_j)(2H + \frac{\beta}{\mu_j})] + B_j e^{-HDD}[-2\lambda_j H + 2H^2 DD(\lambda_j + \mu_j)-$$

$$\frac{\beta}{2\mu_j}(\lambda_j + \mu_j)(1 - HDD)] + C_j H e^{HDD}[(\lambda_j + \mu_j)(2H - \frac{\beta}{\mu_j})]+$$

$$D_j e^{HDD}[2\lambda_j H + 2H^2 DD(\lambda_j + \mu_j) - \frac{\beta}{2\mu_j}(\lambda_j + \mu_j)(1 + HDD)] =$$

$$A_{j+1} H e^{-HDD}[(\lambda_{j+1} + \mu_{j+1})(2H + \frac{\beta}{\mu_{j+1}})]+$$

$$B_{j+1} e^{-HDD}[-2\lambda_{j+1} H + 2H^2 DD(\lambda_{j+1} + \mu_{j+1}) - \frac{\beta}{2\mu_{j+1}}(\lambda_{j+1} + \mu_{j+1})(1 - HDD)]$$

$$+C_{j+1} H e^{HDD}[(\lambda_{j+1} + \mu_{j+1})(2H - \frac{\beta}{\mu_{j+1}})]$$

$$+D_{j+1} e^{HDD}[2\lambda_{j+1} H + 2H^2 DD(\lambda_{j+1} + \mu_{j+1}) - \frac{\beta}{2\mu_{j+1}}(\lambda_{j+1} + \mu_{j+1})(1 + HDD)]$$

$$\text{(A.144)}$$

Using equation A.133 in Equation A.135 (for the nth layer),

$$G_n = (A_n + B_n z)e^{-Hz} + (C_n D_n z)e^{HZ}$$

When $z \to \infty$,

$$(A_n + B_n z)e^{-Hz} + (C_n D_n z)e^{HZ} = 0$$

which gives,

$$C_n = 0 \tag{A.145}$$

$$D_n = 0 \tag{A.146}$$

There are four constants of integration to be calculated for each layer, which means for n layers, there are $4n$ constants to be calculated. Since C_n and D_n are zeros, there are $(4n - 2)$ constants.

The top layer gives two equations and for n layers with $(n - 1)$ interfaces, there are $4(n - 1)$ equations. The total is $2 + 4(n - 1) = (4n - 2)$ equations for $(4n - 2)$

constants, and all constants of integration can be calculated. Solving these equations results in the calculation of stresses and displacements. The matrix given as,

[Coefficients of A_j, B_j, C_j, D_j] * [A_j, B_j, C_j, D_j] = [Right Hand Side of the Equations].

The substitution of the values of A_j, B_j, C_j and D_j in Equations A.119 to A.126, calculates the values of stresses and displacements.